EXPERIMENTAL AND NUMERICAL MODELING OF DUST CONTROL AT GRAIN RECEIVING WITH A HIGH-PRESSURE WATER FOGGING SYSTEM

by

DANIEL L. BRABEC

B.S., Kansas State University, 1982
M.S., Kansas State University, 1990

A DISSERTATION

Submitted in partial fulfillment of the

Requirements for the degree

DOCTOR OF PHILOSOPHY

Department of Biological and Agricultural Engineering
College of Engineering

KANSAS STATE UNIVERSITY
Manhattan, Kansas

2003

Approved by:

Major Professor
Ronaldo Maghirang

ABSTRACT

Grain dust is generated whenever grain is loaded or unloaded into hoppers and equipment. Grain dust at the receiving area is a fire hazard, a health concern, and a sanitation problem and should be controlled. A high-pressure, water-fogging system was evaluated as a potential grain dust control method. The system, which had 0.2 mm (0.008 in.) nozzles, produced 10-40 μm drops. The spray-fog system induced air flow, changed the airflow distribution, and changed the movement of grain dust.

Dust emissions and airflow rates were measured while spouting 2.1 m^3 (60 bu) sublots of corn and wheat into a test chamber. The uncontrolled dust emissions ranged from 5 to 24 g/tonne, depending on grain type and grain-flow rate. The airflow rate ranged from 108% to 172% of the volumetric grain flow rate. Grain dust and spray-fog emissions, deposits, and airflow rates were measured. The spray-fog was tested at four levels along with a control and an air-blower treatment. Dust reductions ranged from 60% to 84% for corn and 35% to 73% for wheat. At the highest spray-fog rate (855 g/min), 32 g/min (3.8%) of spray was emitted. Spray deposits ranged from 1.4 to 7.1 $mg/cm^2/min$ depending on sampling location.

FLUENT, a computational fluid dynamics (CFD) software, was used to predict airflow distribution and particle trajectories within the test chamber during grain flow and during spray operation. During grain flow, the grain pile was modeled as a low velocity air source causing air and dust to be exhausted from both ends of the test chamber. The

spray nozzles were simulated as seven individual pressure sources that induced airflow and forced airflow towards one end. Predicted results indicated that the spray generated air recirculation in the lower portion of the test chamber and directed particles and drop movement back towards the spray nozzles and plume. Smoke test confirmed the recirculation model predictions.

TABLE OF CONTENTS

LIST OF FIGURES

LIST OF TABLES

LIST OF SYMBOLS

A_e	cross sectional area at the east boundary of the control volume
a_P, a_E, a_W	coefficients of the discretized momentum equation
$a_x(t)$	acceleration along the x-axis at time t
C	Cunningham slip correction factor
C	constant in Prandlt's mixing layer model
C_d	Drag coefficient for a particle
CFD	Computational Fluid Dynamics
d	particle or drop diameter
D_e, D_w	diffusion related term for the discretized coefficients equation
d_g	geometric mean diameter
d_p	diameter of drop
D_v	vapor diffusion coefficient
e	unit charge
EPA	Environmental Protection Agency
F_d	Stoke's drag force
F_e	electrostatic force
F_e, F_w	mass flow related terms for the discretized coefficients equation
F_g	gravitational force
$F_x(t)$	forces along the x-axis at time t
FEV	Forced Expiration Volume
FGIS	Federal Grain Inspection Service
g	gravitational acceleration
k	turbulent kinetic energy
L, L_m	Prandlt's mixing length
m	mass of particle
M	molecular weight of water
MEC	minimum explosive concentration
MIT	minimum ignition temperature
n	number of charges
P, P*	pressure
p'	pressure correction used in SIMPLE algorithm
p_∞	partial vapor pressure away from drop
p_d	partial vapor pressure at drop surface
PM10	Particulate matter less than 10 μm (aerodynamic diameter)
q, q'	electro-static charge

q_s	saturation charge on particle or drop
R	ideal gas constant
Re	Reynold's number
S	generic source term
t	time
T_∞	ambient temperature
T_d	surface temperature of drop
TSP	total suspended particulate
TWA	time weighted average
u, $\overline{u}$	average air velocity along the x-axis
u_{max}	maximum air velocity along the x-axis
u_{min}	minimum air velocity along the x-axis
u'	turbulent deviation from average velocity
u'	velocity correction in SIMPLE algorithm
u_i	tensor notation for u, v, and w velocities
USDA-ARS	U.S. Dept. Agriculture, Agriculture Research Service
v, v_a	air velocity along the y-axis
v_o, V_o	initial particle velocity
v_{rel}, V_r	relative velocity between particle and air
$v_x(t)$	particle velocity along the x-axis at time t
v_t	terminal velocity of a particle in still air
VMD	volumetric median diameter
w	air velocity along the z-axis
x(t)	position on the x-axis at time t
x_i	tensor notation for x, y, and z position components
Γ	generic diffusion coefficient as used in conservation equations
γ	surface tension
ε	turbulent dissipation rate
ρ, ρ_a, ρ_g	density of air
ρ_p	density of particle
σ_g	geometric standard deviation
τ	relaxation time of particle
ϕ	generic dependent variable as used in conservation equations
ϕ'	turbulent deviation from average value
μ, μ_a	laminar viscosity of air
μ_t	turbulent viscosity of air
δ	boundary layer thickness

ACKNOWLEDGEMENTS

This research was supported by the USDA-ARS Grain Marketing and Production Research Center and Kansas Agricultural Experimental Station.

Thanks to my graduate committee: Dr. Ronaldo Maghirang, Dr. Mark Casada, Dr. Ekramul Haque, and Dr. Larry Erickson.

Thanks to many in the USDA-ARS Engineering Research Unit:
Floyd Dowell, Tom Pearson, Charles Martin, Robert Rousser, Duane Walker,
Dennis Tilley, Shirley Johnson.

Thanks to many fellow graduate students.

Thanks to retired faculty members Dr. James Steele and Dr. Charles Spillman for consultations regarding modeling.

Thanks to my wife, Susan, and children; Bethany, Benjamin, Joseph.
And thanks to God for my health and the time and resources for completing this research project.

Chapter 1. Introduction

1.1 Background

Grain dust is an inherent part of grain. It is dispersed during grain handling operations such as truck unloading or loading of bucket elevators. It is a continual house-keeping issue, drifting about a facility. Workers are often exposed to dust clouds which could affect their respiratory health. The dust can be a food supply for potential grain infesting insects. Grain dust appears to be a benign substance, quietly lying around. However, the dust can be a fuel for potential grain facility fires and explosions.

In 1976-1977, several large grain facilities were severely damaged and many employees killed from grain dust explosions. In February 1976 near Houston, Goodpasture Grain lost seven people and its facility was destroyed. In December 1977 near New Orleans, 36 people were lost from the grain explosion at Continental Grain facility. Also, in December 1977 at Galveston, 18 were lost at Farmers Export facilities grain explosion (Schoeff, 1995). This group of explosions alarmed the grain industry and gave momentum to significant efforts in the research on grain dust and its control.

In the early 1980's, research evaluated liquid additives for controlling grain dust emissions. A minor portion of the work studied the effectiveness of direct applications of water to grain. In the work by Lai and Martin (1982), water was sprayed directly onto grain as it was spouted into a truck bed. The dust was reduced by 50% and 75% when 0.5% and 1% water was sprayed into the grain stream. In a related study, Lai and Martin (1984) reported an 80% reduction in dust at the head house when 0.3% water was added to the grain at the boot. Also, in the same study, dust emissions were reduced in the head house of the grain storage facility by over 90% when 200 ppm of mineral oil was applied directly to the grain in the boot of the elevator.

In 1993, a fogging system was marketed for grain dust control. The manufacturer claimed effective dust control with only 0.01% moisture addition to the grain stream (Environmental Engineering Concepts, Palm Springs, Calif.). The fogging system clearly contrasted the coarse water sprays in the amount of water and the size of drops and demonstrated some potential as a dust control method.

The main locations in grain facilities where dust emissions are controlled are the bucket elevator and at grain receiving and loading out. Bucket elevators are usually totally enclosed and have limited access. Grain receiving hoppers are more visible and accessible. The dust suppression tests were performed on a pilot scale receiving hopper.

1.2 Objectives

This research investigated the potential of a water fogging system in controlling grain dust emissions for a grain receiving application. The specific objectives were to:

1. Determine the effectiveness of a variety of spray fog treatments in controlling grain dust within a test chamber representing a narrow portion of a receiving hopper.
2. Develop models for estimating the airflow and particle movements during grain receiving and spray fog treatment.

1.3 Organization of dissertation

Besides this introductory chapter, this dissertation has five other chapters and an Appendix section. Chapter two reviews literature related to dust characteristics, hazards, and controls. Chapter three describes mathematical models used to compute airflow and particle motion. Chapter four describes experiments testing the effectiveness of the spray-fog to control grain dust when dropping grain into a test chamber. Chapter five characterizes the spray-fog and the airflow and describes modeling of the spray fog. Chapter six is a summary of the project and list additional research possibilities. The Appendix contains supporting data and procedures.

1.4 Literature cited

Lai, F.S., Miller, B.S., and Martin, C.R. 1982. Control of grain dust with a water spray. Cereal Foods World 27(3): 105-107.

Lai, F.S., Martin, C.R., and Miller, B.S. 1984. Examining the use of additives to control grain dust in commercial grain elevators. ASAE Paper No. 84-3575. St. Joseph, Mich.: ASAE.

Schoeff, R.W. 1995. Feeds Science Presentation: Safety in Grain Storage and Processing Facilities. Kansas State University, Dept Grain Sc. Manhattan, Kans.

Chapter 2. Literature Review

Grain dust control is important in reducing fire/explosions, worker exposure, and impact to neighboring environments. The two main dust control methods, pneumatic systems and oil additives, have strengths and limitations. The use of water sprays was investigated as a potential tool in dust control.

2.1 Grain dust explosions

In 1976-1977, three large grain export facilities were severely damaged and 61 people killed from grain dust explosions at U.S. gulf ports. Many other countries had grain dust explosions during the 1980's: Canada, Germany, Spain, Russia, Thailand, France, Morrocco, Argentina, Australia, and China. From 1992 to 2001, the U.S. has averaged around 12 grain dust explosions per year (Schoeff, 2002).

If the grain dust is lying in a pile and a flame was directed onto the pile, the pile may start to burn but would not explode. When dust is dispersed into the air at a high concentration and a heat source is directed onto the dust cloud, then a flash fire will occur. The flash fire converts the solid particles into gas and heat. In a grain dust explosion at a grain facility, the gases and flames propagate through a piece of equipment or grain facility, idle floor and wall dust is dispersed in secondary reactions and fuels the fire further. This is clearly demonstrated in a dust explosion and safety video available from the Grain Science Department at Kansas State University (Schoeff, 1995).

Several factors influence the explosiveness of grain dust: dust type, dust concentration, particle size, ash content, and moisture content. Garrett and Lai (1982) studied the minimum explosive concentrations, MEC, for corn starch and grain dust using the Hartman Bomb. The smaller, drier, and starchier particles would explode easier. The MECs for cornstarch at 5% and 15% moisture content were 50 and 310 g/m^3, respectively. The MEC for the corn, wheat and sorghum dust ranged from 150 to 550 g/m^3 depending on size fraction and moisture content.

Lesikar et al. (1991) studied MEC and particle size using two plexiglass boxes that were separated by a paper diaphragm. An explosion was defined as the pressure to burst the paper diaphragm (20.7 kPa = 3 psi). The MECs for the sorghum dust were 70 and 150 g/m^3 for the 74 μm and 212 μm size fractions, respectively, while the minimum ignition temperatures, MIT, were 585°C and 890°C, respectively. The MECs for the wheat dust were 110 and 150 g/m^3 for the 74 and 212 μm size fractions, respectively, while the MITs for the wheat dust were 645°C and 670°C, respectively.

2.2 Health hazards from grain dust

Grain workers are exposed to a certain amount of dust. The nose and mouth are fairly effective in removing inhalable dust. However, the smaller respirable dust can enter the lungs. Occupational Safety and Health Administration, OSHA, lists respiratory safety and grain elevator safety requirements in the code of federal regulations (CFR 29, 1910.134 and 1910.272). OSHA listed grain dust permissible exposure limits of 10 mg/m^3, time weighted average, while NIOSH (2002) listed a grain dust recommended exposure limit of 4 mg/m^3.

Enarson et al. (1985) studied the lung capacity and respirable health of grain handlers on the west coast of Canada and attempted to relate the lung functions to the dust exposure in the workplace. All the workers at four Vancouver terminals were part of the study. The workers were given standard questionnaires, tested for skin allergens, and tested for lung capacity. Ten percent of the workers were very sensitive to dust and had a mean decline in lung capacity greater than 100 mL/yr. Normal lung capacity is 600 mL for a medium sized male. For 1978 and 1981, sweepers and cleaners were exposed to maximum dust concentrations of 148 and 72 mg/m^3, respectively, with average dust concentrations of 32 and 6 mg/m^3, respectively; maintenance workers were exposed to maxima of 48 and 24 mg/m^3 with average dust concentrations of 12 and 6 mg/m^3. Enarson et al. (1985) concluded that exposure to dust levels greater than 5 mg/m^3 was associated with serious adverse trends in lung capacity, although, the workers' lung capacities improved over weekends and after extended leave.

Burg and Shotwell (1980) measured the aflatoxin levels around harvesting equipment and compared them with levels around grinding equipment, swine pens, and grain handling equipment in Georgia. Inside the combine cab, airborne aflatoxin was only 0.02 μg/m^3, while in front of the combine, the aflatoxin level was 1.6 μg/m^3. Near the grinder, aflatoxin level was approximately 0.2 μg/m^3. An aflatoxin level of 1.8 μg/m^3 was found in the swine pens. At the truck receiving pit, aflatoxin levels varied from 0.03 to 1.8 μg/m^3. At rail load-out, the aflatoxin levels varied from 0.5 to 2.9 μg/m^3 near the hatch of the car. The work area near the conveyor of the elevator contained the highest levels of aflatoxin with over 13 μg/m^3. Two workers recorded exposures of 1.2 μg/m^3. Four other workers recorded 0.4, 0.2, 0.1, and 0.1 μg/m^3 aflatoxin exposures as measured with personal air samplers.

Richards et al. (1983) exposed male rats for 2 h/d and 5 d/wk for 4 wk with air containing 1000 and 5000 ppm of aflatoxin. The investigators found lung lesions of varying severity in 5 of 8 exposed rats while unexposed rats had no lesions. At 5000 ppm, the total exposure received by the rats was 6 μg aflatoxin per kg of weight.

2.3 Grain dust and emissions

Martin and Lai (1978) measured the total amount of dust particles adhering to corn, sorghum, and wheat. A 50-g portion of grain was rinsed with 600 mL of isopropyl alcohol. The rinse was passed through a 100-mesh sieve and a 0.8 μm filter. The rinsed dust averaged 0.082% by weight for corn, 0.070% for sorghum, and 0.025% for wheat.

Martin (1981) determined particle size distributions, densities, and compositional characteristics of corn, wheat, sorghum, and soybean dust samples, which were collected from a grain elevator cyclone collector. The median particle diameter ranged from 20 to 60 μm. The density of the grain dust ranged from 1.38 to 1.71 g/cm^3 with an average density of 1.49 g/cm^3. The composition of the dust was approximately 65-85% grain matter and the balance was water and soil-type material.

Martin et al. (1985) measured the dust concentration within a grain bin as it was being filled. The dust concentrations at 3 m (10 ft.) above the bin floor were 0.85 and 2.5 g/m^3 for the corn lot and 0.07 and 0.13 g/m^3 for wheat lot while dropping grain into the bin at rates of 0.8 and 1.6 m^3/min (22 and 44 bu/min), respectively.

Kenkel and Noyes (1994) measured the dust emissions at a grain elevator while receiving wheat from end-dump and hopper trailer grain trucks. The receiving area was enclosed with plywood. All the dust leaving the receiving pit was collected by either pneumatic collector or floor sweeping. End-dump grain trucks averaged 44 g/tonne total emissions while hopper bottom trailers averaged 25 g/tonne total emissions. The airborne dust was 20 g/tonne for the end-dump truck and 10 g/tonne for the hopper-bottom trailer.

Shaw et al. (1997) measured dust emissions during grain receiving at feed mills in Kansas and Texas cattle feedlots. The trailer hopper bottoms and receiving pit were covered with plastic while receiving grain shipments. Four high-volume air samplers collected the emitted dust. The average total suspended particle (TSP) emissions were 10 g/tonne of corn dust, with a standard deviation of 10 g/tonne. PM10 was estimated as 15% of the TSP from laboratory particle size distribution test of the dust samples collected.

The U.S. Environmental Protection Agency (1998) contracted with the Midwest Research Institute to compile references with dust emissions data from grain processing and handling facilities. The report averaged data from several research reports. TSP emission factors at grain receiving were 18 g/tonne for a hopper bottom truck and 90 g/tonne for a straight truck. Emission factors for PM10 were 4 g/tonne for a hopper bottom truck and 29 g/tonne for a straight truck.

2.4 Grain dust control methods

The U.S. Congress, Office of Technology Assessment (1995) evaluated methods and policies for suppressing grain dust. The report presented both the advantages and disadvantages of oil, water, and pneumatic dust control methods. The study found no statistical evidence that any one-dust suppression method has reduced dust explosions. Common dust control methods currently used by the grain industry are pneumatic systems and oil additives. These methods are described below.

2.4.1 Pneumatic systems

Pneumatic systems are standard equipment for large facilities. These systems reduce housekeeping, decrease emissions, and minimize the risk of dust explosion by collecting dust and reducing dust concentrations. Most pneumatic collection systems have numerous ducts feeding to a single fan. The ducts need to be carefully sized to maintain a balanced airflow throughout the network of ducts (Kanoski, 1981). Changing duct sizes or the number of inlets in the system could affect the airflow in other ducts.

Pneumatic systems are limited by the air distribution and the capture velocity at the inlet vents. The air velocity quickly decreases outside the inlet vent. The respective air velocities at 1/2 and 1 duct diameter away from the vent are only 30% and 7.5% of the air velocity in the duct (Boumans, 1985). Buss (1981) studied the location of air intakes on elevator legs. He measured dust concentrations of 75-95 g/m^3 with the inlet on top of the boot. By moving inlets to the sides of the up-leg, the measured dust concentration was reduced to 15-25 g/m^3 .

Once the air and dust are in the duct, a cyclone or baghouse is used to separate the dust from the air. The total collection efficiency depends on the size distribution and fractional collection efficiencies of the material collected (Hueman, 1996). The cyclone's efficiency depends on the inlet design and shape of the cyclone and can exceed 95% for raw cotton processing (Hughs and Baker, 1996). Baghouse filters are highly efficient. Many types of filters are over 99% efficient in collecting dust particles greater than 5 μm. However, as the filters becomes loaded, the airflow decreases. The filters require periodic cleaning and maintenance.

2.4.2 Oil spray systems

The Federal Grain Inspection Service, FGIS, allows food-grade oil to be applied to the grain at a rate of 200 ppm. This is equivalent to applying approximately 6 L (1.5 gal) of oil onto a semi-trailer load of grain. Lai et al. (1982a) studied the use of additives to control grain dust. At the point of application, the air was still dusty. Dust suppression was realized after initial transfer and mixing. The oil had some residual effect and dust emissions were reduced for several months.

Youngs et al. (1985) studied the oil content of the bran, shorts, and flour for wheat sprayed with several levels of mineral oil. They found most of the added oil stayed on the bran layer of wheat. The oil content of the bran and shorts was approximately 3 times the application rate, while the oil in the flour was 0.1 times the application rate.

Reid (1987) reported flour sifter problems from grain treated with oil. He stated that the dustiness of the facility was less. A full scale test was conducted to compare treated and non-treated wheat. A 48 h mill-run of oil-treated wheat with was compared with a 48 h mill-run of non-treated wheat. For this test, the oil treated grain had a 1.8% loss in flour yield, a 3 point average drop in Agston color, and many sifter problems.

2.5 Sprays and fogs

Water spray-fog systems could be an alternative grain dust control method. Issues related to this method are discussed below.

2.5.1 Fogs and mist

ASAE standard S327.2 (1992) defined a mist as the distribution of droplets with a volumetric median diameter (VMD) from 50 to 100 μm while distributions with a VMD less than 50 μm was classified as an "aerosol". Hinds (1982) shows several different drop categories depending on the drop size and application; fogs and clouds were 2 to 70 μm, mist was 70 to 200 μm, and drizzle was 200 to 500 μm.

ASAE standard S327.2 (1992) listed several devices for producing mist and fogs: hydraulic atomizer, pneumatic atomizers, and rotary atomizers. The hydraulic atomizer uses high pressure to force the liquid through the nozzle to produce the fog. The pneumatic atomizer combines an air source and a liquid source. The liquid is delivered at lower pressures and the air atomizes the water stream to a fog. The rotary atomizer delivers the liquid at medium pressures against a turning disk. The disk breaks up the stream into a mist. A spray of fog has several characteristics such as drop size distribution, spray direction, spray density, and spray velocity. These characteristics are dependent on nozzle size, water pressure, and other variables (Mawhinney, 1995).

2.5.2 Particulate scrubbers

A scrubber uses liquids to remove dust and gases from air. Particulate scrubbers have been studied since the 1950's and have been described in many air pollution texts (Cooper and Alley, 1994). The basic operating parameters are power consumption, airflow, air velocity, length of contact zone, liquid flow rate, drop size, and fractional collection efficiency.

The overall collection efficiency of a scrubber increases as the power and liquid flow increases. Stairmand (1964) described spray chambers as capable of obtaining 90% collection efficiency for particles larger than 8 μm with power consumption ranging from 0.3 to 1.5 kW per 30 m^3/min of air. Cyclone spray chambers increase the contact zone by their spiral path and can achieve efficiencies of 95% for particles larger than 5 μm and a power consumption of 0.75 to 2.5 kW per 30 m^3/min and liquid flows of 11 to 22 L per 30 m^3/min of air. Further design enhancements will increase collection efficiency such as wet filter packing, wet baffles, rotating baffles, and venturi type constrictions.

2.5.3 Sprays in the mining industry

Like the grain industry, the coal and rock mining industry has worked with many dust emissions problems. The mining industry has decades of experience using water sprays for controlling dust in mines and roads. Water is used to reduce dust, lubricate the machinery cutting points, and reduce the concentration of methane gas during coal mining. Courtney et al. (1978) used top and bottom spray nozzles on a coal mining machine to reduce respirable dust by 10-67%. Page et al. (1981) tested a 0.5-1.5 L/min water suppression system with salt mining equipment. The reduction in respirable dust concentration varied from 0 to 68%. Page (1982) compared external spray systems to sprays through the tips of the mining tools. A spray of water through the tip reduced dust by 91%, while externally mounted nozzles reduced dust by 50-60%. Jankowski et al. (1987) studied system configurations to reduce dust rollback from the mining's face. Top and bottom mounted nozzles reduced rollback by 50% and quartz content totally.

Some mining equipment use a combination of air and water for dust control. Wang et al. (1991) described a mining machinery that uses a pneumatic system to draw the air from the front of the machine into a venturi scrubber that was mounted on the side of the machine. The basic scrubber consisted of a fan, short duct transition, and a wire screen. Water was sprayed at a flow rate of 15 L/min. When maintained properly, the system would capture 99% of the dust particles. Page et al. (1994) described a nozzle configuration that was "tuned" with the mining ventilation. The system spaces and directs the nozzles for optimum scrubbing and sweeping towards the side-wall curtain. The "tuned" system operated with minimal air turbulence.

2.5.4 Pesticides and drift

The problems with spray drift have been considered in many types of agricultural spray applications. Spraying pesticides from small aircraft is a common procedure for treating agriculture acreage. Generally, crop sprayers use VMD from 200 to 400 μm and fly at 180 to 240 km/h within 2 to 4 m of the crop canopy. Computer software (Teske, 1996) was developed to predict spray drift and off-target deposits from many types of small, spray aircraft.

Large aircraft are used for treating mosquitoes in forest, war zones, or natural disaster regions. Factors such as spray drop distribution, flight speed, aircraft type and weight, local wind conditions, and drop evaporation affect the spray trajectory and drift. In one operation, military spray planes flew 50 m above the ground and the spray spread over 650 m downwind (Burkett et al., 1996).

Kohl et al. (1987) examined the drift from two types of low-pressure sprinkler heads used in irrigation systems. The VMDs from a smooth and a serrated impact plate were 1.14 mm and 2.65 mm respectively. With an average ambient wind-speed of 6.5 m/s, over 10% of the spray drifted beyond 12 m with the smooth plate and 10 m with the serrated plate.

2.5.5 Electrostatic sprays and charged fogs

The potential for static electric charges on grain dust were considered. Hoenig et al. (1976) claimed the polarity of the electro-static charge on clay, sand, and foundry dust tended to be negative for particles less than 5 μm. He found that positively charged fog worked significantly better than the uncharged fog at reducing the respirable dust, particularly the particles smaller than 5 μm. Also, Mitchell (1995) studied the precipitation of respirable dust with air ionizers and charged water-fogs.

Law (1978) developed an air-atomizing spray nozzle that had an embedded brass ring near the orifice for electro-statically charging spray drops. The brass ring was energized with a 1.5 kV-dc source. Dai et al. (1992) found the deposition of tracer chemicals on plant foliage was 2.5 fold better with air assisted, charged spray compared to regular hydraulic sprays. Almekinders et al. (1992) studied the trajectories of charged and uncharged sprays in a wind tunnel containing artificial plants. The charged spray improved the deposition of the 94 μm drops but not the 180 μm drops.

2.5.6 Paints

The fogging nozzles used in this grain dust research project produced drops in the 10 to 40 μm range like some paints. Part of the fog either deposits on the grain surfaces or on wall surfaces in a similar manner as paint drops deposit on surfaces.

The fundamental airflow and paint particle distributions were measured and modeled from an air-assisted paint nozzle which was directed towards a flat, vertical plate (Kwok, 1991). The region near the nozzle was called the flow development region. Near the work piece, the airflow made a 90^o change in direction and the paint particles tried to change direction also. The larger particles were deposited on the surface while many of the smaller particles followed the air streams past the work piece.

Paint deposition efficiency was modeled for 10 sizes of drops and for five initial locations. The drop diameters were 2, 10, 20, 30, 40, 50, 60, 70, 90, and 120 μm. The initial positions defined the initial forward and side velocities. At center-line, the initial forward and transverse velocities were 14.2 and 0.2 m/s, respectively. At the edge, the initial velocities were 2.8 and 0.5 m/s. For 2 μm drops, the deposition efficiency was approximately 10% from all entry locations. For 20 μm drops, the deposition efficiency was 60% at the center and 15% at the edge. For 60 μm drops, deposition efficiency was 100% at the center and 60% at the edge.

Two assumptions helped predict the overall deposition efficiency. First, the same drop size distribution existed at each entry position. Second, the mass flow of paint was proportional to the entry velocity. Predicted paint deposits were 62% and 72%. The measured efficiency was 68% for a test work-piece at 25 cm from the nozzle.

2.6 Water sprays for grain dust control

Zalosh (1977) studied the possibility of using a spray mist as an explosion suppression method when applied to the boot and head of a bucket elevator. His theory was that the heat from the burning of the grain dust would be absorbed by evaporation of the mist. Zalosh tried misting grain while it was unloaded at the head of a laboratory scale bucket elevator (40 kg/min). He estimated the liquid flow was 5-10 times the level needed for inhibiting an explosion. At the test spray levels, the grain moisture increased approximately 0.1% to 0.4%.

Lai et al. (1982b) applied water directly to a stream of corn falling from a elevator through a grain chute and into a truck. Water was applied directly to grain in the chute at 0.5% and 1.0% and dust was reduced by 47% and 71%, respectively. During a later study, Lai et al. (1984) applied 0.3% water to corn at the boot of the elevator and realized an 80% reduction of dust at the top of the elevator.

The U.S. Senate Committee on Agriculture, Nutrition, and Forestry had a hearing regarding the use of water to control grain dust (U.S. Congress, 1993). FGIS was proposing to ban the practice of directly adding 0.3% water for dust control. FGIS investigated and found some U.S. grain companies were adding in excess of 0.3% water for the purpose of increasing the weight of the shipment. FGIS had received formal complaints from several foreign grain buyers like Japan and South Africa and many U.S. grain companies.

Roughly 2/3 of the comments at the hearing were in favor of the ban. National Grain and Feed Association (NGFA) spoke out against water addition citing that grain weight was being affected. NGFA stated that some possible exceptions to the ban should be allowed such as using water for pesticides, dyes, and grain processing.

A regulation to prohibit the direct addition of water to grain, except for milling, malting, or similar processing operations, was passed and published in the Code of Federal Regulations. However, FGIS encouraged the continued research into spray fogging because insufficient data was available to conclude whether or not fogging was a viable dust control method (Federal Register, 1994).

2.7 Summary

Pneumatic and oil suppression dust control methods both have their limitations. Oils are not effective at the initial point of application, but require some mixing before their benefit is realized. A pneumatic system requires large airflow handling equipment to control dust at grain receiving because the hopper has limited confinement. The water fogging system could be a good method of dust control at grain receiving especially for country elevators that receive the bulk of their grain during the summer or fall harvest periods. The fogging system is clearly different from direct application of water method. The spray fog is applied at much lower dosage with the plume covering the hopper opening. The direct application uses fan spray nozzle to apply 0.3% water onto the grain stream.

2.8 Literature cited

Almekinders, H., Ozkan, H.E., Reichard, D.L., Carpenter, T.G., and Brazee R.D. 1992. Spray deposit patterns of an electrostatic atomizer. Trans ASAE 35(5):1361-1367.

ASAE Standards. 1992. S327.2. Terminology and definitions for agricultural chemical applications. St. Joseph, Mich.: American Society of Agricultural Engineers.

Boumans, G. 1985. Grain handling and storage. New York: Elsevier.

Burg, W.R. and Shotwell, O.L. 1984. Aflatoxin levels in airborne dust generated from contaminated corn during harvest and at an elevator in 1980. J. Assoc. Off. Anal. Chem 67(2):309-312.

Burkett, D.A., Biery, T.L., and Haile, D.G. 1996. An operational perspective on measuring aerosol cloud dynamics. Journal of American Mosquito Control Assoc. 12(2): 380-383.

Buss, K.L. 1981. Dust concentrations in bucket elevators. In Proc. Dust Control for Grain Elevators, pp. 64-87. Washington, D.C.: National Grain & Feed Assoc.

Code of Federal Regulations. 1994. 29 CFR 1910.134. OSHA, respiratory protection. Washington, D.C.: U.S. Government Printing Office.

Code of Federal Regulations. 1994. 29 CFR 1910.272. OSHA, grain elevator facilities. Washington, D.C.: U.S. Government Printing Office.

Cooper, D.C. and Alley, F.C. 1994. Air pollution control: A design approach. Prospect Heights, Ill.: Waveland Press, Inc.

Courtney, W.G., Jayarman, N.I., and Behum, P. 1978. Effect of water sprays for respirable dust with a research continuous-mining machine. USBM Report No.8283. Pittsburgh, PA: U.S. Bureau of Mines.

Dai, Y., Cooper, S.C., and Law, S.E. 1992. Effectiveness of electrostatic, aerodynamic, and hydraulic spraying methods for depositing pesticide sprays onto inner plant regions. ASAE Paper No. 92-1094. St. Joseph, Mich.: American Society of Agricultural Engineers.

Enarson, D.A., Vedal, S., and Chan-Yeung, M. 1985. Rapid decline in FEV in grain handlers. American Review of Respiratory Disease 132(4):814-817.

EPA. 1998. Emission factor document for EPA AP-42, section 9.9.1 Grain Elevators and Grain Processing Plants. Research Triangle Park, N.C. U.S. Environmental Protection Agency.

Federal Register. 1994. Prohibition on adding water to grain. Vol. 59, no.198.

Garrett, D.W. and Lai, F.S. 1982. Minimum explosive concentration as affected by particle size and composition. ASAE Paper No. 82-3580. St. Joseph, Mich.: American Society of Agricultural Engineers.

Hinds, W.C. 1982. Aerosol technology: properties, behavior, and measurement of airborne particles. New York: John Wiley & Sons, Inc.

Hoenig, S.A., Russ, C.F., and Bidwell, J.B. 1976. Application of electrostatic fog techniques to the control of foundry dusts. Amer. Foundrymen's Society 84:55-64.

Hueman, W. 1996. Wet scrubbers (workshop). Int. Conf on Air Pollution from Agricultural Operations. Kansas City, MO. Sponsored by Midwest Plan Service, Ames, Iowa.

Hughs, S.E. and Baker, R.V. 1996. Effectiveness of cyclone design in collecting gin trash particulate emissions. In Proc. Int Conf on Air Pollution from Agricultural Operations, pp. 301-308. Ames, Iowa: Midwest Plan Service.

Jankowski, R.A., Jayarman, N.I., and Babbitt, C.A. 1987. Water spray systems for reducing the quartz dust exposure of the continuous miner operator. Proc 3rd Mine Ventilation Symposium, Littleton, Colo.: Society of Mining Engineers

Kanoski, T.E. 1981. Operating dust aspiration systems. Proc Dust Control for Grain Elevators. St. Louis, MO: National Grain & Feed Association.

Kenkel, P. and Noyes, R. 1994. CR-1108 OSU grain elevator dust emission study. Stillwater, Okla.: Oklahoma Cooperative Extension Service.

Kohl, R.A., Kohl, K.D., and DeBoer, D.W. 1987. Chemigation drift and volatilization potential. Applied Engineering in Agriculture 3(2): 174-177.

Kwok, K.C. 1991. Fundamentals of air spray painting. Ph.D. dissertation, University of Minnesota.

Law, S.E. 1978. Embedded-electrode electrostatic-induction spray-charging nozzle: theoretical and engineering design. Trans ASAE 21(5):1096-1104.

Lai, F.S., Martin, C.R., and Miller, B.S. 1982a. Examining the use of additives to control grain dust. NGFA #OAC-82-036, NGFA, Washington, D.C.: National Grain and Feed Association

Lai, F.S., Miller, B.S., and Martin, C.R. 1982b. Control of grain dust with a water spray. Cereal Foods World 27(3):105-107.

Lai, F.S., Martin, C.R., and Miller, B.S. 1984. Examining the use of additives to control grain dust in commercial grain elevators. ASAE Paper No. 84-3575. St. Joseph, Mich.: American Society of Agricultural Engineers.

Lesikar, B.J., Parnell, C.B., and Garcia, A. 1991. Determination of grain dust explosibility parameters. Trans ASAE 34(2):571-576.

Martin, C.R. 1981. Characterization of grain dust properties. Trans ASAE 24(3):738-742

Martin, C.R., Aldis, D.F., and Lee, R.S. 1985. In situ measurement of grain dust particle size distribution and concentration. Trans ASAE 28(4):1319-1327.

Martin, C.R. and Lai, F.S. 1978. Measurement of grain dustiness. Cereal Chem. 55(5):779-792.

Mawhinney, J.R. 1995. Water mist fire suppression systems: applications, principles, and limitations. National Research Council, Canada.

Mitchell, B.W. 1995. Effectiveness of negative air ionization on the precipitation of inhalable sized particles in a poultry house environment. ASAE Paper No. 95-4592. St. Joseph, Mich.: American Society of Agricultural Engineers.

NIOSH. 2002. Pocket guide to chemical hazards. www.cdc.gov/niosh. National Institute for Occupational Safety and Health (NIOSH). Washington, D.C.

Page, S.J., Urban, C.W., and Vokwein, J.C. 1981. Effectiveness of wet cutter bars in reducing salt mine dust. USBM Report No.8512. Pittsburgh, Pa.: U.S. Bureau of Mines.

Page, S.J. 1982. An evaluation of three wet dust control techniques for face drills. USBM Report No. 8596. Pittsburgh, Pa.: U.S. Bureau of Mines.

Page, S.J., Mal, T., and Volkwein, J.C. 1994. Unique water spray system improves exhaust face ventilation and reduces exposure to respirable dust on continuous miners in laboratory test. J.Mine Ventilation Society of South Africa Oct94:196-205.

Reid, R.G. 1987. Dust control-additive update. In Proc. of the Grain Elevator and Processing Society 58th Int Technical Conf. Minneapolis, Minn.

Richards, J.L., Cheville, N.F., Songer, J.R., and Thurston, J.R. 1983. Exposure of rats to aerosols of aflatoxin containing particles. Proc. 8th International Congress of Human and Animal Mycology. Ed. M. Baxter. Palmerstown, New Zealand.

Schoeff, R.W. 2002. Agricultural dust explosions in 2001. January Newsletter. Kansas State University, Dept Grain Sc. Manhattan, Kans.

Schoeff, R.W. 1995. Deadly dust III. Video Tape. Dept of Comm., Kansas State University, Manhattan, Kans.

Shaw, B.W., Buharivala, P.P., Parnell, C.B.Jr., and Demny, M.A. 1997. Emission factors for grain receiving and feed loading operations at feed mills. Trans. ASAE 41(3):757-765.

Stairmand, C.J. 1964. Removal of dust from gases. In Gas Purification Processes, ed. G. Nonhebel, pp.469-522. Bristol, Great Britain: J.W. Arrowsmith Ltd.

Teske, M. 1996. An introduction to aerial spray modeling with FSCBG. Journal of the American Mosquito Control Association 12(2): 353-358.

US Congress. 1993. Subcommittee on Agricultural Research. U.S. Senate. Hearing for Use of water to control grain dust. Washington, D.C.: U.S. Government Printing Office.

U.S. Congress, Office of Technology Assessment. 1995. Technology and policy for suppressing grain dust explosions in storage facilities. OTA-BP-ENV-177. Washington, D.C.: U.S. Government Printing Office.

Youngs,Y.L., Kunerth, W.H., and Crawford, R.D. 1985. Mineral oil added to wheat for dust control: effects on milling and baking quality. AOM Bulletin May 1985: 4476-4479.

Wang, Y.P., Tien, J.C., Wilson, J.W., and Erten, M.H.. 1991. Use of surfactants for dust control in mines. Proc. of 5th US Mine Ventilation Symposium. West Virginia University: Society of Mining Engineers.

Zalosh, R. 1977. Water mist for the prevention and mitigation of grain dust explosions. In Proc. Int. Symposium on Grain Dust Explosions. Minneapolis, Minn.: Grain Elevators and Processing Society.

Chapter 3. Model Development and Preliminary Analysis

3.1 Introduction

A cloud of grain dust is a mixture of air and dust. Air movement controls the movement of dust and fog. One approach to predicting dust or spray emissions is to follow the movement of individual particles within an enclosure or chamber. Such an approach requires the air velocity within a enclosure to be determined either experimentally or numberically. Then, trajectories can be calculated for particles and drops of known sizes, densities, and initial locations. For grain dust, the particles are released into the air when the grain stream impacts the top of the grain pile. Thus, the initial location would be around the top of the grain pile. For the fog spray, the drops were initially located near the nozzles. An array of particle and drop sizes and initial locations were used to describe a group of grain dust particles or spray drops. The particle and drop sizes were measured to determine the appropriate sizes to model.

There are two airflow conditions that result in distinctly different particle movements: still-air and moving-air. In still air, the main force acting on the particle is gravity. Modeling of well dispersed grain dust particles in still air is a one-dimensional problem. A plume of dust particles can be divided into several size categories. The larger dust particles of the plume settle out faster. The total settling is the summation of the settling from the weighted size-distribution.

With moving air ($v_a >> v_t$), the main force acting on the particle is the drag force from the air. Modeling particle movement in air requires knowledge of the particle initial conditions, test geometry, and airflow profile. The problem is three-dimensional and both the drag force and gravitional force are accounted for during each time step.

Besides air movement, several other possible factors were considered such as drop or particle interactions, potential drop evaporation, and the potential electro-static forces. These factors are affected by relative concentrations, relative velocities, and environmental influences. Detailed particle-drop and drop-drop interaction models were not pursued and left for later studies because they were beyond the scope of this project. For this study, the airflow and particle trajectory testing and modeling were emphasized.

3.2 Terminal velocity in still air

A basic characteristic of a particle is its settling velocity in air. Terminal velocity is the maximum velocity of a falling particle in still air. It occurs when the particle's acceleration reaches zero and the air-drag force is equal to the particle weight. When the particle's Reynold number (Re) is less than one, the drag force is defined as,

$$F_d = \text{Stoke's drag force} = \frac{3\pi\mu v_{rel} d}{C} \tag{3.1}$$

where μ is air viscosity, v_{rel} is relative velocity between the particle and air, d is particle diameter, and C is the slip correction factor. The weight of the particle is written as,

$$F_g = \text{weight} = m\,g = \frac{\rho_p \pi d^3}{6} g \tag{3.2}$$

where m is mass, g is gravitational acceleration, and ρ_p is particle density. At the particle's terminal settling velocity,

$$F_d = F_g \tag{3.3}$$

so that,

$$v_{rel} = v_t = \frac{\rho_p d^2 g C}{18\mu} \tag{3.4}$$

The settling velocity for a 10 μm grain dust particles (particle density, ρ_p= 1.5 g/cm^3) in still-air is only 0.45 cm/s and would drop only 27 cm (11 in.) in one minute. A 100 μm particle has a terminal velocity of 45 cm/s or 2.7 m/min. Air currents of similar small magnitudes would suspend and carry these particles.

When working with particles with diameters less than 100 μm, Re (eqn 3.5) is usually less than one and the Stokes's drag force (F_d, eqn 3.1) is valid (Hinds, 1982).

$$\mathrm{Re} = \left(\frac{\rho_a}{\mu_a}\right) * V_r * d = 6.6 * V_r * d \quad \text{(20C air, } V_r \text{ (cm/s), d (cm))} \tag{3.5}$$

When Re>1, Newton's drag equation and coefficient of drag (C_d) should be employed (Hinds, 1982):

$$F_d(Newton's) = C_d \frac{\pi}{8} \rho_a V_r^2 d^2 \tag{3.6}$$

$$C_d = \frac{24}{\mathrm{Re}}\left(1 + \frac{\mathrm{Re}^{2/3}}{6}\right) \tag{3.7}$$

3.3 Spray induced airflow

During preliminary laboratory work with the spray system, a hot wire anemometer was positioned just between two spray nozzles and indicated induced air velocities between 1 and 3 m/s. The induced air resulted from the momentum exchange with the spray jet and helped carry the small drops down-stream of the nozzle.

Many authors have studied induced airflow from spray nozzles. Jones and James (1987) studied induced airflow from extraction tubes, which were used to reduce respirable coal dust during mining. When the high pressure spray was operating within a tube, air was sucked into the tube. Several sizes and shapes of tubes were tested: 10 cm (4 in.) to 60 cm (24 in.), round and rectangular. Several nozzles were tried with some having flow over to 16 L/min (3.6 gal/min). Ford et al. (1987) used a group of nine extraction tubes to produce airflow of 85 m^3/min (3000 cfm) to scrub the dust generated from an 8 ton/min coal mining equipment.

St. Georges and Buchlin (1994) developed a one-dimensional model to predict the plume envelope, drop velocities, and gas flow from a single nozzle directed vertically downward. The authors theorized that air is sheared from the circumference of the spray plume and that the mass of the air sheared from the circumference was equal to the mass of the air within the plume. The gas flow was related to the distance from the tip of the nozzle and the pressure of the spray.

For this work, the spray was modeled as two parts: a small pressure source in the fluid phase and a discrete-particle phase representing a group of drops. Details of the individual nozzle pressure values and dimensions and the array of drop characteristics are given in Chapter 5.

3.4 Numerical modeling of airflow

The airflow from grain-displaced air and spray-induced air can be modeled with computational fluids dynamics (CFD). CFD is a numerical method developed to study fluid flows and heat transfer problems. Commercially available softwares are available including FLUENT (Fluent Inc., 2002), which was used in this research. A general description of one CFD modeling technique is given below. Additional information regarding CFD modeling is available from Patankar (1980). Specific applications of FLUENT to grain and spray operations models are given in Chapter 5.

The geometry is defined with inlets, outlets, and obstructions. The geometry is meshed into sub-volumes. CFD uses the conservation of mass and momentum equations to solve for the pressure and velocity fields. When there are temperature gradients, then the conservation of energy would be included. The conservation of momentum equations in the x, y, and z directions have a common type of differential equation. The four parts of this differential equation are the time dependent, flow dependent, diffusion dependent, and source components (eqn 3.8).

$$\frac{\partial}{\partial t}(\rho\phi)+\frac{\partial}{\partial x_i}(\rho u_i\phi)=\frac{\partial}{\partial x_i}(\Gamma\frac{\partial\phi}{\partial x_i})+S \tag{3.8}$$

(time) (flow) (diffusion) (source)

ϕ is a dependent variable and could be either *u*, *v*, or *w* velocity. Γ is the associated diffusion coefficient and would be viscosity (μ) for momentum equations. S is the associated source term and would be pressure-change or a body force for the momentum equations. The momentum equation for the *u*-velocity (x direction) appears as follows:

$$\frac{\partial}{\partial t}(\rho u)+\frac{\partial}{\partial x}(\rho uu)+\frac{\partial}{\partial y}(\rho vu)+\frac{\partial}{\partial z}(\rho wu)=\frac{\partial}{\partial x}(\mu\frac{\partial u}{\partial x})+\frac{\partial}{\partial y}(\mu\frac{\partial u}{\partial y})+\frac{\partial}{\partial z}(\mu\frac{\partial u}{\partial z})-\frac{\partial P}{\partial x} \qquad (3.9)$$

The momentum equations are discretized or converted to an algebraic form for each meshed volume. The following is an example of discretization of the steady-state, one-dimensional general equation. Consider the following one-dimensional control volume (fig 3.1):

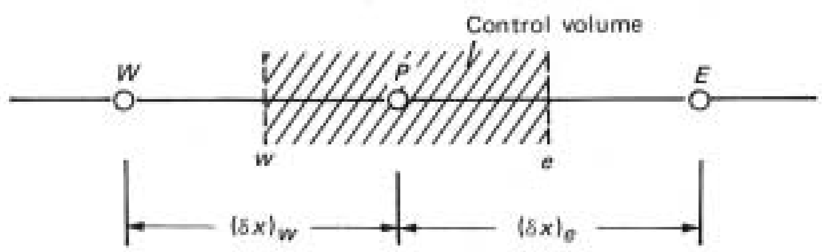

Figure 3.1: Control volume (P) and neighboring points on the east and west. (Patankar, 1980)

The common differential equation (eqn 3.8) can be simplified for the 1-d control volume at steady state as:

$$\frac{d}{dx}(\rho uu) = \frac{d}{dx}(\mu\frac{du}{dx}) + S \qquad (3.10)$$

When the left side of equation 3.10 is integrated across the control volume (eqn 3.11), the terms on the right side of the integration can be discretized as in equations 3.12 and 3.13. The subscripts on the following terms indicate their locations and represent the center or one of the faces of a control volume (figure 3.1)

Integrated flow terms:
$$\int \frac{d}{dx}(\rho uu)dx = (\rho uu)_e - (\rho uu)_w \tag{3.11}$$

$$(\rho uu)_e = (\rho u)_e \frac{(u_E + u_P)}{2} \tag{3.12}$$

$$(\rho uu)_w = (\rho u)_w \frac{(u_W + u_P)}{2} \tag{3.13}$$

When the diffusion term of equation 3.10 is integrated (eqn 3.14), the terms on the right side of the integration can be discretized as in equations 3.15 and 3.16.

Integrated diffusion flux:
$$\int \frac{d}{dx}(\mu \frac{du}{dx})dx = (\mu \frac{du}{dx})_e - (\mu \frac{du}{dx})_w \tag{3.14}$$

$$(\mu \frac{du}{dx})_e = \frac{\mu_e}{(\delta x)_e}(u_E - u_P) \tag{3.15}$$

$$(\mu \frac{du}{dx})_w = \frac{\mu_w}{(\delta x)_w}(u_P - u_W) \tag{3.16}$$

After setting the integrated flow equations (eqns 3.12 and 3.13) equal to the integrated diffusion equations (eqns 3.15 and 3.16), the control volume's dependent variable, u_P, can be expressed as a function of its neighboring values and coefficients.

$$a_P u_P = a_E u_E + a_W u_W + S \tag{3.17}$$

where, $$a_E = D_e - \frac{F_e}{2} \qquad a_W = D_w + \frac{F_w}{2} \qquad a_P = a_E + a_W \tag{3.18}$$

$$D \equiv diffusion \equiv \frac{\mu}{\delta x} \qquad F \equiv flow \equiv \rho u \tag{3.19}$$

The influence of the flow directions should be included in the coefficients of the discretized equations to avoid some types of false computations. Several methods are possible, including upwind, hybrid, and power-law schemes (Patankar, 1980). The upwind scheme is considered here and the coefficients are given as an example:

$$\text{For } F \geq 0 \qquad a_E = D_e \qquad a_W = D_w + F_w \tag{3.20}$$

$$\text{For } F \leq 0 \qquad a_E = D_e - F_e \qquad a_W = D_w \tag{3.21}$$

For two and three dimensional models, the equations are expanded and include the velocities and pressure influences of neighboring control volumes:

$$a_P u_P = a_E u_E + a_W u_W + a_N u_N + a_S u_S + S \tag{3.22}$$

Discretized equations are applied to all the control volumes. A single-line solution method is repeatedly applied line-by-line through the geometry until the changes in the dependent variables from sequential sweeps are within a convergence criteria. The single-line solution method commonly used is the Tri-Diagonal-Matrix-Algorithm (Patankar, 1980).

For the momentum equations, the source term is the pressure difference between two grid points. Pressures are computed at the centers of the control volumes while the velocities are computed at the faces of the control volumes. One technique for handling pressure at the volume's center and velocities at the faces uses staggered computational grids. The offset grid aligns the pressure terms (P_P, P_E) on the face of the velocity grid. The discretized momentum equation for the u-velocity appears as follows:

$$a_e u_e = \Sigma a_{nb} u_{nb} + A_e (P_P - P_E) \tag{3.23}$$

For most of the control volumes, neither the pressure nor the velocity is initially known. A computational protocol, semi-implicit method for pressure linked equations (SIMPLE), was developed which uses pressure information in momentum equations to determine velocity values and velocities in continuity equation to determine pressure corrections until the two equations converged.

The basic steps of SIMPLE computational procedures are:

0. Estimate the initial pressure = P*

1. Solve for the '*' velocities (u*, v*, w*) using P* and the momentum based equations.

2. Solve for pressure corrections, P', using the '*' velocities and the continuity equations.

3. Solve for velocity corrections, u', v', w', using momentum equations.

4. Solve for the velocities: u = u* + u';   v = v* + v'; w = w* + w'

5. new P* = P* + P';   if not converged then goto #1.

The above overview of CFD modeling is a partial description of the equations used to solve the pressure and velocity profiles and the techniques which can be used to solve them.

The discussion of the airflow model to this point has been for laminar flow. However, the flow inside a receiving hopper with high-pressure spray is expected to be tuburlent. The development of turbulent models are decribed in this section (Patankar, 2002). Turbulent flow modeling combines time averaged velocities $(\bar{u})$ with velocity fluctuations;

$$u = \bar{u} + u' \; . \tag{3.24}$$

When the average and fluctuating velocity terms are included in the conservation of momentum equations, an additional set of terms are present, which are called the turbulent stress or Reynold's stresses:

conservation of momentum: $$\frac{\partial}{\partial t}(\rho\bar{\phi}) + \frac{\partial}{\partial x_i}(\rho\bar{u_i}\bar{\phi}) = \frac{\partial}{\partial x_i}(\Gamma\frac{\partial\bar{\phi}}{\partial x_i} - \rho\overline{u_i'\phi'}) + \bar{S} \tag{3.25}$$

turbulent stress terms: $$-\rho\overline{u_i'\phi'} \text{ or } -\rho\overline{u_i'u_j'} \tag{3.26}$$

Turbulent models provide a means of calculating the turbulent stresses. In 1877, Boussinesq expressed the turbulent stresses in terms of turbulent kinetic energy, *k*, and turbulent viscosity, μ_t:

$$-\rho\overline{u_i'u_j'} = \mu_t\left(\frac{\partial u_i}{\partial x_j} + \frac{\partial u_j}{\partial x_i}\right) - \frac{2}{3}k\rho\delta \tag{3.27}$$

$$k = \frac{1}{2}\left(\overline{u_1'^2} + \overline{u_2'^2} + \overline{u_3'^2}\right) \tag{3.28}$$

The turbulent viscosity term was initially determined experimentally and was assumed constant. It was larger than the laminar viscosity term, μ, and represented the viscosity imposed by colliding eddy currents.

Around 1925, Prandtl proposed equations to express the turbulent viscosity as a function of boundary layer properties. One model, free-shear-layer, is written as:

$$\mu_t = C\rho\delta(u_{\max} - u_{\min}) \tag{3.29}$$

where C = 0.01 for a mixing layer and δ was the thickness of the shear layer.

Another model, mising-length model, is given as:

$$\mu_t = \rho {L_m}^2 \left(\frac{\partial u}{\partial y}\right) \tag{3.30}$$

where the turbulent viscosity was a function of velocity gradient and mixing length, L_m .

In 1940, Kolmogorov proposed an expression relating the turbulent viscosity to turbulent kinetic energy: $\mu_t = \rho k^{1/2} L$. (3.31)

Further developments involved differential equations and the *k*-ε models.

$$\frac{\partial}{\partial t}(\rho k) + \frac{\partial}{\partial x_i}(\rho u_i k) = \frac{\partial}{\partial x_i}(\mu_t \frac{\partial k}{\partial x_i}) + P - \rho\varepsilon \tag{3.32}$$

$$\frac{\partial}{\partial t}(\rho\varepsilon) + \frac{\partial}{\partial x_i}(\rho u_i \varepsilon) = \frac{\partial}{\partial x_i}(\frac{\mu_t}{1.3}\frac{\partial \varepsilon}{\partial x_i}) + (1.44P - 1.92\rho\varepsilon)\frac{\varepsilon}{k} \tag{3.33}$$

$$P = \mu_t(\frac{\partial u_i}{\partial x_j} + \frac{\partial u_j}{\partial x_i})\frac{\partial u_i}{\partial x_j} \tag{3.34}$$

$$\mu_t = 0.09\rho\frac{k^2}{\varepsilon} \tag{3.35}$$

The k-ε model solves three terms; *k, ε,* μ_t *,* which are then used to determine the Reynold's stresses and velocity fluctuations. The equation for turbulent dissipation, ε, is semi-empirical. The *k*-ε model has been widely tested and has been useful in describing a variety of turbulent flow solutions.

3.5 Modeling particle and drop trajectories

Given the airflow profile and the initial particle conditions, particle or drop trajectories can be computed from equations based on Newton's second law of particle motion. The particle motion is described in terms of forces, acceleration, velocity, displacement, and time as described in an engineering physics book (Shortley and Williams, 1971). From the trajectories, the fate of the particles can be estimated.

The following equations illustrate the general sequence for determining the acceleration, velocity, and position of a particle for a time increment and in two-dimensions. The routine requires the particle diameter, density, initial position, and velocities to be specified.

Forces: $$ma_x = \Sigma F_x = \mathrm{F_d(x)} \qquad ma_y = \Sigma F_y = \mathrm{F_d(y) + mg} \tag{3.36}$$

Acceleration: $$a_x(t) = \frac{\Sigma F_x(t-1)}{m} \qquad a_y(t) = \frac{\Sigma F_y(t-1)}{m} \tag{3.37}$$

Velocity: $$v_x(t) = v_x(t-1) + dv_x(t) \qquad v_y(t) = v_y(t-1) + dv_y(t) \tag{3.38}$$

$$dv_x(t) = \left(\frac{a_x(t) + a_x(t-1)}{2}\right) * dt \qquad dv_y(t) = \left(\frac{a_y(t) + a_y(t-1)}{2}\right) * dt \tag{3.39}$$

Position: $x(t) = x(t-1) + dx(t)$ $y(t) = y(t-1) + dy(t)$ (3.40)

$$dx(t) = \left(\frac{v_x(t) + v_x(t-1)}{2}\right) * dt \qquad dy(t) = \left(\frac{v_y(t) + v_y(t-1)}{2}\right) * dt \tag{3.41}$$

Time: $t = t + dt$ (next step: loop to force equations) (3.42)

The drag force from air and gravitational force were the only forces considered in the particle trajectory models. The effect of turbulence was included. The CFD software provided particle tracking computations and used similar equations of motion.

3.6 Modeling the potential for particle/drop collisions

The relative coverage of the spray flux to the area of the plume gives some insight to the amount of energy the spray exchanges with the air and the chance of drop and particle interactions. At 15 cm from the nozzle, the diameter and cross sectional area of the spray plume were approximately 15 cm and 120 cm^2, respectively. The spray plume contains a large flux of drops. The liquid flow from a single nozzle at 6.9 MPa (1000 psi) was 1.6 cm^3/s. Approximately 70% of the spray were 18 μm drops and the drop flux was over 360,000,000 drops/s. The cross sectional area of a single drop was 2.5×10^{-6} cm^2. The area covered by the spray flux would be 933 cm^2/s. The spray flux totally sweeps the plume's cross section 7.7 times per second at 15 cm. Depending on the distance from the nozzle, plume diameter, and the overlap (figure 3.2), the drop flux totally covers a region close to the nozzles from 5 to 15 times per second.

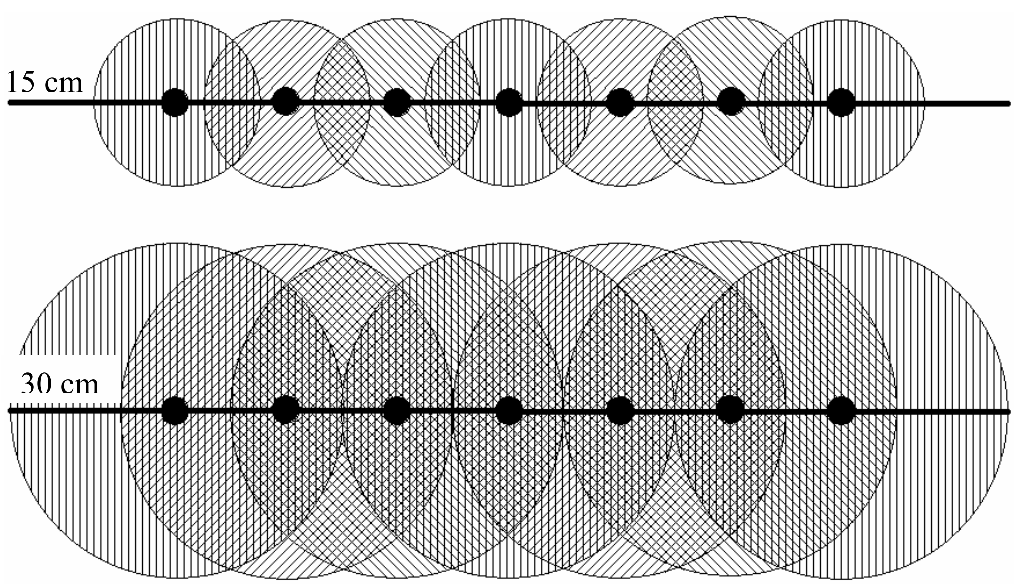

Figure 3.2: Spray plumes at 15 and 30 cm from the nozzles.

The potential of collisions was considered on a smaller scale of 1000 µm x 1000 µm. Figure 3.3 shows the relative size of the micro-volume with a single 14 µm dust particle in the center and twenty 18 µm drops randomly positioned. For the spray described previously, over 20,000 drops/s would pass through the area. Opportunities for agglomeration or collisions depend on many factors. Collisions depend on the concentration of the drops and particles, the relative velocities, the flow patterns (co-flow or cross-flow), turbulence, and the effects of potential static electric attractions (Friedlander, 1977).

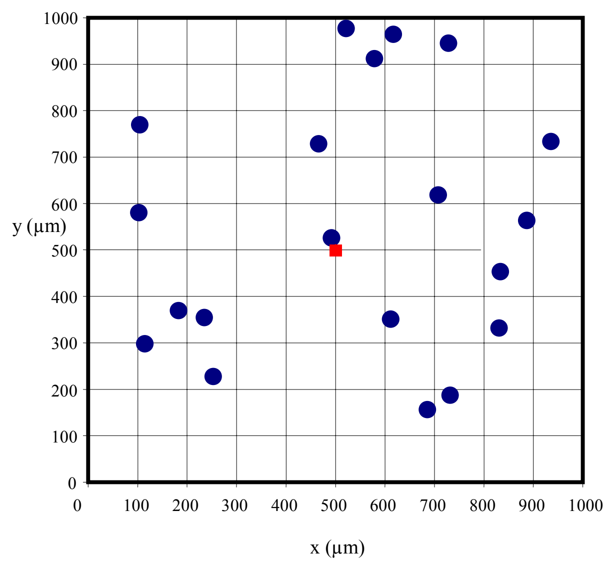

Figure 3.3: 1000 µm x 1000 µm cross sectional area with drops and particle.

Drop-drop interaction was evident in the pre-trials with the agglomerated drops falling out from under the spray plume. The greater concentration of drops and the largest potential for drop-particle interactions are near the spray nozzles, and spray concentration decreases with distance from the nozzle. However, drop-drop and drop-particle *interactions* models were not further developed.

3.7 Modeling potential electro-static forces between particles

Electro-static forces are known to affect particulate motion in many situations. For instance, air cleaners have been designed using electro-static ionizers and voltage fields to remove particles (Cooper and Alley, 1994). The following analysis is to provide some estimates of the potential influence of electro-static charging to particles and drops on particle motion.

Electro-static forces between particles are based on Coulomb's principle, which states that the electro-static force (F_e, dynes) between two point charges is proportional to their charges (q) and inversely proportional to the square of the distance (x) separating them (Hinds, 1982):

$$F_e = k \frac{(qq')}{x^2} \tag{3.43}$$

The total charge (q) is the product of the number of charge units (n) and the unit charge (e), that is, $q = n\ e$, where $e = 4.8 \times 10^{-10}$ stC (3.44)

The maximum charge for a particle depends on its surface area, whether it is liquid or solid, and the polarity of the charge. The maximum charge that a liquid drop can carry depends on its liquid surface tension (γ). Solid particles can hold more positive charges before the spontaneous discharge limit is reached. The equations for charge saturation (unit of stC) on spherical particles were derived by combining Hind's (1982).

$$q_S \text{ (liquid, -)} = (2\ \pi\ \gamma\ d^3)^{0.5} \qquad \gamma\text{(water)} = 72 \text{ dyne/cm} \tag{3.45}$$

$$q_S \text{ (solid, +)} = 7 \times 10^5 \ (d^2 / 4) \qquad q_S \text{ (solid, -)} = 3 \times 10^4 \ (d^2 /4) \tag{3.46}$$

The number of charges or the sign of the charges is not known specifically for this work. However, the maximum number of charges was estimated with the above equations. For 10, 20, and 30 μm water drops, the saturation negative charges were estimated as 0.7×10^{-3}, 1.9×10^{-3}, and 3.5×10^{-3} stC, respectively. For 8, 14, and 20 μm solid dust particles, the saturation positive charges were 0.11, 0.34, 0.70 stC, respectively. The saturation charges of the drops were much less than those of the solid particles. The forces of attraction depend on matching of positive and negative charges, thus the electro-static force is limited by the low charge on the drops.

Table 3.1 summarizes hypothetical electro-static forces and compares them to the gravitational and drag forces. A 20 μm drop and a 14 μm particle were used. The force of gravity on a 14 μm particle (ρ_p= 1.5 g/cm^3) is 2.1×10^{-6} dynes. For the 14 μm particle subjected to 50 cm/s air, the maximum drag force is 1.2×10^{-4} dynes. The amount of charge on the drop determines the electro-static force of attraction. The charge on the drop was varied. The table indicates that when the charges are small and the distance between the particle is greater than 1000 μm, then the force of gravity outweighs the electro-static force. However, as the charge increases and the gap decreases, then the electro-static attraction becomes larger. However, the collisions of a drop and particle from static forces is further complicated by the time dependent movements of the drops and particles during spray conditions.

Table 3.1: Electro-static force (F_e) versus drag force (F_d) and gravity (F_g).
A 20 um drop at various levels of charge and a 14 µm dust particle with V_{rel}= 50 cm/s.

%Saturation	Drop charge	Separation distance	F_e	F_e/F_g	F_e/F_d
%q(sat)	stC	µm	dynes		
1%	1.6E-05	1000	2.6E-08	0.0	0.0
1%	1.6E-05	500	1.1E-07	0.0	0.0
1%	1.6E-05	100	2.6E-06	1.2	0.0
10%	1.6E-04	1000	2.6E-06	1.2	0.0
10%	1.6E-04	500	1.1E-05	5	0.1
10%	1.6E-04	100	2.6E-04	125	2.2
50%	8.1E-04	1000	6.6E-05	31	0.5
50%	8.1E-04	500	2.6E-04	125	2.2
50%	8.1E-04	100	6.6E-03	3123	55.0

A limited test was performed on the spray-fog to measure the static-charge as described in Appendix O. The spray-fog quickly neutralized the static charge obtained by rubbing a glass rub against fabric material. Also, electro-static charge measurements of the nozzle and the spray indicated no level of charge. Static charge on the fog appeared to be minimal and was not included in model development.

3.8 Modeling potential drop evaporation

The drops of the spray-fog either deposit on some surface or evaporate. The spray-fog system has been used for evaporative cooling in hot/dry climates. The following drop evaporation model was used to provide some estimates of droplet lifetime under various conditions (Hinds, 1982). The evaporation model expresses the change in drop diameter with time as a function of vapor diffusion (D_v), molecular weight (M), ideal gas constant (R), drop density (ρ_p), drop diameter (d_p), drop vapor pressure (p_d), drop temperature (T_d), air vapor pressure(p_∞), and air temperature (T_∞):

$$\frac{d\left(d_p\right)}{dt} = \frac{4 D_v M}{R \rho_p d_p}\left(\frac{p_\infty}{T_\infty} - \frac{p_d}{T_d}\right) \tag{3.47}$$

The drop size ranges from 5 to over 30 µm for much of the spray-fog plume and are carried by induced air currents traveling 1 to 2 m/s. Figure 3.4 represents the evaporation of a 15 µm drop at 40% rh and a 20 µm drop at 65% rh as determined from the equation above. For the 20 µm drop at 65% rh , the following parameters were used:

T_∞ = 20 C,	T_d = 14.8 C,
p_∞ = 11.4 mm Hg	p_d = 12.6 mm Hg,
D_v = 0.241 cm^2/s,	R = 62400 mm Hg*cm^3/K/mole,
ρ_p = 1 g/cc,	M = 18.

The 15 μm drop had completely vaporized after 0.35 s. The 20 μm drop shrank to 16 μm after 0.5 s.

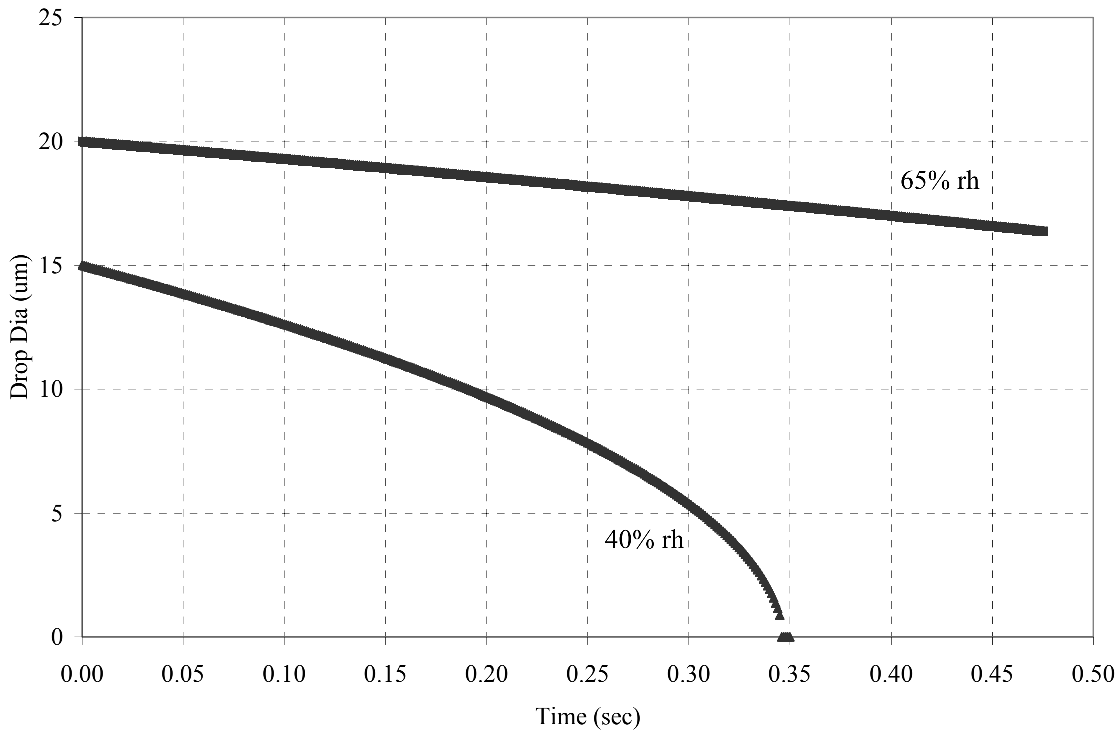

Figure 3.4: Estimated evaporation of 15 μm and 20 μm pure water drops at 20^{o}C.

The spray tests were performed in Central Kansas during warm weather months of May through October. The test conditions ranged from 20-30^{o}C with humidity ranging from 40% to 60%. Under these environments, the evaporation losses appeared to be small within the test chamber and spray levels. However, in a more arid condition, the evaporation of the spray plume would increase, potentially decreasing the effectiveness of sprays and requiring spray level adjustments. Evaporation was not included in further model development.

3.9 Summary

The spray system is more than just particle motion in still air. The main features of the modeling were the modeling of the airflow and the modeling of particle and drop movement. Airflow modeling was done with computational fluid dynamics (CFD) software. Many features of CFD were presented such as the basic conservation equations, discretization methods of the equations, and one pressure-velocity computational procedure. The equations involved with particle/drop tracking were reviewed. Those equations were based on Newton's second law of motion with the main force of the particle being that exerted by air and expressed through Stoke's F_d equation.

Some preliminary work with the spray-fog indicated that electro-static interaction and evaporation were secondary factors, although simplified mathematical analyses were performed. The potential for electro-static attractions depended on the charges and the gaps between particles. The charge on a drop was estimated as being low and limiting the force of attraction. Evaporation was computed for two small drops at low and medium humidity. At the test conditions, the evaporation appeared to be minor. But, evaporation would be significant at low humidity environments, vaporizing the spray plume and reducing the extent of plume dispersion.

The particle and drop interactions are more challenging to model. The spray plume has a high drop concentration near the nozzles, which completely covers the cross-sectional area 5-15 times/sec. Drop collisions and agglomerations were apparent from the drop fall-out under the plume. However, the dynamics and changes in particle sizes and velocities were left for future research.

3.10 Literature cited

Cooper, C.D. and Alley, F.C. 1994. Air pollution control, a design approach. Prospect Heights, Ill.: Waveland Press, Inc.

Fluent, Inc. 2002. Computational fluid dynamics software. Lebanon, NH.

Ford, V., Brierley, T., and Brooks, D. 1987. Water-powered extraction systems for dust control on coalface production machines. Ann. Occup. Hyg. 31(2):147-160.

Friedlander, S.K. 1977. Smoke, dust, and haze: Fundamentals of aerosol behavior. New York: John Wiley & Sons, Inc.

Hinds, W.C. 1982. Aerosol technology: properties, behavior, and measurement of airborne particles. New York: John Wiley & Sons, Inc.

Jones, A.D., and James, G.C. 1987. Air movement and cleaning by water sprays. Ann. Occup. Hyg. 31(2):161-179.

Patankar, S.V. 1980. Numerical heat transfer and fluid flow. Hemisphere Publishing Corp.: New York, N.Y.

Patankar, S.V. 2002. Computational fluid dynamics: engineering, analysis, and applications. ASME Continuing Education Institute: New York, N.Y.

Shortley, G. and Williams, D. 1971. Elements of physics. Englewood Cliffs, New Jersey: Prentice-Hall Inc.

St. Georges, M. and Buchlin, J.M. 1994. Detailed single spray experimental measurements and one-dimensional modeling. Int. J. Multiphase Flow 20(6):979-992.

Chapter 4. Effectiveness of a High-Pressure, Water Fogging System in Controlling Dust Emissions at Grain Receiving

4.1 Abstract

Grain dust at the receiving area is a fire hazard, a health concern, and a sanitation problem and should be controlled. The effectiveness of a high-pressure, water-fogging system in controlling grain dust emissions was evaluated with corn and wheat while spouting 2.1 m^3 (60 bu) of grain into a test chamber. Dust/fog emissions and deposits along with entrained airflows were measured for four treatments, a control, and an air-blower treatment each at two grain flow rates. The uncontrolled dust emissions varied with grain type and grain-flow rate. Water-fog sprays, when applied across the top of the test chamber, redirected the airflow downstream of the spray nozzles and reduced dust emissions significantly. Dust reductions from the spray fog treatments ranged from 60% to 84% for corn and 35% to 73% for wheat. However, the sprays produced significant fog emissions and deposits in proportion to the liquid supply. At the highest spray-fog rate (855 g/min), fog emission was 32 g/min (3.8%) and fog deposits ranged from 1.4 to 7.1 $mg/cm^2/min$.

4.2 Introduction

Grain dust clouds are generated whenever grain is mechanically conveyed, agitated, or processed. The resulting airborne dust concentrations are a nuisance and a potential respiratory risk for workers. High concentrations of dust in equipment provide fuel for a probable flash fire or dust explosion. The settled dust that layers in facilities can fuel a secondary dust explosion. The dust also provides food for insects that can infest stored grain.

Dust emissions are a function of air movement and the dustiness of the grain. Grain dust particles commonly range in size from less than 5 to over 100 μm (Martin, 1981). These particles have relatively low settling velocities in air, ranging from 0.001 to 0.25 m/sec (Hinds, 1982), and are carried downstream by airflow. In a grain receiving area, some air movement is generated as grain falls into the hopper and displaces the air. Additional airflow is entrained while the grain falls into the receiving hopper; the amount of entrained air depends on grain drop height and flow-rate (Cooper and Arnold, 1995).

Grain dustiness varies with grain type and condition. Corn is generally dustier than wheat. Using an alcohol rinse, Martin and Lai (1978) found that corn samples averaged 0.082% residual dust while wheat samples averaged 0.025%. Converse and Echkoff (1989) observed that the amount of dust collected in the grain elevator pneumatic system from corn dried with propane-heated air was over twice that of corn which was natural air dried with an aeration system.

Recent research has quantified dust emissions in grain receiving areas. Kenkel and Noyes (1994) measured dust emissions at a grain receiving area of a country grain elevator while receiving wheat. For a hopper-bottom semi-truck trailer, the average airborne dust emission was 9.5 g/tonne (0.019 lb/ton) and the average floor dust was 17 g/tonne (0.034 lb/ton). For an end-dump grain truck, the average airborne dust emission was 19.5 g/tonne (0.039 lb/ton) and floor dust was 24.5 g/tonne (0.049 lb/ton). Shaw et al. (1997) studied corn dust emissions at feed-mill grain receiving operations of cattle feedyards. Dust emissions during unloading of a hopper bottom trailer averaged 8.5 g/tonne (0.017 lb/ton) with a standard deviation of 9.0 g/tonne (0.018 lb/ton). Based on published data, Midwest Research Institute (1998) has recommended total-suspended-particulate (TSP) emission factors at grain receiving of 17.5 g/tonne (0.035 lb/ton) for hopper bottom trucks and 90 g/tonne (0.180 lb/ton) for straight trucks.

Common dust control methods currently used by the grain industry are pneumatic systems for dust collection and oil additives for dust suppression. Pneumatic systems are generally an effective method of reducing dust at grain transfer points; however, they require high capital cost and large airflow rates, especially in areas with minimal confinement (Mains, 1998). Adding oil to grain is also effective in suppressing dust. Lai et al. (1984) showed that applying mineral oil at the elevator boot reduced the dust emissions by 90% at the elevator's gallery level. In addition, they observed that the oil treatment remained effective for several months after treatment. However, oil additives could reduce milling yields and increase sifter problems as reported by Reid (1987) and the FGIS maximum application rate of 200 ppm may be exceeded in multiple handlings.

Water sprays have been used for controlling dust in mines and roads (Page, 1982; Jankowski et al., 1987; Ford et al., 1987; Page et al., 1994). In 1993, Environmental Engineering Concepts (Palm Springs, Calif.) marketed a water fogging system for grain dust control, claiming effective dust control with only 0.01% moisture addition (1.0 kg

H_2O / 10,000 kg grain) to the grain stream. Water fog systems potentially could be an alternative dust control method. However, the effectiveness of such a system in controlling grain dust emissions has not been documented.

This research investigated the effectiveness of a water fogging system in controlling grain dust emissions for a grain receiving application. The specific objectives were to:

1. Determine the effectiveness of the fogging system in reducing dust emissions,
2. Determine airflow associated with the grain flow and spray treatments, and
3. Determine potential dust and fog emissions and deposits.

4.3 Materials and methods

4.3.1 Spray system

The spray system used in this study (Model E1, Environmental Engineering Concepts, Palm Springs, Calif.) consisted of water filters, an electric motor, a pump, lines, pressure gauges, and nozzles. The nozzles had a 0.20 mm (0.008 in.) diameter orifice and internal impellers. The pump was attached to a city water line via a garden hose. For the test, the pump was operated from 5.5 MPa (800 psi) to over 8.3 MPa (1200 psi). The systems have been used mainly for localized cooling for outdoor businesses in arid climates and, in some cases, for dust control in mineral processing facilities.

Two randomly selected nozzles were tested first at a commercial laboratory (Spraying Systems, Wheaton, Ill.) for measurement of droplet size distributions at 7.6 cm (3 in.) and 30.5 cm (12 in.) from the tip of the nozzle. Details of the measurement and results are presented in chapter 5 The volume-median diameters (VMD) of the droplets were 12.5 and 21 μm at 7.6 cm and 30.5 cm, respectively, along the center-line of the nozzle with the nozzle pressure at 6.9 MPa (1000 psi). Particles were falling out of the plume after 30.5 cm and most of those particles had VMD ranging from 100 to 200 μm.

The average liquid flow-rate for the nozzles listed by the manufacturer was 84 cc/min (0.02 gpm) at 5.5 MPa (800 psi). To determine uniformity among nozzles, a group of 36 nozzles were tested individually by collecting the spray into a graduated cylinder while timing with a stopwatch. The measured flow-rates ranged from 76 to 104 cc/min. Sixteen nozzles, which had flow rates ranging from 79 to 88 cc/min, were then selected for this research. Nozzle liquid flow variability data is given in Appendix H.

Four spray levels were prepared by using 16 nozzles and two spray lines. The spray levels are defined in table 4.1. For the first spray level (S1), one line had nine nozzles which were spaced 7.6 cm (3 in.) apart. For the second spray treatment (S2), the nine nozzle line was reduced to seven nozzles. For the third spray level (S3), a second line was used, which had seven nozzles that were spaced 10.2 cm (4 in.) apart. For the fourth treatment (S4), the seven nozzle line was reduced to five nozzles. The distances between the outside nozzles were 61.0 cm (S1), 45.7 cm (S2), 61.0 cm (S3), and 40.6 cm (S4). The spray-fog system produced overlapping plumes (figure 4.1) and induced airflow.

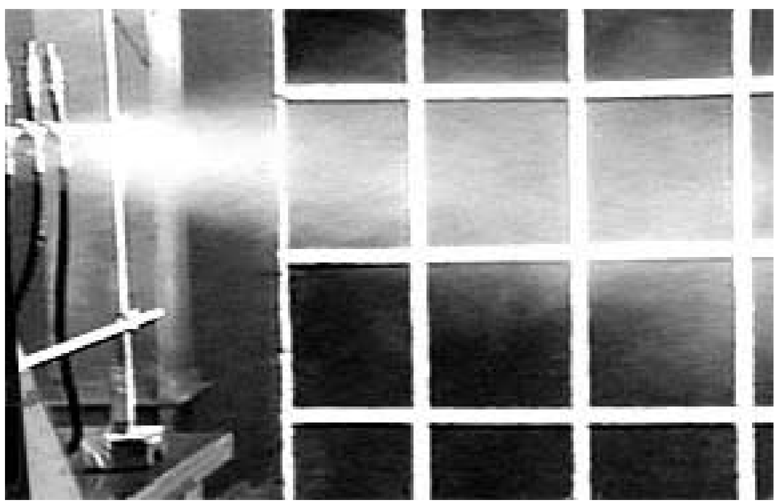

Figure 4.1: A line of fogging nozzles generating a plume of fine drops. The grid in the background has 30.5 cm (1 ft) spacing.

4.3.2 Test chamber

All tests were conducted using a test chamber that represented a portion of a grain-receiving hopper. Typical grain receiving hoppers hold from 17.6 to 35.2 m^3 (500 to 1000 bu) of grain so that a truck can dump its complete load into the hopper in 2 to 5 min. The test chamber was 244 cm (8 ft) long, 76 cm (30 in.) wide, and 183 cm (6 ft) high (figure 4.2). During the test, the chamber was filled to a grain peak height of 137 cm (54 in), equivalent to a volume of approximately 2.1 m^3 (60 bu) of grain. The top 30.5 cm (12 in.) of the chamber served as headspace for airflow and dust. Photographs of the test chamber and the experimental setup are given in Appendix A.

To facilitate airflow and dust emission measurements, the chamber was designed with three openings. The top had a 20.3 cm (8 in.) x 30.5 cm (12 in.) opening for the incoming grain. Each end had a 76.2 cm (30 in.) wide x 30.5 cm (12 in.) high opening for the inlet and outlet airflow. The spray lines were mounted at the inlet end and sprays were directed toward the outlet end. Air-flow transitions were made at both ends for attaching a 25 cm (10 in.) diameter, thin-walled tube, which held propeller anemometers. Propeller anemometer calibration data are presented in Appendix B.

The test chamber was positioned in the truck-bay of the grain receiving area at the USDA-ARS research grain elevator at Manhattan, KS. Grain was dropped from an overhead bin into the test chamber through a grain chute. After each test, the grain was emptied from the chamber into the receiving pit. The doors of the receiving area were closed during testing to eliminate any effects of ambient wind.

4.3.3 Experimental parameters and designs

Two series of tests were performed. The first series studied the effectiveness of spray-fog treatments when applied across the test chamber opening (figure 4.2). The second series compared the cross-flow application to directly applying the spray-fog to the grain stream just prior to entering the test chamber.

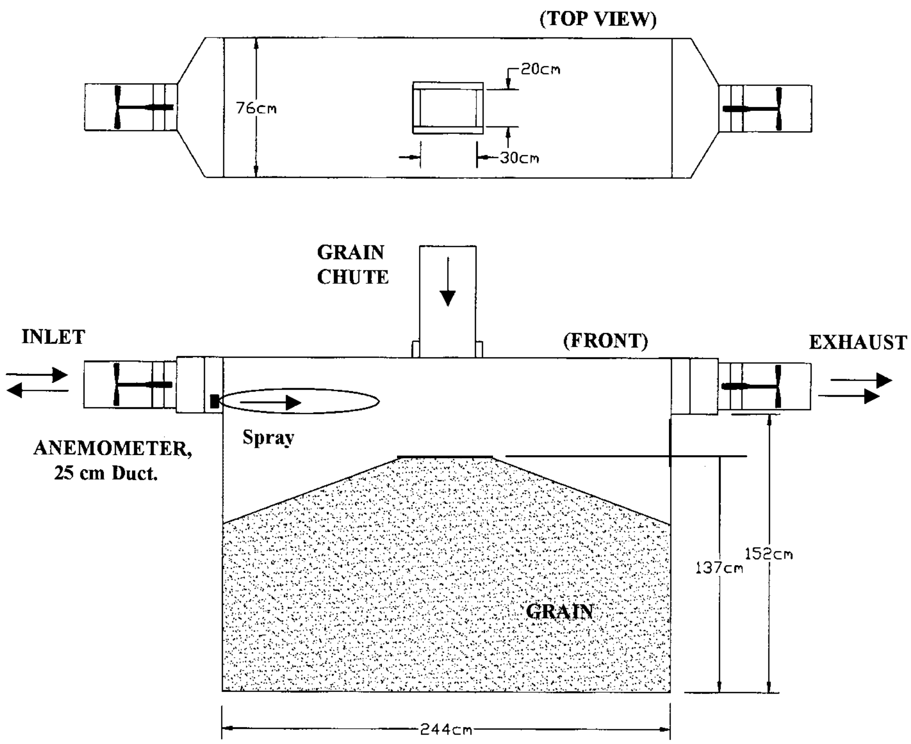

Figure 4.2: The top and front views of the experimental chamber.

4.3.4 Test I: Spray-fog directed over grain receiving hopper

The following factors were considered for the first series of tests: spray treatment, grain samples, and grain-flow rate (table 4.1). There were 24 test combinations each with three replicates for a total of 72 trials. Treatments included four spray treatments, one cross-flow of air from a blower, and the control. The four spray-fog treatments provided a range of coverage, liquid flow-rates, and induced airflow rates.

Table 4.1: Experimental parameters and variables
for study of the effectiveness of a fogging system to control grain dust.

Grain Samples	*Test Treatments*[1]
Wheat (U.S. Grade #1)	C: Control
Corn (U.S. Grade #5)	blw: Blower (Fan)
	S1: 9n at 6.9 MPa (1000 psi)
Grain Flow Rates	S2: 7n at 6.9 MPa (1000 psi)
2.5 m^3/min (72 bu/min)	S3: 7n at 5.5 MPa (800 psi)
1.7 m^3/min (48 bu/min)	S4: 5n at 5.5 MPa (800 psi)

[1]In spray treatments S1-S4, the number of nozzles (n) and nozzle pressure varied. The treatments were replicated three times for each grain and grain-flow.

As mentioned above, the spray induced additional airflow. The blower treatment was included to compare the effects of airflow (without fogging) and spray-fog treatments on dust emissions. For this treatment, a shaded pole blower (Model 4c004, Grainger, Topeka, Kans.) was fitted on the end of a 25.4 cm (10 in.) diameter x 61.0 cm (24 in.) long tubing. This unit was mounted to the anemometer unit at the inlet end of the chamber. A baffle was added in the test chamber inlet to reduce the blower vent opening to 7.6 cm (3 in.) high x 76.2 cm (30 in.) wide and to distribute the blower airflow uniformly to approximate the airflow induced by the nozzles.

The grain sample and grain-flow rates were chosen to provide a range of dust and airflow conditions. The study used approximately 35 m^3 (1,000 bu) of wheat and 35 m^3 of corn. To determine the dustiness of the grain and the repeatability of the drop test, 12 sequential 2.1 m^3 (60 bu) drop trials at full grain flow were done with each grain. The corn emission sub-samples averaged 4.5 g with a standard deviation of 0.22 g. The wheat emission sub-samples averaged 1.5 g with a standard deviation of 0.52 g. For this test set, the high-volume air sampler captured about 40% of the total emissions. Thus, the corn and wheat averaged 12.2 and 4.2 g/tonne emissions, respectively. Appendix D contains the data for the sequential grain drop tests.

During the spray test, each 35 m^3 grain lot provided 12, 2.1 m^3 trials and represented one replication of the spray treatments at two grain-flows. The first 4.2 m^3 (120 bu) of grain was used to purge the spouting and the last 4.2 m^3 (120 bu) was emptied from the holding bin. The 35 m^3 grain lot was cycled into the holding bin for the next replication.

Grain flow rate was controlled with the gate from the holding bin. When the gate was fully-opened, grain flow rate was approximately 2.5 m^3/min (72 bu/min). When the gate was partially-opened, grain flow was approximately 1.7 m^3/min (48 bu/min). The test chamber represented about 25% of the full-sized hopper. The fully-opened-gate grain flow represented approximately 4 x 2.5 m^3/min or 10 m^3/min (288 bu/min) full scale grain flow while the partially-opened-gate grain flow represented 6.8 m^3/min (192 bu/min). If a grain truck would empty its 17.6 m^3 (500 bu) load in two minutes, then the full scale grain flow would be 8.8 m^3/min (250 bu/min).

Each grain lot was sampled and graded three times. The grain lots were sampled with an automatic sample diverter while the 35 m^3 (1,000 bu) batch was cycled into the holding bin. For both the wheat and corn, the visual inspection and grain odor indicated no obvious mold growth. The average moisture, test weight, and dockage of the wheat were 13.0%, 61.8 lb/bu, and 1.7%, respectively. The wheat samples met US Grade #1 standards. The average moisture, test weight, and broken corn and foreign materials (bcfm) of the corn were 11.2%, 58.6 lb/bu, and 6.1%, respectively. The corn had higher than normal fine material causing it to grade as US#5. The corn and wheat lots provided two distinct levels of dust emission and were not selected to compare wheat and corn.

4.3.5 Test II: Spray-fog directed on the incoming grain stream

For testing of direct application of spray-fog to the grain, the spray configuration was varied and included one cross-flow spray, two direct applications (D1 and D2), and a control. The cross-flow spray treatment was similar to treatment S2 in Test I; it used seven nozzles at 6.9 MPa (1000 psi). The direct method, D1, used four nozzles while D2 used six nozzles at 6.9 MPa (1000 psi) as shown in figure 4.3. An equal number of nozzles were positioned on each side of the grain chute, 15 cm (6 in.) above the test chamber and directed through two, 12 cm x 30 cm, openings. The four test combinations and three replicates yielded 12 trials for this series. Corn was used at full grain flow.

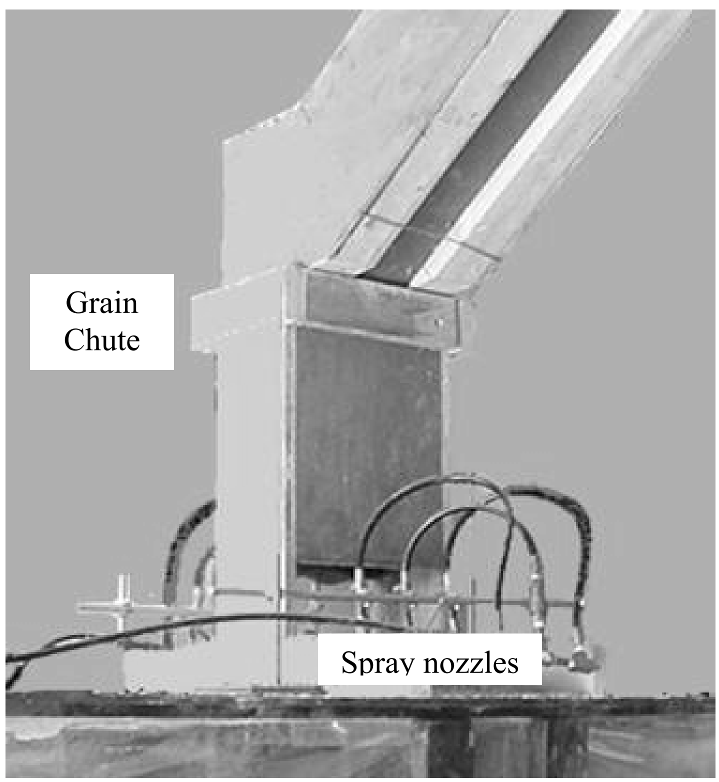

Figure 4.3: Configuration of fogging nozzles for Test II
-direct application of fog on the incoming grain.

4.3.6 Measurement methods

The experimental dependent variables were dust emissions, fog emissions, dust deposits, fog deposits, and volumetric airflow rates. The emissions were collected with high-volume air samplers (PN 3-115-10, Bendix Corp., Env. Process Instr. Div.). The air-sampling inlet had an opening of 6.4 cm (2.5 in.) x 20.3 cm (8 in.). The sampler was positioned next to the exit of the anemometer tube. Because the air sampling area represented 25% of the anemometer outlet area, the speed of air sampler was adjusted to maintain a flow-rate near 25% of the exiting air flow-rate. The high-volume air sampler calibration data are presented in Appendix C.

The air filters were Type A/E, 20.3 cm (8 in.) x 25 cm (10 in.), glass fiber filters (Pall-Gelman Sciences, Ann Arbor, MI). The filters were weighed before and immediately after each trial to determine the filter's wet weight. The filters were placed on trays and stored in racks while dried at 25^{o}C and 60% rh for at least 24 h, then re-weighed to determine dry weight. The difference between the wet weight and the dry weight represented the fog emissions. The difference between the dry weight and the pre-weight represented the weight of the collected dust. The equilibrium moisture content of the dust was near 12%. These filters were weighed on an electronic balance (Mettler Instr., PC180), which was accurate to 1 mg.

Dust and fog deposition samples were collected after each trial from six locations in the chamber. The samples were collected using filters located on the boundary surfaces. Figure 4.4 is a schematic of filter locations at the outlet end. A similar group of filters was positioned at the inlet end. These filters (Model PA41, Pall-Gelman, Ann Arbor, MI) were 12.7 cm (5 in.) in diameter and placed into a filter holder with an 11.4

cm (4.5 in.) diameter opening, thus exposing an area of 102 cm^2 (15.9 in^2). The deposition filters were handled and analyzed following the procedure above, but using an electronic balance that was accurate to 0.1 mg (Precisa Balance, model 40SM-200A).

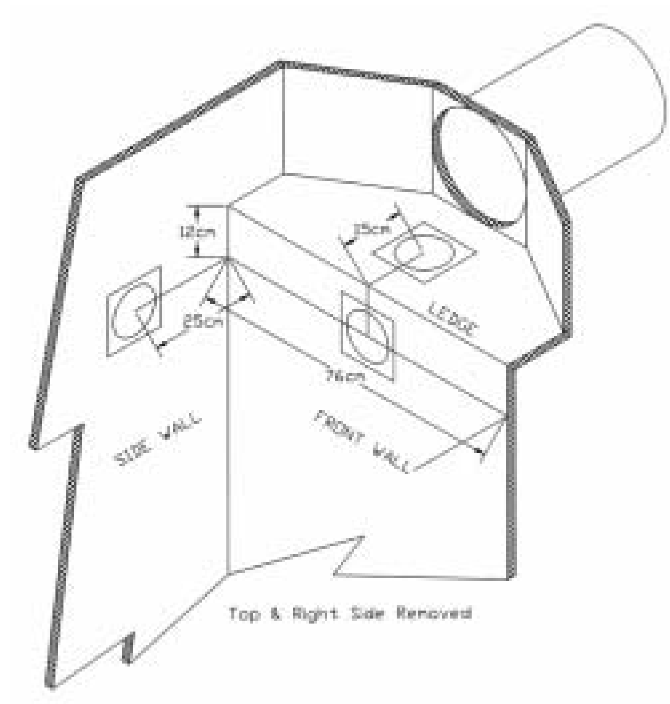

Figure 4.4: Positions of deposition sampling filters
at the outlet end of the experimental chamber.

For each test, the following procedures were followed:

1. The high-volume air samplers and the spray system were turned on about 5 seconds before the grain-flow was started. Several seconds were required for the spray lines to become fully charged and functioning.
2. The grain was dropped into the test chamber at the prescribed flow rate.
3. The sprayer was turned off immediately after the grain-flow had stopped. The high-volume air samplers were operated for an additional 5 sec after to account for the delayed response of the airflow and emissions after the grain-flow was stopped.
4. The emission sample filters and the dust sample filters were weighed and dried.
5. The test chamber was emptied into the grain receiving hopper and prepared for the next test.

Airflow was measured during each trial with two propeller anemometers, one mounted at each end of the test chamber (figure 4.5). The anemometers had a 22 cm (8.7 in.) diameter propeller (Model 27106 R.M.Young Co., Traverse City, MI). They were mounted to a bracket inside of 25.4 cm (10 in.) diameter tubes. The anemometers were pre-calibrated using a wind tunnel, which was designed in accordance with AMCA standard 210-85 (AMCA, 1985). The anemometer voltage signals were recorded with a computer data acquisition system.

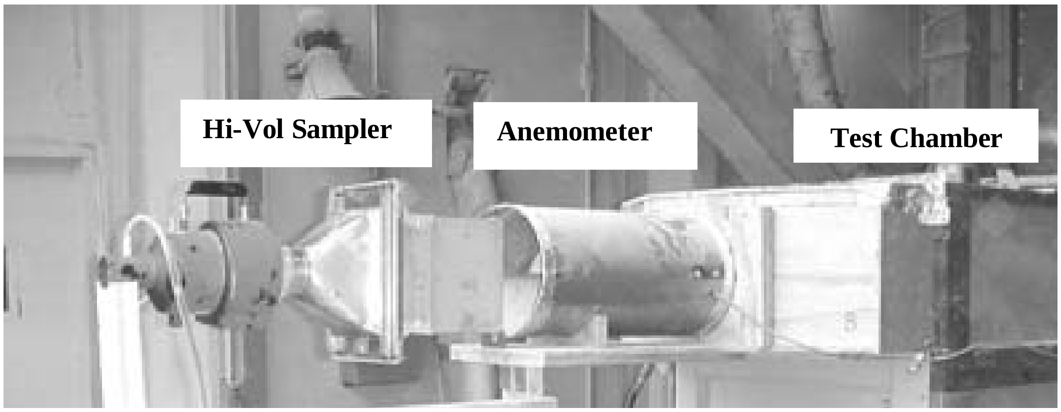

Figure 4.5: High-volume air sampler and propeller anemometer at the inlet of the experimental chamber.

The time required to drop 2.1 m^3 (60 bu) of grain into the test chamber varied with gate opening and grain type. When the gate was fully opened, both wheat and corn were dropped in 48-52 sec. When the gate was partially opened, the wheat was delivered in 68-72 sec while the corn was delivered in 78-82 sec. The drop time was recorded with a stop watch for each trial.

4.3.7 Data analysis

The effect of spray treatment on dust emission for each grain type and grain flow rate was determined using the PROC MIXED technique in PC-SAS (version 8.02, SAS Institute, Cary, NC) with a 5% level of significance. PROC MIXED is an analysis of variance (ANOVA) procedure used with split-plot experiments. The LSMEANS (least square means) method was used to determine statistical significance of differences among treatment dust emission means. The reduction in dust emissions and the variance were determined as follows:

$$\%reduction = 100\% - 100 * \frac{Avg.(treatment)}{Avg.(control)} \tag{4.1}$$

$$Var.\left(\frac{treatment}{control}\right) = \frac{Std.(trt)^2}{Avg.(ctrl)^2} + Std.(ctrl)^2 \frac{Avg.(trt)^2}{Avg.(ctrl)^4} \tag{4.2}$$

The variance for the ratio of means, $\frac{Avg.(treatment)}{Avg.(control)}$, was determined as outlined by Casella and Berger (1990). This variance was a function of the treatment standard deviation, the treatment mean, the control standard deviation, and the control mean. The variance was transformed to a standard error by taking its square root.

4.4 Results and discussion

4.4.1 Airflow rates from grain and spray-fog

The movement of dust particles depends on air movement because of the low settling velocities for small dust particles. Air was displaced from the box as grain was dropped into the chamber. The measured airflow for the control trials ranged from 108% to 172% of the volumetric grain flow (table 4.2). The amount of additional or entrained air depended on the grain type and flow rate.

Table 4.2: Volumetric grain flow versus measured airflow.
The airflow was measured from the test chamber and computed from three trials.

	Grain flow rate	Measured airflow rate[1]		Air/grain
		Avg.	Std. dev.	
	m^3/min	m^3/min	m^3/min	
Wheat	2.55	2.75 a	0.01	108%
Corn	2.55	2.89 b	0.05	113%
Wheat	1.84	2.32 c	0.07	126%
Corn	1.61	2.78 a	0.03	172%

[1]Means with the same letter are not significantly different at 5% level.

Airflow was also induced by spray-fog treatments. Figure 4.6 shows the average exhaust airflow rates from the test chamber during the corn trials with full grain-flow. For the control, the air exhausted from each end of the hopper enclosure at approximately 1.4 m^3/min (50 cfm). The sum of exhausting airflow rates from both ends was 2.8 m^3/min (100 cfm) and represents the air displaced by the grain plus entrained air in the grain stream. For spray treatment S1, air was exhausted at the outlet at 4.0 m^3/min (140 cfm) and entered the inlet at 1.2 m^3/min (42 cfm), with the net airflow displaced by the grain of 2.8 m^3/min (100 cfm). The spray-fog treatments provided a curtain of airflow over the test chamber and towards the exit while some air recirculated within the chamber back towards the nozzles. Test Series I airflow, emissions, and deposition data are presented in appendix E.

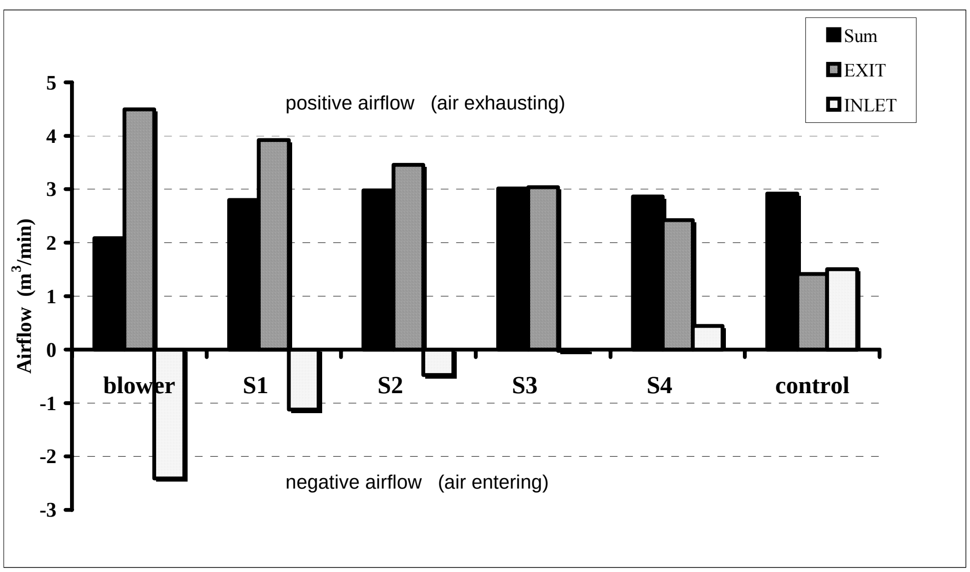

Figure 4.6: Average inlet and average outlet airflow measurements
For corn trials at full grain flow, spray treatments S1-S4 are outlined in table 4.1.

4.4.2 Emissions

4.4.2.1 Test I: Spray-fog directed over grain receiving hopper

Dust and fog emissions varied with grain sample, grain flow rate, and spray treatment as determined with ANOVA at the 5% level of significance. During spray treatments, emissions contained both dust and fog. Air and dust were exhausted through the inlet and exhaust openings of the chamber for treatment S4 and control. However, for the other spray treatments, the air and emissions were exhausted only from the outlet end (figure 4.6) because the induced airflow from the spray process had greater inertia and mass flow than the air displaced by the grain.

Control and blower trial emissions results were not significantly different (figures 4.7 and 4.8), thus the cross airflow from the blower did not reduce dust emission. The spray treatments produced significant reductions in dust emissions (figures 4.7 and 4.8, table 4.3). Reductions were calculated as a ratio of the treated sample to the control sample as described in the data analysis section. The reductions varied with the grain sample and spray treatment. Reductions were higher for the corn sample, with its greater dustiness, than for wheat. For corn, mean reductions ranged from 60% to 84%, while for wheat, mean reductions ranged from 35% to 73%. In general, the dust emissions from spray-fog treatments S1, S2, and S3 were not statistically different from each other ($p>0.05$) but were all significantly lower than treatment S4. SAS ANOVA procedures and Least Square Means differences are presented in Appendix F.

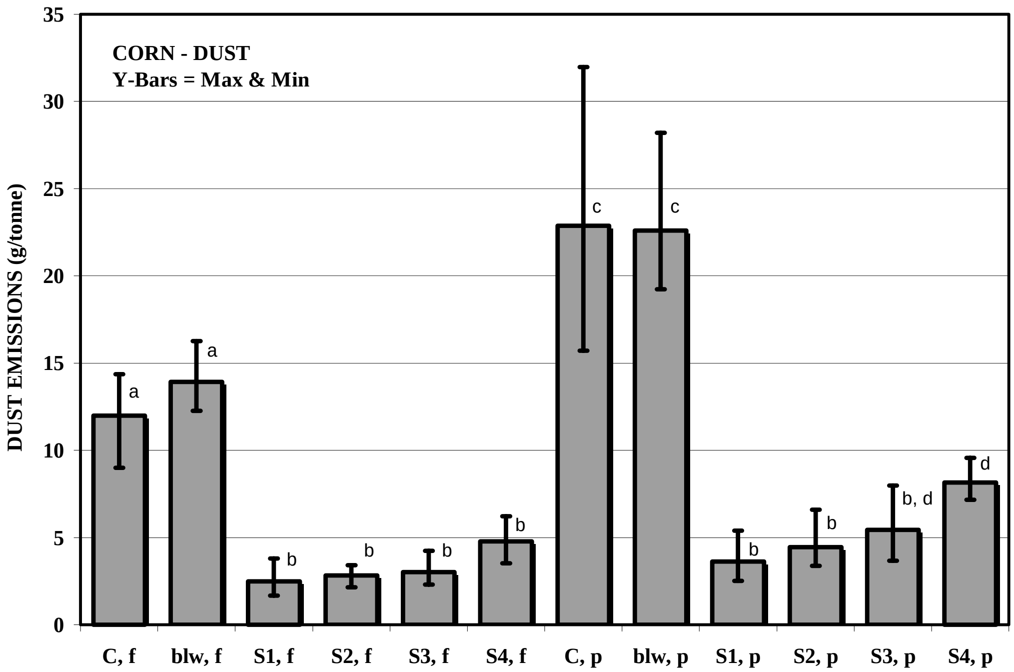

Figure 4.7: Average, maximum, and minimum corn dust emissions

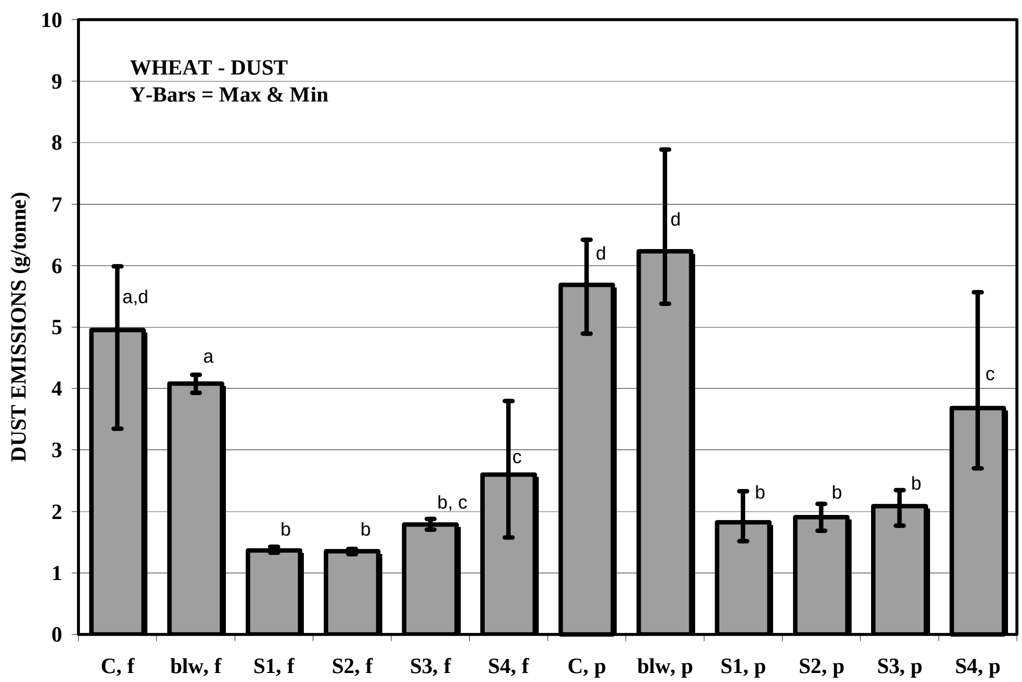

Figure 4.8: Average, maximum, and minimum wheat dust emissions for full (f) and partial (p) grain flows. S1-S4 are outlined in table 4.1. Means with common letter are not significantly different at 5% level.

Table 4.3: Reductions of dust emissions
for spray-fog treatments, grain, and grain-flow.

	Corn: full flow		Corn: partial flow	
Trt.[1]	1-Trt/Ctrl	Std error	1-Trt/Ctrl	Std error
S1	79%	11%	84%	9%
S2	76%	8%	81%	11%
S3	75%	11%	76%	13%
S4	60%	15%	64%	14%
	Wheat: full flow		Wheat: partial flow	
Trt.[1]	1-Trt/Ctrl	Std error	1-Trt/Ctrl	Std error
S1	72%	8%	68%	9%
S2	73%	8%	66%	6%
S3	64%	10%	63%	7%
S4	47%	27%	35%	30%

[1] Spray treatments S1-S4 are outlined in table 4.1.

The water-fog emissions varied with spray treatments and ranged from 2.2% to 3.8% of the liquid supply (table 4.4). The liquid supply was calculated by multiplying the number of nozzles by the approximate flow per nozzle. At 5.5 MPa (800 psi) and 6.9 MPa (1000 psi), the manufacturer's literature rated flows were 84 and 95 g/min/nozzle, respectively.

Table 4.4: Spray-fog liquid flowrate and fog emissions.

	Supply	Emissions	Emitted
Trt.[1]	g/min	g/min	
S1	855	32	3.8%
S2	665	24	3.7%
S3	588	16	2.7%
S4	420	9	2.2%

[1] Spray treatments S1-S4 are outlined in table 4.1.

4.4.2.2 Test II: Spray-fog directed on the incoming grain stream

Table 4.5 summarizes the dust and fog emissions for the control, cross-flow (S2), and direct-spray configurations (D1 and D2). Dust emissions for the control in this series averaged 17 g/tonne. S2 reduced dust emissions to 4 g/tonne (76% reduction) while the D1 and D2 treatments increased dust emissions to 23 g/tonne. It appears that the small amount of water directly applied to the grain had no benefit in reducing the grain dust and that the air generated by the spray and entrained in the grain stream enhanced dust emissions. Test Series II data are presented in Appendix G.

Table 4.5: Dust and fog emissions for Test II
spray-fog directed on incoming grain stream.

Trt.	Dust (g/tonne)		Water (g/tonne)	
	Avg.	Std. dev.	Avg.	Std. dev.
C	17.0	3.1	0.1	0.2
S2	4.0	1.1	12.4	1.2
D1	22.6	2.6	0.4	0.2
D2	23.1	4.2	0.8	0.4

[1] Treatments C and S2 are outlined in table 4.1.
Treatments D1 and D2 were sprays applied directly to the grain

4.4.3 Deposits on ledges and walls

The dust deposits on the side-wall and front-wall for the corn trials ranged from 0.01 to 0.04 $mg/cm^2/min$. The dust deposits on the inlet and outlet ledges ranged from 0.15 to 1.25 $mg/cm^2/min$ (table 4.6). For the control trials, the amount of deposits at the inlet was close to that at the outlet. For the blower, S1, and S3, the deposits at the inlet were smaller than those at the outlet. For S2 and S4, the deposits at the inlet were greater than those at the outlet. The greater amount of deposits for S2 and S4 at the inlet compared to the outlet can be due to the wider nozzle spacing at the side-wall, which may have allowed some back-swirling airflow and dust.

Table 4.6: Dust deposits ($mg/cm^2/min$) on inlet and outlet ledges for corn at full grain-flow (2.5 m^3/min).

Trt.[1]	Inlet		Outlet	
	Avg.	Std. dev.	Avg.	Std. dev.
C	0.87	0.12	0.95	0.12
blw	0.15	0.03	1.25	0.16
S1	0.38	0.11	0.70	0.16
S2	1.06	0.27	0.80	0.13
S3	0.30	0.06	0.55	0.15
S4	0.82	0.19	0.63	0.08

[1] Treatments C, blw, and S1-S4 are outlined in table 4.1.

Table 4.7 shows the average fog deposition rates at the outlet ledge, front-wall, and side-wall for the spray treatments. The fog deposition rate varied with the spray treatment and sampling location. The deposition rate for spray S1 was 7.14 $mg/cm^2/min$ at the ledge and 3.72 $mg/cm^2/min$ on the front-wall. The approximate exposed surface area for the ledge was 2300 cm^2 (2.5 ft x 1 ft). For the front-wall, the exposed surface was approximately 7000 cm^2 (2.5 ft x 3 ft). The fog deposits for the ledge and front-wall were 19 g and 35 g during the partial grain flow trials. These deposits were roughly 1.5% and 3% of the supply.

Table 4.7: Fog deposits ($mg/cm^2/min$) at exit ledge, front-wall, and side-wall for corn at full grain-flow (2.5 m^3/min).

Trt.[1]	Ledge		Front		Side	
	Avg.	Std. dev.	Avg.	Std. dev.	Avg.	Std. dev.
S1	7.14	0.75	3.72	1.36	1.44	0.41
S2	5.28	0.59	1.50	0.36	1.19	0.19
S3	2.34	0.25	0.59	0.15	0.54	0.19
S4	2.03	0.10	0.51	0.16	0.48	0.08

[1] Spray treatments S1-S4 are outlined in table 4.1.

4.5 Potential application

The spray fog system could be used in country elevators, terminal elevators, and feedmills receiving dry grain products, such as wheat, corn, or milo, during harvest. Receiving grain from producers using end-dump trucks is a dusty job. A short interval of fogging in the grain hopper would offer some relief. Fogging may not work in combination with pneumatic systems because the spray would drift into the air ducts and deposit, causing a buildup and caking on the sidewall, which might eventually plug them. Also, the 0.2 mm (0.008 in.) nozzle orifices need to be checked periodically for wear and maintained. As a reminder of U.S. legal restrictions, it is unlawful to add water to merchandised grain for the purpose of adding weight (Federal Register, 1994).

4.6 Summary and conclusions

This study evaluated the effectiveness of a high-pressure water fogging system in controlling grain dust emissions. Results showed the following:

1. Air movement was generated by both the grain flow and the spray fogging system. Dropping 2.5 m^3 (60 bu) of grain in 50 sec displaced about 2.8 m^3/min (100 cfm) airflow for the given test chamber geometry. The spray treatments induced additional airflow and redirected dust emissions towards one end of the receiving test chamber.
2. The spray fogging treatments S1, S2, and S3, which used 7 to 9 nozzles per 0.76 m of width, reduced dust emissions by 75%-84% for corn and 63%-73%

for wheat, depending on the spray treatment and grain flow. Spray treatment S4, which used 5 nozzles per 0.75 m, was less effective and more variable.

3. Direct application of the spray-fog to the incoming grain stream increased dust generation and emissions. The control trials and direct application trials (D1) averaged 17.0 and 22.6 g/tonne dust emissions, respectively.
4. The spray fogging system generated considerable fog emissions and deposits depending on the spray treatment. The liquid supply and fog emissions were 855 g/min and 32 g/min, respectively, for spray-fog S1 which used 9 nozzles per 0.76 m. The rate of depositions for S1 ranged from 1.4 to 7.1 $mg/cm^2/min$, depending on sample location.

Overall, the spray-fog system reduced dust emissions and redirected air movement significantly. It also produced significant fog emissions and deposits. In some environments, the fog emissions would simply evaporate. Some additional screening or mist collection material may have to be added to the receiving hopper to reduce fog emission. The small amount of deposits would mix into grain shipments and not be considered a problem. However, the concerns with fogging need to be weighed with the potential dust control benefit. As such, the adoption of such a system in the grain industry would likely be limited to special applications and processes and must meet regulatory limits.

4.7 Literature cited

AMCA. 1985. Laboratory methods for testing fans for rating. AMCA Standard 210-85. Arlington Heights, IL.: Air Movement and Control Association.

Casella, G. and Berger, R.L. 1990. Point estimation. In: Statistical Inferences, pp. 331. Belmont, CA: Duxbury Press.

Converse, H.H. and Eckhoff, S.R. 1989. Corn dust emissions with repeated elevator transfers after selected drying treatments. Trans. ASAE 32(6):2103-2107.

Cooper, P. and Arnold, P.C. 1995. Air entrainment and dust generation from a falling stream of bulk material. KONA Powder and Particle. No.13:125-134.

Federal Register. 1994. Vol. 59, no.198. Prohibition on Adding Water to Grain.

Ford, V.H.W., Brierley, T., and Brooks, D.J. 1987. Water-powered extraction systems for dust control on coalface production machines. Ann. Occup. Hyg. 31(2):147-160.

Hinds, W.C. 1982. Aerosol technology; properties, behavior, and measurement of airborne particles. New York, N.Y.: John Wiley & Sons.

Jankowski, R.A., Jayarman, N.I., and Babbitt, C.A. 1987. Water spray systems for reducing the quartz dust exposure of the continuous miner operator. Proc 3rd Mine Ventilation Symposium, Littleton, CO. Society of Mining Engineers

Kenkel, P. and Noyes, R. 1994. CR-1108 OSU Grain elevator dust emission study. Stillwater, OK: Oklahoma Cooperative Extension Service.

Lai, F.S., Martin, C.R., and Miller, B.S. 1984. Examining the use of additives to control grain dust in a commercial grain elevator. ASAE Paper no. 84-3575. St. Joseph, MI: American Society of Agricultural Engineers.

Mains, D.G. 1998. How to balance a dust system? Paper presented at the GEAPS Plains States Regional Meeting, Aug 14-15, 1998, Manhattan, KS.

Martin, C.M. 1981. Characterization of grain dust properties. Trans. ASAE 24(3):738-742.

Martin, C.R. and Lai, F.S. 1978. Measurement of grain dustiness. Cereal Chem. 55(5):779-792.

Midwest Research Institute. 1998. Emission factor documentation for EPA AP-42, section 9.9.1 Grain Elevators and Grain Processing Plants. MRI Project #4945. Midwest Research Institute, Kansas City, MO.

Page, S.J. 1982. An evaluation of three wet dust control techniques for face drills. USBM Report No. 8596. Pittsburgh, PA.: U.S. Bureau of Mines.

Page, S.J., Mal, T., and Volkwein, J.C. 1994. Unique water spray system improves exhaust face ventilation and reduces exposure to respirable dust on continuous miners in laboratory test. J. Mine Ventilation Society of South Africa, October 1994:196-205.

Reid, R.G. 1987. Dust Control-Additive Update. Proc. of the Grain Elevator and Processing Society 58th Int Technical Conf. Minneapolis, MN.

Shaw, B.W., Buharivala, P.P., Parnell, C.B. Jr., and Demny, M.A. 1997. Emission factors for grain receiving and feed loading operations at feed mills. Trans. ASAE 41(3):757-765.

Chapter 5. Characterization and Modeling of a High-Pressure Fogging System for Grain Dust Control.

5.1 Abstract

Grain dust is generated whenever grain is loaded or unloaded into hoppers and equipment. This research investigated a high-pressure spray-fog system as a potential method for dust control at the grain receiving hopper. The spray-fog was characterized in terms of drop size, drop velocities, and airflow distributions.

The spray nozzle, which had a 0.2 mm (0.008 in.) orifice, produced a plume of fog with 90% of the drops ranging from 10 to 40 µm. Average drop velocities were over 10 m/s at 7.6 cm from the nozzle. The air velocity pressures at 7.6 cm were parabolic with maximum pressures over 275 Pa.

Experiments were also conducted to measure the spray deposits that were collected on both the side walls and the grain surface. The side wall deposits were 11 mg/cm^2/min in the middle where the test chamber cross sectional area was reduced by the incoming grain. The side wall deposits decreased to 1.5 mg/cm^2/min near the outlet. Grain surface deposits generally ranged from 0.1 to 0.4 mg/cm^2/sec.

Airflow and particle trajectories were modeled using FLUENT, a computational fluid dynamics (CFD) software. Airflow distributions, grain dust transport, and spray droplet trajectories were predicted within a test chamber that represented a narrow section of a grain receiving hopper. The induced airflow from the spray-fog caused recirculation of the air and dust particles in the lower part of the chamber. This

recirculation pattern transported the dust back to the nozzle where the dust and spray-fog would interact.

5.2 Introduction

The amount of dusty-air produced during grain handling varies with grain type, grain condition, and handling methods. The problems created by grain dust range from minimal to extreme. Workers exposed to dusty environments can develop respiratory problems. Enarson et al. (1985) found grain elevator employees experiencing reduced lung function depending on individual sensitivity and dust exposure. High concentrations of dust in grain facilities and equipment provide fuel for potential flash fires or dust explosions. An annual average of 12 grain dust related fire/explosions of varying intensities were reported from 1992 to 2001 in the U.S. (Schoeff, 2002).

The primary methods for controlling dust emissions in grain handling facilities are pneumatic dust collection systems and direct application of food-grade oils to grain streams. Each method has its advantages and limitations as cited by the U.S. Congress, Office of Technology Assessment (1995) and was presented in Chapter 2. The dust capture efficiency of a pneumatic system varies depending on airflow and the proximity of the dust to the inlet vent. In addition, pneumatic systems are expensive to install, maintain, and operate. Oil additives, while not effective at the initial point of application, are effective after initial mixing and at later transfer points. However, oiled grain has been reported as adversely affecting milling processes (Reid, 1987).

High-pressure spray systems, which produce jets of fog and mist, have demonstrated some potential to confine and suppress grain dust. The spray-fog differs from the coarse spraying methods in the amount of water and the size of drops produced. Research is needed to characterize the spray-fog systems. As noted in chapter four, considerable airflow is induced by the spray-fog. It is necessary to establish the induced airflows. In addition, it is necessary to determine the fate of the droplets to determine if the grain or equipment is being negatively affected. Such investigations could be done through experimental research using full-scale or small-scale prototypes or research using computational fluid dynamics (CFD).

Previous researchers have demonstrated the applicability of CFD in predicting airflow within structures such as greenhouses (Al-Arifi et al., 2001) and swine buildings (Sun et al., 2002). Additionally, several researchers have analyzed spray systems using CFD (Brown and Sidahmed, 2001; Tsay et al., 2002).

5.3 Objectives

This study was conducted to:

1. Characterize the high-pressure fog system in terms of drop size and airflow distributions; and
2. Model the airflow distribution, particle trajectories, and drop trajectories from fog sprays in a pilot scale receiving hopper using CFD.

5.4 Materials and methods

5.4.1 Characterization of the spray system

The spray system (Model E1, Environmental Engineering Concepts, Palm Springs, CA) contained an electric motor with controls, pump, pressure gauges, water filters, and lines with nozzles (Appendix figure A.3). The nozzles had a 0.20 mm (0.008 in.) diameter orifice and internal impellers. The pump was attached to a city water line via a garden hose and operated from 5.5 MPa (800 psi) to over 8.3 MPa (1200 psi) with 10 to 60 nozzles. Characterization of the spray system involved measurement of : (1) drop size and velocity distributions for individual nozzles; (2) induced airflow rates associated with the spray system in a test chamber; and (3) deposits of spray-fog.

5.4.1.1 Drop size and velocity distributions for individual nozzles

Two randomly selected nozzles, from a group of over 32 nozzles, were tested at a commercial testing laboratory (Spraying Systems, Wheaton, Ill.) to determine droplet size and velocity distributions. The nozzles were tested at the normal operating pressure of 6.9 MPa (1000 psi). A phase-doppler particle analyzer, which had a low power laser as the light source, was used. In this instrument, the laser beam is split producing two laser beams, which later intersect at the drop sampling location. When a drop passes through the intersection of the laser beams, a light interference pattern is formed and detected by several parallel detectors. Drop velocity and size were determined from the frequency information of the interference pattern and the phase shift information from the detectors (Spraying Systems, 2000).

Sampling was located at 7.6 cm (3 in.) and 30.5 cm (12 in.) horizontally from the tip of the nozzle and at 11 vertical test point locations across the plume (figure 5.1). At 7.6 cm, the vertical test points were 4.4 cm above the horizontal center-line and 4.4 cm below. At 30.5 cm, the vertical test points were located 1.9 cm above and 12.7 cm below. A total of 30,000 samples or approximately 30 sec of data were collected at each test location.

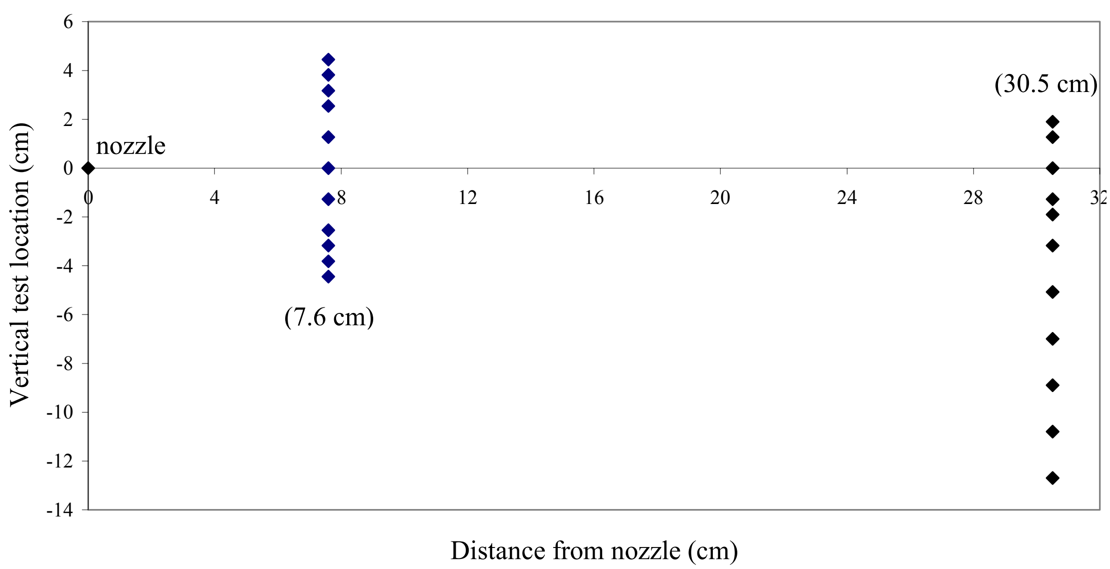

Figure 5.1: Side view of test locations for spray-fog drop size distributions. Eleven test points were located at each of two horizontal distances.

5.4.1.2a Airflow profile associated with individual nozzles

Induced airflow was determined qualitatively and quantitatively. Induced airflow was qualitatively investigated using smoke and photography. The induced airflow was also quantified for an individual nozzle at 6.9 MPa (1000 psi) using a pitot tube (Model no. 160S, Dwyer Instruments, Michigan City, Ind.) and an inclined manometer (figure 5.2). Pressure data were collected at 7.6 cm (3 in.), 15.2 cm (6 in.), 30.5 cm (12 in.), and 61.0 cm (24 in.) horizontally from the nozzle and from 0 to 10.2 cm (4 in.) below the horizontal center-line.

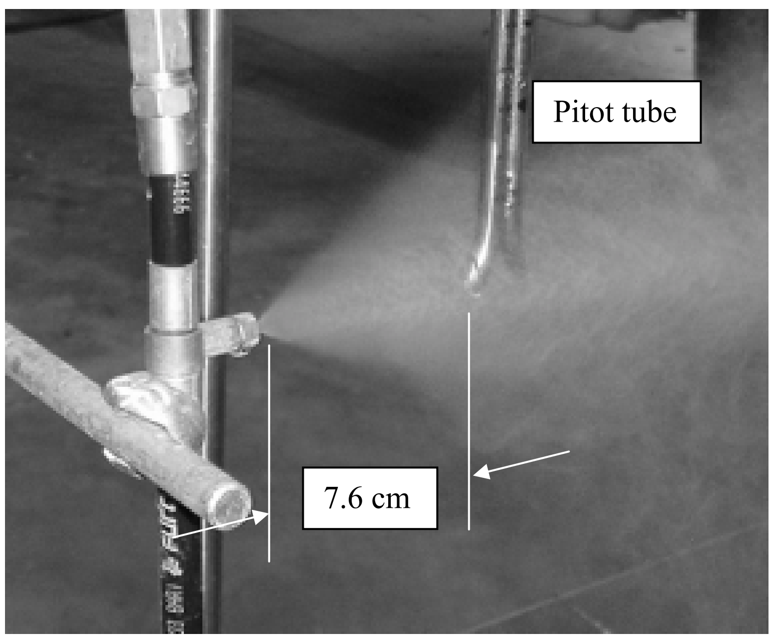

Figure 5.2: Measurement of spray-fog velocity pressure distribution.

5.4.1.2b Airflow measurements in test chamber

A line of seven nozzles was mounted at the opening of a test chamber. The nozzles were spaced 10 cm (4 in.) apart and operated at 6.9 MPa (1000 psi). The test chamber was 76 cm (2.5 ft) wide x 244 cm (8 ft) long and 183 cm (6 ft) high. Openings were at each end of the test chamber. Two sizes of opening were considered: a 25.4 cm (10 in.) diameter opening and a 30.5 cm x 76.2 cm (1 ft x 2.5 ft) opening. For the smaller circular opening, a single 22 cm propeller anemometer was used to measure the airflow rate. For the larger rectangular opening, the average air velocity was determined by conducting a velocity traverse using a 10 cm vane anemometer (Appendix J).

The recirculating airflow pattern within the test chamber was visualized using smoke and a video camera. Smoke was injected into the test chamber at 30.5 cm (1 ft) below the outlet while the spray system was operating. Video data was transferred from a video cassette player to a computer with an imaging circuit board and software (EPIX, Inc., Buffalo Grove, Ill.).

5.4.1.3a Spray-fog side-wall deposits

Total deposits (grain dust and water drops) on the wall of the test chamber were measured using dust collection filters while grain was dropped and the spray system was operated. Sampling locations were at the m(0) = middle, m(30) = mid+30 cm, and m(90) = mid+90 cm (figure 5.3). The filters had a diameter of 12.5 cm (Model PA41, Pall-Gelman, Ann Arbor, MI) and placed into a filter holder having an 11.4 cm diameter opening, thus exposing an area of 102 cm^2 (15.9 in^2). Filters were weighed before and after each trial using an electronic balance with a sensitivity of 0.1 mg (Model 40SM-200A, Precisa Balance, Zurich, Switzerland).

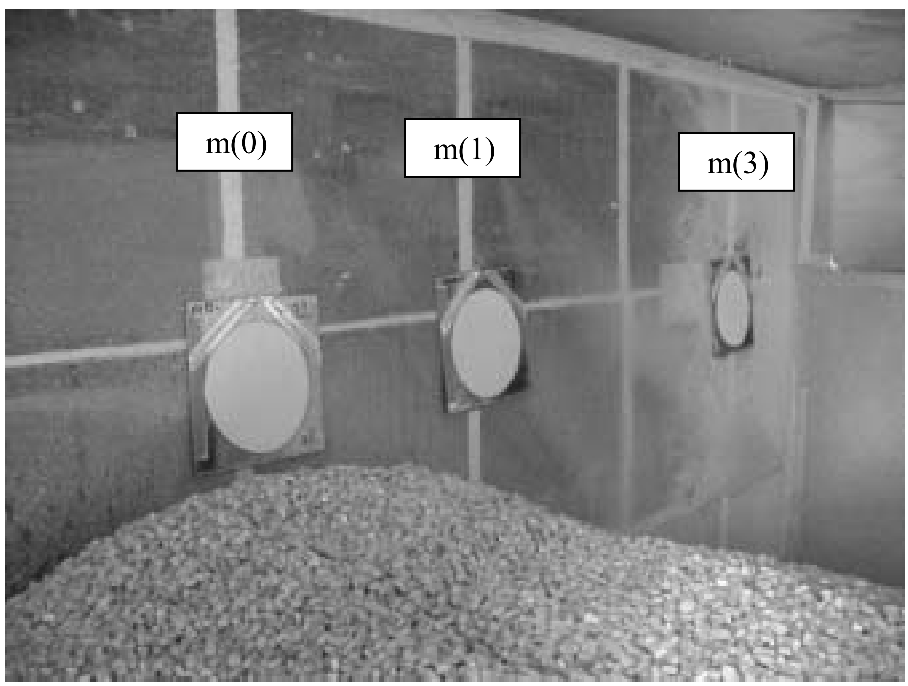

Figure 5.3. Side-wall deposit sampling filters.
The grid was on 0.30 m (1 ft) spacing with m(0) located in the middle of the chamber.

5.4.1.3b Spray-fog grain surface deposits

Drop deposits on the grain pile were collected for three levels of grain: 138 cm (floor), 106 cm, and 60 cm below the nozzle. Grain was first loaded into the test chamber at the specified level, then filters were placed at six locations on the grain (Appendix figure L.3). Three filter samples were evenly spaced on the front half and three on the back half of the grain pile. A wooden barrier, 10 cm deep x 30 cm wide x 180 cm high, was positioned in the middle of the test chamber to simulate the volume occupied by the incoming grain (Appendix figure L.5). The filters were 18.5 cm (7.25 in.) in diameter (CMS # 263-806) and had an area of 268 cm^2. They were weighed on an electronic balance (Model: PC 180, Mettler, Hightstown, New Jersey) before and after sampling. The spray was operated for 30 sec per trial.

5.4.2 CFD modeling

Numerical simulation of airflow and of fate of particles was accomplished using FLUENT (version 6.0, Fluent Inc). Airflow was simulated using three dimensional conservation of momentum equations with the k-ε turbulence model where k is the turbulent kinetic energy and ε is the turbulence dissipation rate. Transport of particles (grain dust or spray drops) was calculated using the equations of motion of a particle. The geometry, grid, and boundary conditions were specified with GAMBIT, a geometry meshing software. The geometry was 3-dimensional and matched the dimensions of the test chamber (figure 5.4).

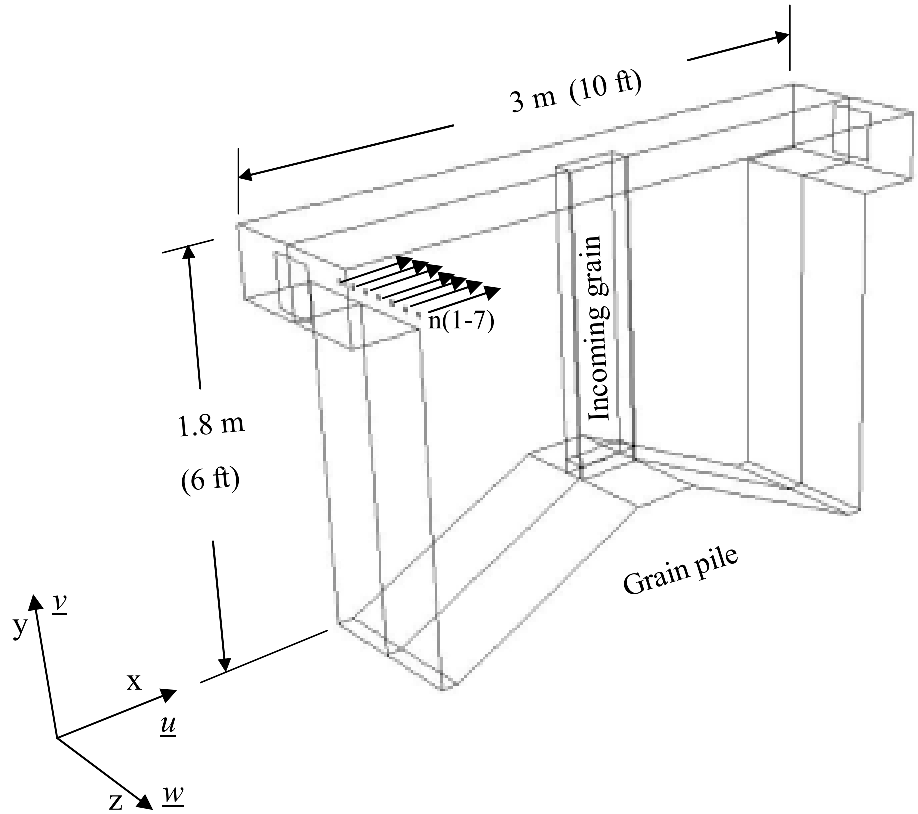

Figure 5.4: Three-dimensional outline of the test chamber
showing the grain pile, incoming grain stream, inlet, outlet, and spray nozzles.

The grid system used finer mesh around the nozzle locations and coarser grid in the lower portion of the chamber. CFD airflow models were computed for grain receiving, grain receiving with spray operations, recirculating air smoke test, and large test chamber inlets. Particle and drop trajectory modeling accompanied most of the airflow models.

The CFD airflow model computed the following parameters for each control volume:

- Pressure at the center of the control volume, P.
- Component velocities u, v, and w.
- Turbulent kinetic energy, k, and turbulent dissipations, ε.

The pressure and velocity components were determined from mass continuity and the x, y, and z conservation of momentum equations. The turbulent components of k and ε were determined with semi-empirical equations which were provided by FLUENT (Fluent Inc., 2002). The turbulence parameters, k and ε, are related to velocity gradients and turbulent air viscosity. They were used to estimate the deviations from the mean velocities within each control volume.

The components of the particle tracking model were (x, y, z) forces, accelerations, velocities, and positions. The particle tracking equations are based on:

- Newton's second law of motion; $\Sigma F = ma$.
- Stoke's particle/air drag force, $F_d = 3\pi\mu V_{rel} d$; where μ is air viscosity, V_{rel} is the relative velocity of the particle to the air, and d is the particle diameter. The velocity of the air included turbulent deviations as determined with the k- ε model.
- Gravitational force, $F_g = mg$.

The boundary conditions are described in the following sections and table 5.1. Also, some modeling details are given in Appendix K.

Table 5.1: Boundary conditions applied to the test chamber.

Geometry	Boundary Descriptions		Size	Turbulence	
			length x width	intensity	length
inlet	pressure-inlet	1 atm.	25 cm x 25 cm	0.020	0.244 m
outlet	pressure-outlet	1 atm.	25 cm x 25 cm	0.030	0.244 m
grain pile	velocity inlet	0.025 m/s	265 cm x 78 cm	0.005	0.762 m
grain impact zone	velocity inlet	0.12 m/s	6 cm x 81 cm	0.050	0.031 m
grain column	moving wall	1.4 m/s	134 cm x 81 cm		
individual nozzles	fan	200 Pa	0.18 cm x 0.18 cm		
walls	wall	default	180 cm x 480 cm		

Some of the basic model assumptions were: 3-dimensional space, steady-state flow, and isothermal conditions. Three more assumptions were required;

- The spray was modeled as two parts: an air source which was located 7.6 cm from the nozzle and a group of drops. Although, the drops were a source of momentum and induced the airflow.
- The entrained air from grain receiving was modeled as a small air source near the top of the grain pile. The entrained air came with the incoming grain; however, once it reaches the top of the pile, it could not advance into the grain pile.
- Particle and drop interactions were not considered, although drop agglomeration was evident and surface deposits measured.

5.4.2.1 Modeling airflow from grain receiving

Grain enters the chamber at 2.55 m^3/min (72 bu/min) and the grain pile height rises approximately 2.5 cm/sec (1 in./sec) displacing air from the chamber. In the CFD model (figure 5.5), the grain pile boundary was considered fixed and was specified as an air velocity source having a constant velocity of 2.5 cm/s. Air was entrained with the incoming grain as seen in chapter four. The entrained air was 0.34 m^3/min and was determined from the difference between the measured airflow rate and the volumetric flow rate of corn at full flow. The bottom 6 cm (2.4 in.) of grain column was considered the impact zone. The entrained air was modeled as air released from the impact zone surfaces with a velocity of 0.12 m/s. The geometry also contained a solid section in the middle representing the incoming grain column. The grain column was modeled as a wall moving at 1.4 m/s downward with a roughness constant of 0.5.

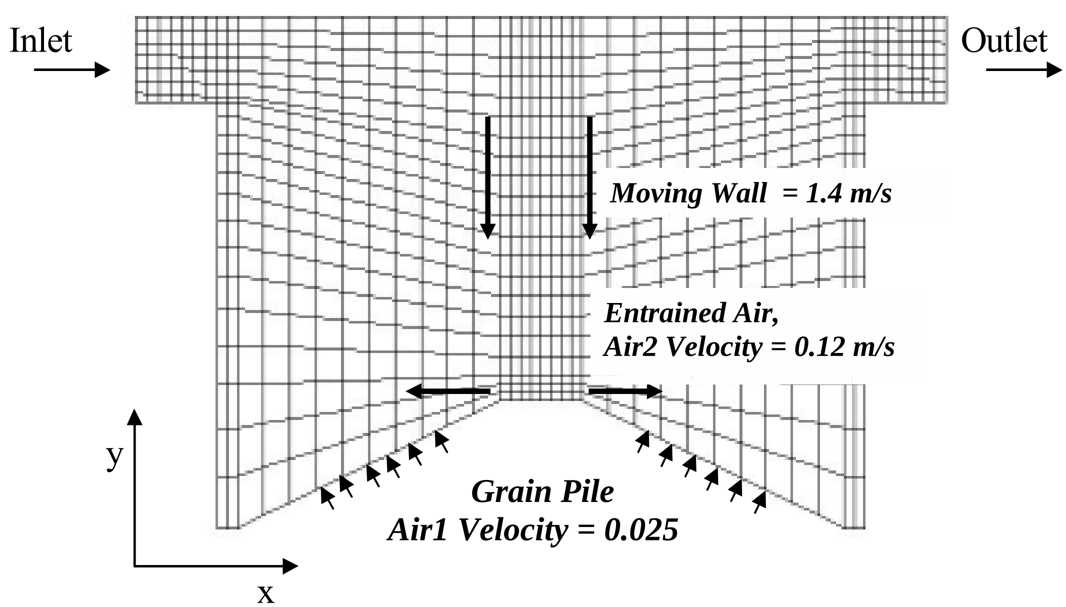

Figure 5.5: Model of airflow from grain movement
Two-dimensional side view of the test chamber showing the grid pattern.

5.4.2.2 Modeling airflow from a spray nozzle

Each nozzle location was defined as a cross-sectional area (figure 5.6) and a pressure jump that produced airflow similar to that determined experimentally for a single nozzle. The pressure jump was based on air velocity pressure measurements taken 7.6 cm (3 in.) from a single nozzle operating at 6.9 MPa (1000 psi). Seven nozzles were specified and each nozzle's cross sectional area and pressure jump were 18 mm x 18 mm and 200 Pa, respectively. The boundaries of the inlet and outlet were selected as pressure inlet/outlet having atmospheric pressure.

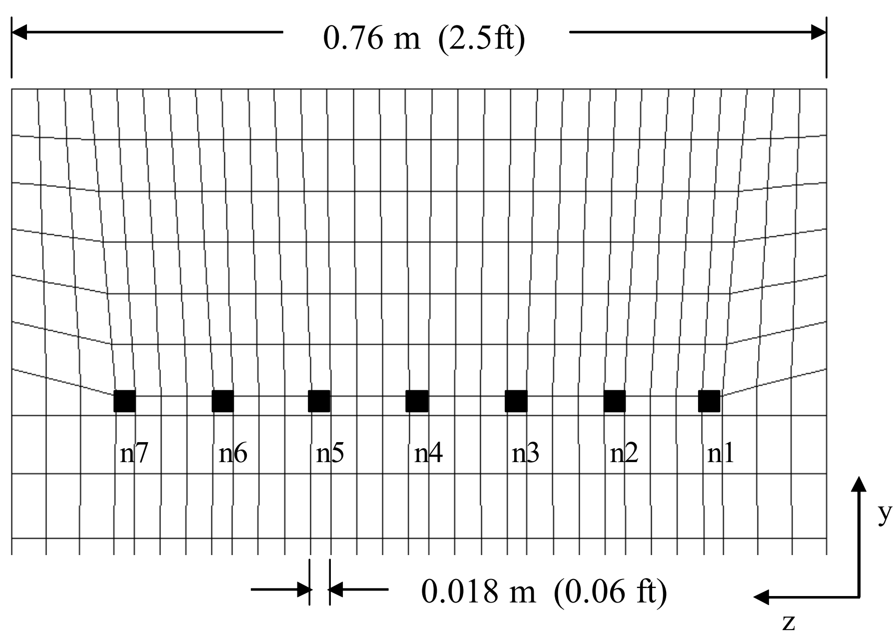

Figure 5.6: Cross-section of the top portion of the chamber's inlet showing the seven nozzles (black squares).

5.4.2.3 Modeling dust during grain receiving with spray operations

Particle tracking was accomplished through FLUENT using similar procedures as outlined in section 3.5. An array of grain dust particle sizes (d_p = 5-40 µm, ρ_p = 1.5 g/cm^3) were tracked. They were initially positioned around the grain pile peak and incoming grain column. The discrete phase model calculated the position of the particles after each 1.8 mm of movement. With each time step, the drag force, and gravitational force, acceleration, velocity, and position were computed. The effect of local turbulence was included. Particle sizes were determined from corn dust samples taken with the high-volume sampler during grain drop test. They were analyzed by a commercial laboratory (Appendix M). A particle size of 14 µm was the approximate geometric mean diameter.

5.4.2.4 Modeling small and large test chamber inlets

Although grain receiving hoppers are not normally covered, the top of the test chamber in this study was covered to facilitate airflow measurements. Inlets were positioned on ends and had a rectangular cross-section with dimensions of 30.5 cm x 76.2 cm (1 ft x 2.5 ft). The average velocity was determined during spray operation from measurements taken at 15 locations across the rectangular opening with a 10 cm (4 in.) diameter vane anemometer. The inlets on each end were reduced to 25.4 cm (10 in.) diameter tubing and a single, large vane anemometer with a diameter of 22 cm (Model 27106 R.M.Young Co., Traverse City, MI) was installed at each tube. CFD models were prepared to estimate the change in airflow resulting from the two sizes of inlets and different grain flow conditions.

5.4.2.5 Modeling drop deposits on side-wall

Spray drop trajectories were computed for 9600 tracking events from each nozzle location. At each nozzle, the spray was simulated as a cone of 32 injection locations having a radius of 4 cm and a cone angle of 40^o and as 18 μm drops and an initial velocity of 10 m/s. The discrete phase model was allowed a maximum of 3500 steps and a scale length of 1.8 mm (0.006 ft) or a maximum of 12 sec of particle motion. The turbulent dispersion option was enabled. Predicted results were expressed in terms of the number of particles which had escaped through the outlet, were trapped on a surface, or were still drifting. From these results, the fraction of drops that deposited on side wall surfaces was determined. The surfaces were 30 cm x 30 cm and located 0, 30, and 90 cm from the middle of the incoming grain. These surfaces were referred to as m(0)cfd, m(30)cfd, and m(90)cfd, respectively. A relative deposit was computed for m(0)cfd and m(30)cfd by dividing each surface deposit estimate by the surface deposit m(90)cfd.

5.4.2.6 Modeling drop deposits on grain and wall surfaces

Spray drop trajectories were computed separately for 18, 30, and 180 μm drops. The 18 μm and 30 μm drops were selected to represent the main plume. A total of 9600 tracking events were computed with these drops initially located near the nozzle. Agglomerated drops and fall-out from the spray plume were represented by the 180 μm drops. These drops were initially located along the x-axis, 60 cm to 240 cm from the tip of the nozzle and 8 cm below the center line of the nozzle. Their initial x- and y-velocities were 1 and -1 m/s, respectively. Various surfaces of the CFD geometry were sampled for trapped drops: grain column walls, grain pile, near and far end walls.

5.5 Results and discussion

5.5.1 Spray drop size and velocity distributions

The drop size and velocity distribution varied with horizontal and vertical locations in the spray plume. The volumetric median diameters (VMD) for two nozzles and at 7.6 cm (3 in.) and 30.5 cm (12 in.) from the nozzle tip and for all vertical test locations across the spray plume are shown in figure 5.7. Both nozzles have similar size distributions. At 7.6 cm, the drops have a 15-25 μm VMD. At 30.5 cm from the nozzle and 8 cm below the nozzle center line, the drop VMD dramatically increased to over 150 μm, indicating that drops had agglomerated and were falling out of the plume. The observed liquid flow distribution across the spray plume at 7.6 cm from the tip depicted a hollow cone spray with most of the drops located at +/- 3.8 cm (1.5 in.) from the center line.

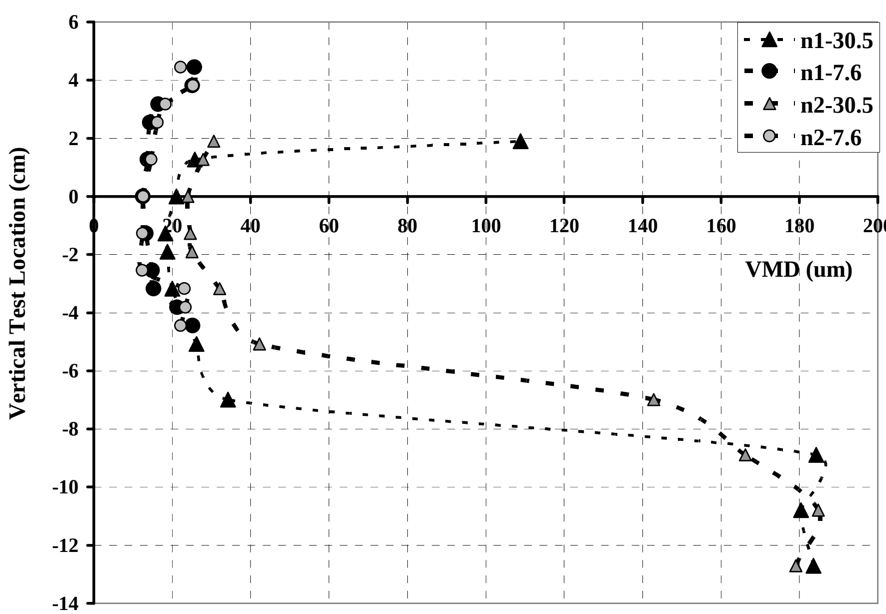

Figure 5.7: VMD for two spray-fog nozzles operated at 6.9 MPa (1000 psi).

The drop size distributions at the single sampling point located 3.8 cm below center line (location 0313) shows the variation in drop sizes near the nozzle (figure 5.8). The volumetric distribution was bimodal with peaks at 19 μm and 31 μm. Approximately 98% of the spray volume ranged from 10 μm to 40 μm. The count distribution indicates that, by count, 50% and 18% of the drops were approximately 18 μm and 28 μm, respectively.

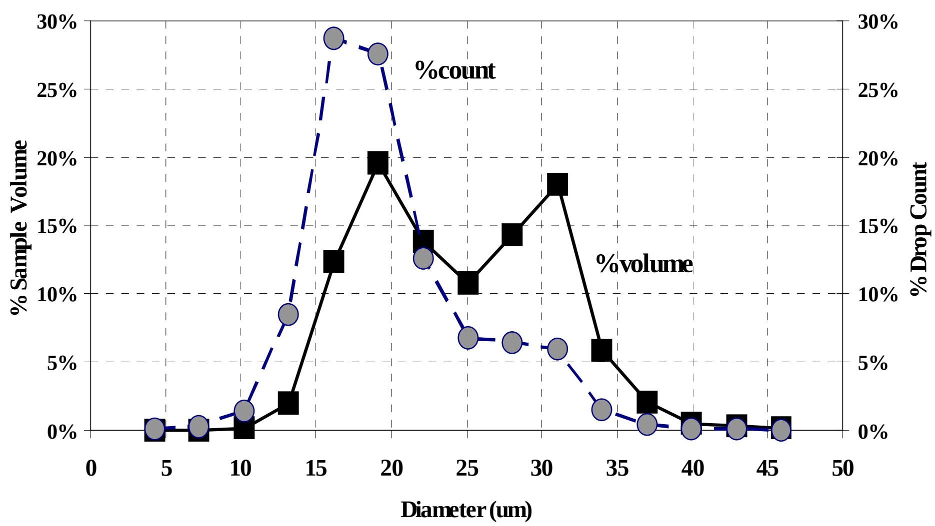

Figure 5.8: Drop size distribution at location 0313
at 7.6 cm from nozzle tip and at 3.8 cm below the center line

Average drop velocities for the spray plume at all vertical test points and at 7.6 cm and at 30.5 cm from the nozzle tip are shown in figure 5.9. The maximum average velocities were 11.5 m/s at 7.6 cm from the nozzle and 5.8 m/s for the 30.5 cm location. The drops were slowing down with distance as momentum was exchanged with the air.

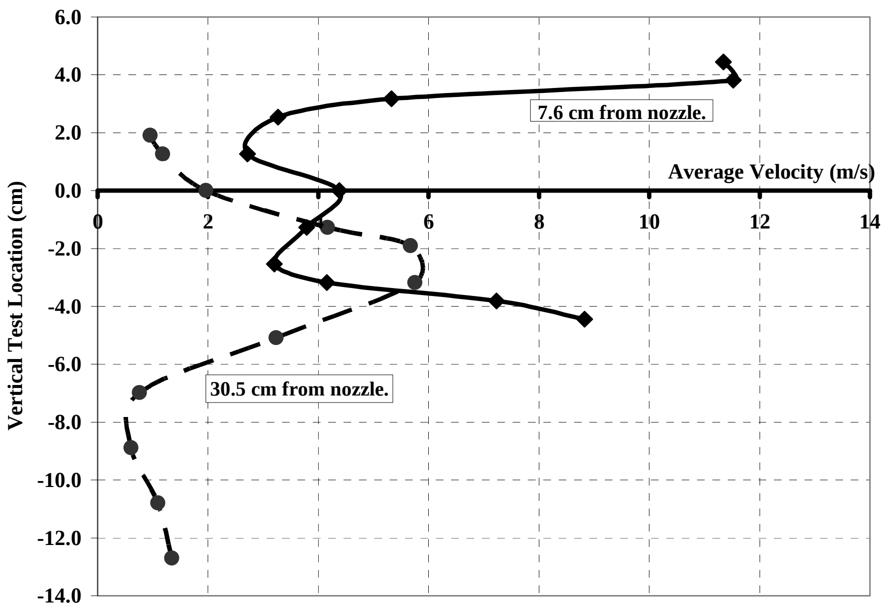

Figure 5.9: Mean drop velocities for a nozzle at 6.9 MPa.

The drop velocity data was examined more closely at two sampling locations, location 0313 and 1217. Location 0313 was 7.6 cm from the nozzle and 4 cm below the center line. Location 1217 was 30.5 cm from the nozzle and 3 cm below centerline. At location 0313, the 19 μm and 31 μm drops had velocities of 5 m/s and 22 m/s, respectively. At location 1217, the drop velocities were approximately 5.5 m/s for all sizes. The velocity of the larger drops decreased with distance while the velocity of smaller drops remained roughly constant. Additional data on spray VMD distributions, velocities, and location data are given in Appendix I.

5.5.2 *Induced airflow from the spray*

Induced airflow was demonstrated qualitatively using a heavy smoke plume, generated from a smoke stick. When the smoke plume entered the underside of the spray (figure 5.10), the entire smoke plume was swept to one side and diffused with the spray. In stationary air, when smoke is directed under a porous medium, most of the smoke passes through a porous medium. With the spray-fog, the induced air redirected particle movement.

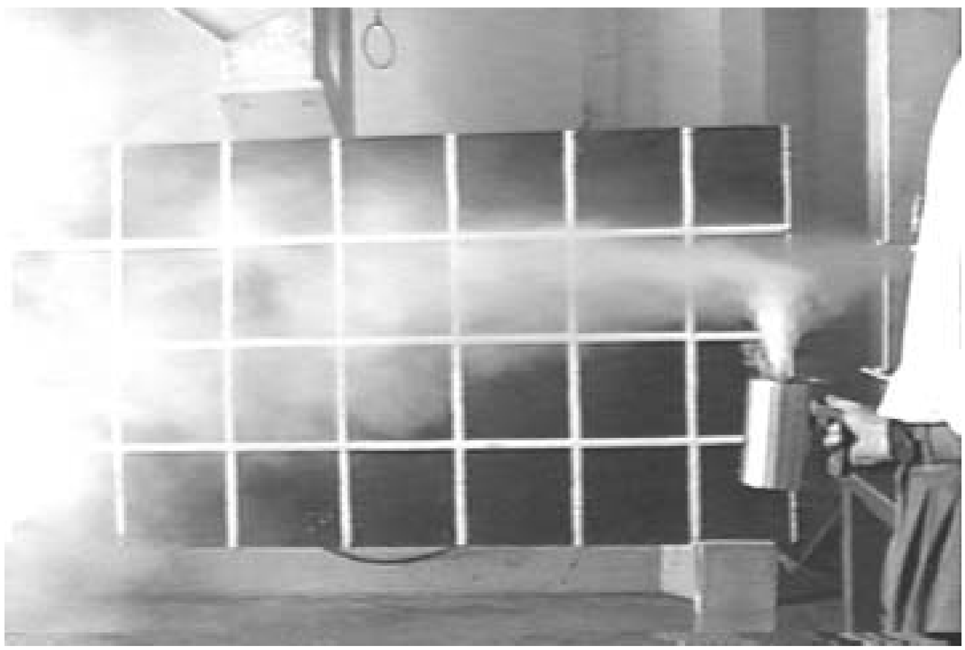

Figure 5.10: Spray induced airflow demonstrated with smoke.
Photograph showing how smoke, positioned underneath the spray, was redirected and diffused with the spray. White grid spacing was 0.30 m.

The maximum velocity pressure for three nozzles and at 7.6 cm (3 in.) was greater than 250 Pa (1 in. H_2O) (figure 5.11). From Hinds (1982), pressure measurements from a pitot tube are related to velocity by $V(m/s) = 20.3\sqrt{P}\ (in.\ H_2O)$. Thus, the maximum spray-fog pressure translates into a maximum air velocity of over 20 m/s. The pressure profile was parabolic with a base width of approximately 3-4 cm. The maximum velocity pressures at 15 cm (6 in.) and 30.5 cm (12 in.) from the nozzle tip were approximately 110 Pa (0.45 in. H_2O) and 42 Pa (0.17 in. H_2O), respectively. The average measured pressure is shown by the shaded rectangle.

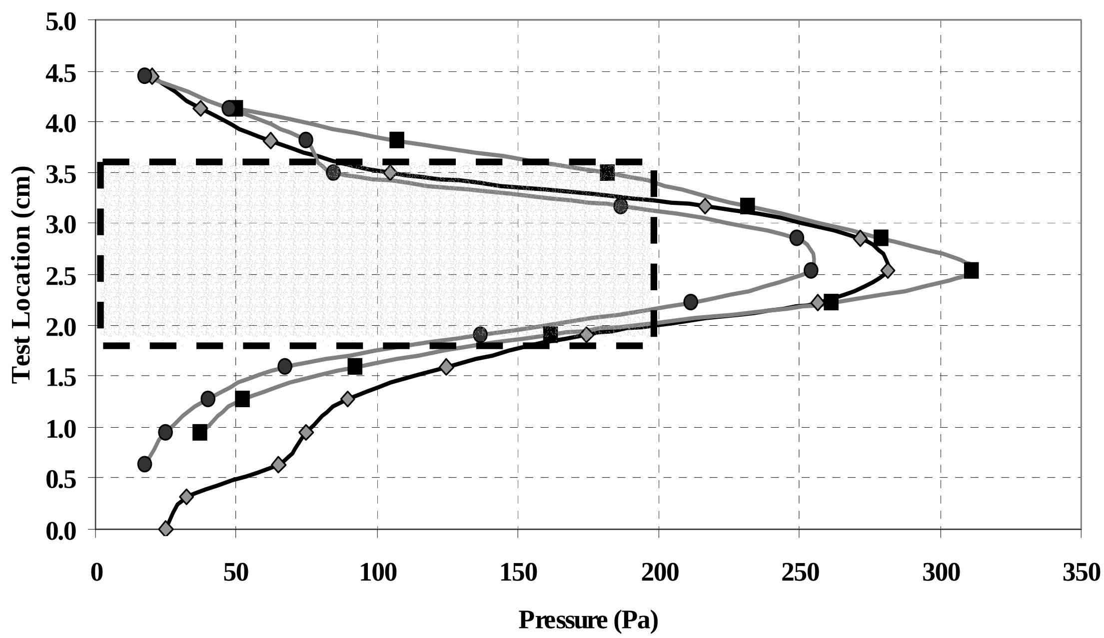

Figure 5.11: Velocity pressure profiles for three nozzles at 6.9 MPa. Data was obtained with an inclined manometer and pitot tube positioned 7.6 cm (3 in.) from the tip and at 15 vertical locations.

5.5.3 CFD airflow and particle emission modeling of grain receiving

The control airflow and dust movement was predicted for grain dropping in the test chamber without spray application. Predicted results showed that the air and 14 μm dust particles moved out of both ends of the test chamber (figure 5.12). The particle distributions of emitted dust indicate a maximum emitted particle size of approximately 25 μm (table 5.2). CFD particle tracking models estimated a maximum size between 30-40 μm (table 5.3). Possibly, the area of the impact zone was undersized. If the impact zone area was a larger for the same entrained airflow, then the air velocity from the impact zone would have been reduced. Also, the maximum size of particles emitted would be decreased as predicted by terminal settling velocity calculations (Hinds, 1982).

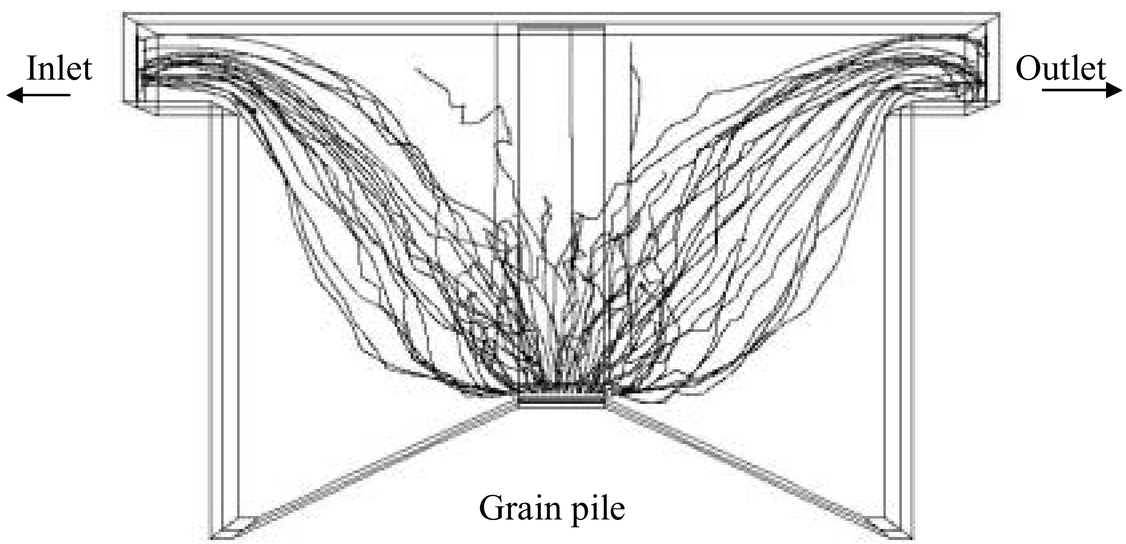

Figure 5.12: Predicted trajectories of grain dust particles.
Particles released around the top of the grain pile.
(d_p = 14 μm, ρ_p = 1.5 g/cm^3, n = 72)

Table 5.2: Particle size distribution of emitted wheat and corn dust. Samples were collected with a high-volume air sampler during the 2.1 m^3 (60 bu) grain receiving trials.

%Vol	Wheat dust (μm)	Corn dust (μm)	Avg. size (μm)
5%	4.0	5.4	5
16%	7.3	8.9	8
28%	11.3	12.3	12
28%	14.7	15.4	15
16%	18.3	18.8	19
5%	23.1	23.5	23

Table 5.3: Dust particle tracking in the test chamber resulting from 5600 events per particle size with particles released from the grain impact zone.

size μm	escaped avg. (%)	trapped avg. (%)	drifted avg. (%)
5	73	10	16
8	74	12	14
12	74	12	14
15	73	13	14
20	63	19	18
25	39	49	12
30	16	83	1
40	2	98	0

5.5.4 CFD airflow and particle trajectories during spray operations

When the line of seven nozzles was added to the control test case, the airflow pattern was changed to a cross flow at the top of the chamber. Additionally, a fraction of the air was exhausted through the outlet and a fraction recirculated down the back wall and towards the inlet side. The predicted trajectories of the 18 μm drops illustrate this recirculating airflow pattern (figure 5.13).

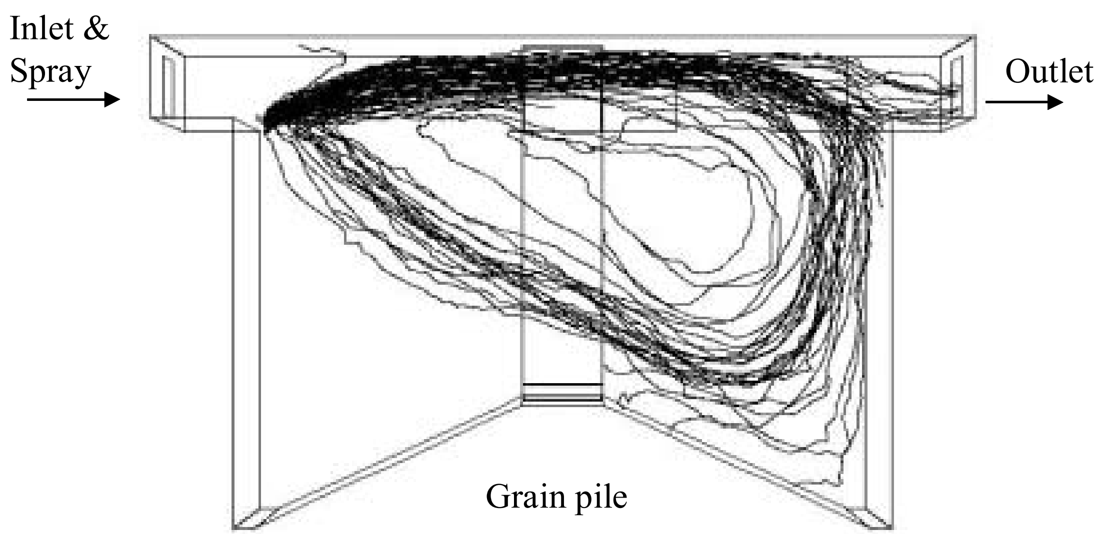

Figure 5.13: Predicted trajectories of spray drops.
Drops (d_p = 18 μm, ρ_p = 1 g/cm^3, n = 64) were released from the middle nozzle (n4) during the incoming grain and the induced airflow from seven nozzles.

Table 5.4 summarizes the predicted fates of the 18, 30, and 180 μm drops for all nozzles. Approximately 49-53% of the 18 μm and 30 μm drops were trapped on some surface while 29-31% were still drifting after 12 sec of computation. The 18 μm and 30 μm drops were released from seven nozzle locations with 9600 tracking events per nozzle location. The 180 μm drops were released under the spray plume and across the length of the chamber.

Table 5.4: Predicted fates of spray droplets.

	Droplet size (μm)		
Fate	18	30	180
Escaped (%)	22	16	0
Drifted (%)	29	31	0
Trapped (%)	49	53	100

Due to the recirculating airflow pattern associated with the spray, the dust particles from the grain pile moved towards the spray nozzles and entered the spray plume near the tip of the nozzles (figure 5.14). The airflow near the grain pile was changed considerably with the spray. The new airflow profile could have affected the amount and the size of grain dust emitted. Possibly, less dust was emitted from the pile since the spray fog recirculated and covered closely the top of the grain pile. Also, the potential for dust and drop interaction was enhanced since the dust particles were concentrated and mixed with the spray near the nozzles where the spray was concentrated.

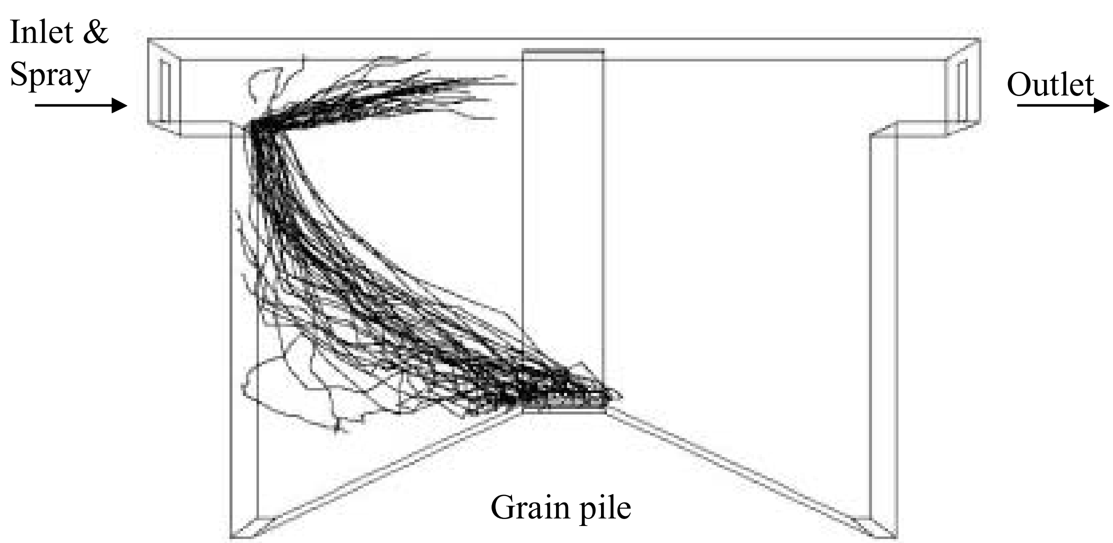

Figure 5.14: Predicted trajectories of grain dust during spray operation.
Particles (d_p = 14 μm, ρ_p = 1.5 g/cm^3, n = 72) were released at grain pile.

The predicted airflow pattern associated with the spray-fog was validated qualitatively using smoke. To simplify the model geometry, the grain pile was removed and smoke particles were released near the outlet (figure 5.15). The smoke particles (d_p = 1 µm, ρ_p = 1 g/cm^3) moved in a counter-clockwise direction. Enhanced images of the smoke test showed similar behavior as the modeled particles (figure 5.16). The smoke moved down the right side of the chamber during the first second and then diffused as it moved upward on the left side which is similar to the CFD model prediction in the empty chamber.

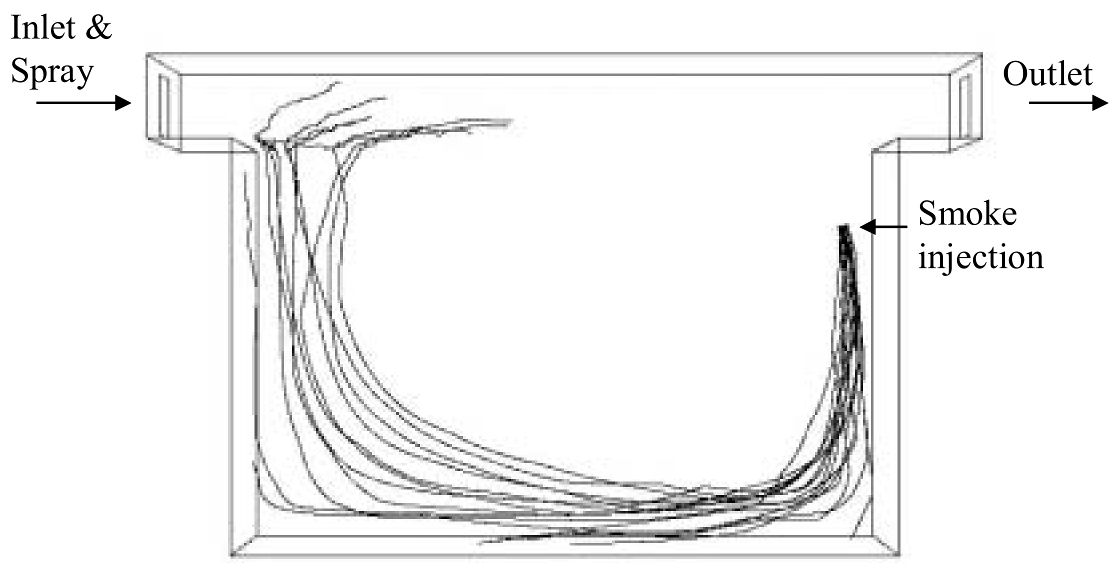

Figure 5.15: Smoke tracking in a revised CFD model.
The particles were 1 µm in size and released 30 cm below the outlet

(a)

(b)

Figure 5.16: Enhanced video images of recirculating air. Smoke test images were collected during spray operation.

5.5.5 CFD airflow modeling for small and large air inlets

Observed and predicted results of the mass flow rate of the inlet air for two sizes of inlets were compared to the measured values (table 5.5). The observed mass flows were 0.009 kg/s versus 0.171 kg/s for inlet(1) and inlet(2), respectively. Inlet(2) mass flow was 19 times larger than inlet(1). This large difference was due to differences in test conditions. First, inlet(1) had an opening of 0.05 m^2 while inlet(2) had an opening of 0.23 m^2. Secondly, inlet(1) had both air from grain flow and the spray nozzles. For inlet(2), the spray operation induced all of the air from the inlet.

With a CFD pressure of 200 Pa, the model estimated the outlet(1) mass flow 0.062 kg/s while the observed outlet mass flow was 0.060 kg/s. When the same CFD pressure was applied to outlet(2), the model estimated 0.228 kg/s while the observed flow was 0.171 kg/s. The CFD nozzle pressure was reduced and additional computations were performed. When the CFD nozzle pressure was reduced to 150 Pa, the model estimated outlet(1) mass flow as being 10% under the observed. In addition, the model estimated outlet(2) mass flow of as being 15% over the observed.

Several factors possibly affected the closeness of the model results. The meshing of subsections of the test chamber and sizing of the control volumes were challenging to adjust. Sizing of the model nozzles and inlet geometry could be improved. Possibly, the nozzle dimensions should be adjusted by 10% to 20%. So, instead of having 1.8 mm x 1.8 mm nozzle area, it would be reduced to 1.6 mm x 1.6 mm. Also, for inlet(1), the CFD model used a 0.06 m^2 opening, because of the rectangular meshing design. The actual size of inlet(1) was 0.05 m^2.

These models demonstrate that the amount of induced air depends on inlet size. Also, the model demonstrates the affects of differences in test conditions i.e., grain and spray versus spray only. For a more open inlet design like in a full-scale operation, more air would be induced than was induced in the test chamber with the restricted inlets.

Table 5.5: Observed and CFD computed mass airflow rates.
The CFD mass airflow rate (kg/s) was computed for three pressure levels.
The spray treatments used seven nozzles at 6.9 MPa (1000 psi).

	Observed flow	CFD nozzle pressure		
		150 Pa	175 Pa	200 Pa
	kg/s	kg/s	kg/s	kg/s
Inlet(1)	0.009	0.002	0.005	0.009
Grain(1)	0.051	0.053	0.053	0.053
Outlet(1)	-0.060	-0.055	-0.058	-0.062
Inlet(2)	0.171	0.197	0.213	0.228
Grain(2)	0.000	0.000	0.000	0.000
Outlet(2)	n.a.	-0.197	-0.213	-0.228

5.5.6 Spray-fog side-wall deposits and modeling

The test chamber was narrow compared to a full size grain receiving hopper. The chamber cross section was further restricted in the middle by the grain stream. This restriction temporarily increased particle concentrations and impingement on the wall at the middle portion of the chamber. Table 5.6 gives the experimental fog deposits on the side wall and above the grain from seven nozzles at 6.9 MPa. The highest deposits were at the narrowed cross section, *m(0)*, and decreased with distance from the middle.

Predicted results were summarized in table 5.7. Most of the side-wall deposits came from a single nozzle, n1, which was closest to the wall, the remaining nozzles, n2 and n2, had little effect. Also, like the observed deposits, the particle tracking model estimated the largest deposits at the middle of the test chamber, *m(0)cfd*. The relative deposits, $\frac{m(0)}{m(3)}$, for observed and predicted data were 7.3 and 4.5, respectively. The model used larger sampling surfaces and the increased area may have caused the reduction in relative amount of trapped drops, because part of the CFD sampling surface was outside the spray plume. Additional photographs of grain and fog deposits are given in Appendix L.

The incoming grain column in a full scale case would have less influence on the side ways movement of the spray-fog, because the walls are further from the grain. Thus, the full scale case would have less mid-wall deposits than seen in the narrow test chamber.

Table 5.6: Test chamber side-wall fog deposits measurements. Sample locations were above the grain pile and exposed to 30 seconds of continuous spray.

Filter position	Side-wall deposit $mg/cm^2/min$ Avg.	Std. dev.	Relative deposit[1]
m(0)	11.0	2.8	7.3
m(1)	5.3	1.2	3.5
m(3)	1.5	0.3	1.0

[1] Relative deposit was determined by dividing the deposit by m(3) deposit.

Table 5.7: CFD estimate of side-wall deposits from spray. Drop deposits were computed for three nozzle positions and at three side-wall locations. 9600 tracking events were computed from each nozzle using 18 µm drops as released in a cone.

Filter position	Nozzle position n1	n2	n3	Relative deposit[1]
m(0)cfd	338	0	0	4.5
m(1)cfd	228	0	0	3.0
m(3)cfd	51	24	0	1.0

[1] Relative deposit was determined by dividing the deposit by m(3) deposit.

5.5.7 Spray drop modeling and surface deposits

Various surfaces within the test chamber were modeled for potential drop deposits: the walls of incoming grain (t1), the far slope of the grain pile (t2), and the far end of the test chamber (t3). Table 5.8 summarizes the independent movement of 18 μm drops from seven nozzle locations. Nozzles n1 and n7 were located next to the chamber's sides and showed the greatest percentage of trajectories trapped. Nozzles n3 and n4 had large fractions of drops deposit on the incoming grain stream. The chute for the incoming grain was centered in the top, however, the grain only used one half of the chute and was shifted to one side. Nozzles n2, n5, and n6 had no side wall or grain interference, and significant portions of those plumes were deposited on the far end wall. Some of the drops from nozzles n2-n6 recirculated and deposited on the back side of the grain pile. The front side of the grain pile and the near-nozzle end wall trapped minimal drops according to the CFD modeling conditions. The CFD particle tracking did not account for changes in the drop sizes due to agglomeration.

Table 5.8: Spray deposits for three selected test chamber surfaces.
18 μm drops were model with 9600 events per nozzle (%deposit/nozzle).

Nozzle Position	n1 side	n2	n3 grain	n4 grain	n5	n6	n7 side
Escaped (%)	15	38	17	13	31	32	8
Drifting (%)	25	20	38	39	29	22	31
Trapped (%)	60	42	45	47	40	46	60
t1) in-grain (%)	0	2	22	30	3	0	0
t2) back of pile (%)	0	2%	3	3	5	4	1
t3) far end (%)	5	14	10	6	16	14	3

5.5.8 Spray-fog grain surface deposits

The spray deposits on the grain surface varied with grain height and horizontal proximity to the nozzle (figure 5.17). The deposits generally ranged from 0.4 mg/cm^2/sec near the nozzle to 0.1 mg/cm^2/sec near the outlet wall. The non-uniformity was more evident as the pile moved closer to and into the spray plume. The heaviest deposit was 1.2 mg/cm^2/sec when the peak of the grain moved within the plume of the spray.

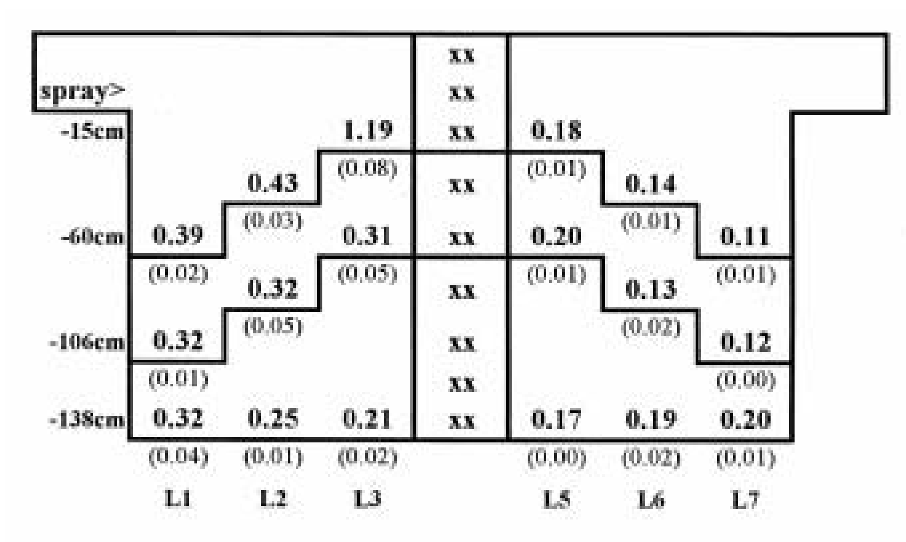

Figure 5.17: Schematic view of the test chamber and spray deposits.

Three levels of grain were used for the spray agglomeration and deposit test. The spray deposits at each level are shown at each sample location (mg/cm^2/sec). Standard deviations are in parentheses.

5.6 Summary and conclusions

The following conclusions were drawn from the study:

1. Over 90% of the measured spray-fog drops ranged from 10 to 40 μm. Drop velocities were over 10 m/s at 7.6 cm and decreased to 4-6 m/s at 30.5 cm from the nozzle.

2. The velocity pressures from a single nozzle at 7.6 cm were parabolic with a base diameter of approximately 3-4 cm, with maximum pressures over 275 Pa, and an average pressure of 200 Pa.

3. The grain receiving CFD model predicted a maximum emitted particle size of 35-40 μm while the emitted dust had a maximum particle size of 25 μm, possibly because the modeled impact zone velocity was overestimated.

4. The spray CFD model predicted air and grain dust recirculation back towards the entrance in the lower portion of the test chamber during spray operation and grain receiving. The predicted results qualitatively agreed well with a smoke test showing the movement of smoke and air from the exit towards the entrance.

5. Spray side wall deposits were 11 $mg/cm^2/min$ at the middle of the test chamber where the grain column reduced the path and 1.5 $mg/cm^2/min$ near the outlet. Deposits of mist on the grain varied with depth of grain and proximity to the nozzle and generally ranged from 0.1 to 0.4 $mg/cm^2/sec$.

6. The observed mass airflows were 0.06 and 0.17 kg/s for the small and large test chamber inlets, respectively. The CFD models for large and small inlets demonstrated that the amount of spray induced air depended on inlet size and test treatments (i.e., spray during grain-flow versus spray alone).

Airflow and particle tracking models were useful in describing the recirculation of the air, drops, and grain dust particles during grain receiving and spray operation. CFD modeling of the individual nozzles demonstrated potential of application to larger inlets and full scale models. Full scale models would require further validation.

Modeling accuracy could be improved. In the grain receiving model, the impact zone velocities were estimated. Validation test should measure the impact zone velocities. If the modeled velocity were decreased, then the modeled maximum emitted particle size would match more closely the dust sample size distribution. Also, the small and large inlet scalability should be improved. The current model could be optimized by modifying the mesh to more accurately represent the nozzle size and pressure and other boundary condition discrepancies. Possibly, the modeling strategy should try to couple the discrete phase with the fluid phase rather than treating them separately. Initial attempts at CFD coupled computations did not work well during this project.

Drop and particle interactions were not modeled effectively. Each nozzle produced millions of drops/sec having a range of drop sizes, initial velocities, and projections. With distance from the nozzles, the spray plumes overlapped. Also, with distance, the high speed drops slow down to the surrounding air velocities or they collide with other drops and agglomerated. Air stream turbulence added variability and influenced interactions. Spray/air momentum exchange, drop agglomeration, and changes in drop sizes and velocities are challenging modeling topics and require much more time and effort to develop useful particle interaction models.

5.7 Literature cited

Al-Arifi, A., Short, T., and Ling, P. 2001. Validating the CFD model for air movements and heat transfer in ventilated greenhouses. ASAE Paper No. 01-4056. St. Joseph, Mich.: American Society of Agricultural Engineers.

Brown, R.B. and Sidahmed, M.M. 2001. Simulation of spray dispersal and deposition from a forestry airblast sprayer – Part II: droplet trajectory model. Trans ASAE 44(1):11-17.

Enarson, D.A., Vedal, S. and Chan-Yeung, M. 1985. Rapid decline in FEV in grain handlers. Am. Rev. Respir. Dis. 132:814-817.

Fluent, Inc. 2002. Computational fluid dynamics software. Lebanon, NH.

Hinds, W.C. 1982. Aerosol technology: properties, behavior, and measurement of airborne particles. New York: John Wiley & Sons, Inc.

Jones, A.D. and James, G.C. 1987. Air movement and cleaning by water sprays. Ann. Occup. Hyg. 31(2):161-179.

Kwok, K.C. 1991. Fundamentals of air spray painting. Ph.D. thesis, University of Minnesota, Minneapolis, Minn.

Office of Technology Assessment. 1995. Technology and policy for suppressing grain dust explosions in storage facilities. OTA-BP-ENV-177. Washington, D.C.

Reid, R.G. 1987. The affects of the use of oil on wheat on milling. AOM Technical Bulletin 1987:4981-4985. Leawood, Kans.: Association of Operative Millers.

Schoeff, R.W. 2002. Agricultural dust explosions in 2001. January Newsletter. Kansas State University, Dept Grain Sc. Manhattan, Kans.

Spraying Systems Co. 2000. Technical bulletin: drop size measurement. Wheaton, Ill.

St. Georges, M. and Buchlin, J.M. 1994. Detailed single spray experimental measurements and one-dimensional modelling. Int. J. Multiphase Flow. 20(6):979-992.

Sun, H., Stowell, R.R., Kenner, H.M., and Michel, F.C. 2002. Two-dimensional computational fluid dynamics (CFD) modeling of air velocity and ammonia distribution in a high-rise hog buidling. Trans ASAE 45(5):1559-1568.

Tsay, J., Ozkan, H.E., Brazee, R.D., and Fox, R.D. 2002. CFD simulation of moving spray shields. Trans ASAE 45(1):21-26.

.

Chapter 6. Conclusions and recommendations

6.1 Summary and conclusions

A high-pressure, water-fog spray was evaluated as a potential dust control method. The spray system was characterized for drop size distributions and airflow distributions. The spray nozzles had a 0.2 mm (0.008 in.) orifice and produced 10-40 μm drops. The spray-fog system induced air flow, changed the airflow profiles, and changed the movement of grain dust.

Dust emissions were generated while spouting 2.1 m^3 (60 bu) sublots of corn and wheat into a test chamber. The test chamber represented a narrow portion of a receiving hopper and was 244 cm (8 ft) long, 76 cm (30 in.) wide, and 183 cm (6 ft) high. The uncontrolled dust emissions ranged from 5 to 24 g/tonne varying with grain sample and grain-flow rate. The exhaust airflow ranged from 108% to 172% of the volumetric grain flow rate.

Dust and spray-fog emissions along with entrained airflows were measured for four water-fog treatments, a control, and an air-blower treatment each at two grain flows. Dust reductions ranged from 60% to 84% for the corn sample and 35% to 73% for the wheat sample. At the highest spray-fog rate (855 g/min), fog emission was 32 g/min (3.8%).

FLUENT, a computational fluid dynamics (CFD) software, was used to predict airflow distribution and particle trajectories within a test chamber during grain flow and during spray operation. During grain flow, the grain pile was modeled as a very low velocity air source causing air and dust to be exhausted from both ends of the test chamber. The spray nozzles were simulated as seven individual pressure sources that induced airflow and forced airflow towards one end. Predicted results showed that the spray generated air recirculation in the lower portion of the test chamber and directed particles and drop movement back towards the spray nozzles and plume. Smoke test confirmed the recirculation model predictions.

6.2 Recommendations for future research

The following studies are recommended:

1) Full scale, airflows should be measured and compared with the CFD model estimates. The velocity and directions of the air near the impact zone should be confirmed. It was assumed that the dust was released at the top of the grain pile and released with the entrained airflow from the grain. (Appendix N)

2) Full scale, pneumatic system variations should be tried and compared with CFD model. The results should help confirm or improve CFD modeling techniques used to specify and optimize pneumatic dust collection designs such as recommendations of pneumatic airflow based on maximum receiving grain flow or the potential effects of baffles and air distributions.

3) Spray-fog and dust interactions studies would improve the particle-drop modeling. Better electro-static testing of grain dust and spray-fog should be done (Appendix O). The charge levels, polarity, and variation with time of the electro-static charge on grain dust are uncertain. Spray-fog agglomerates as seen by the large drops

falling from the spray plume, however, a better understanding of the spray agglomeration would be helpful for modeling drop-drop interaction.

4) Some grain quality parameters and other properties could be evaluated using a laboratory aspiration and filter test (Appendix P). Further developments of this procedure could provide a tool for evaluating dust emissions potential and identify mold and insect contamination levels in the grain.

Appendices

Appendix A: Grain drop test chamber and setup

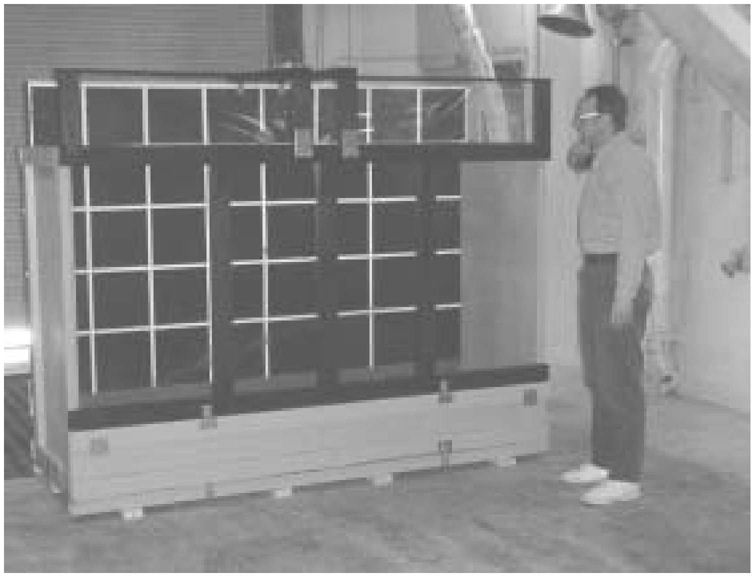

Figure A.1: Photo of empty test chamber.
The test chamber was 183 cm (6 ft.) tall by 244 cm (8 ft.) long by 76 cm (2.5 ft.) wide.

Figure A.2: Photo of test chamber full of grain.

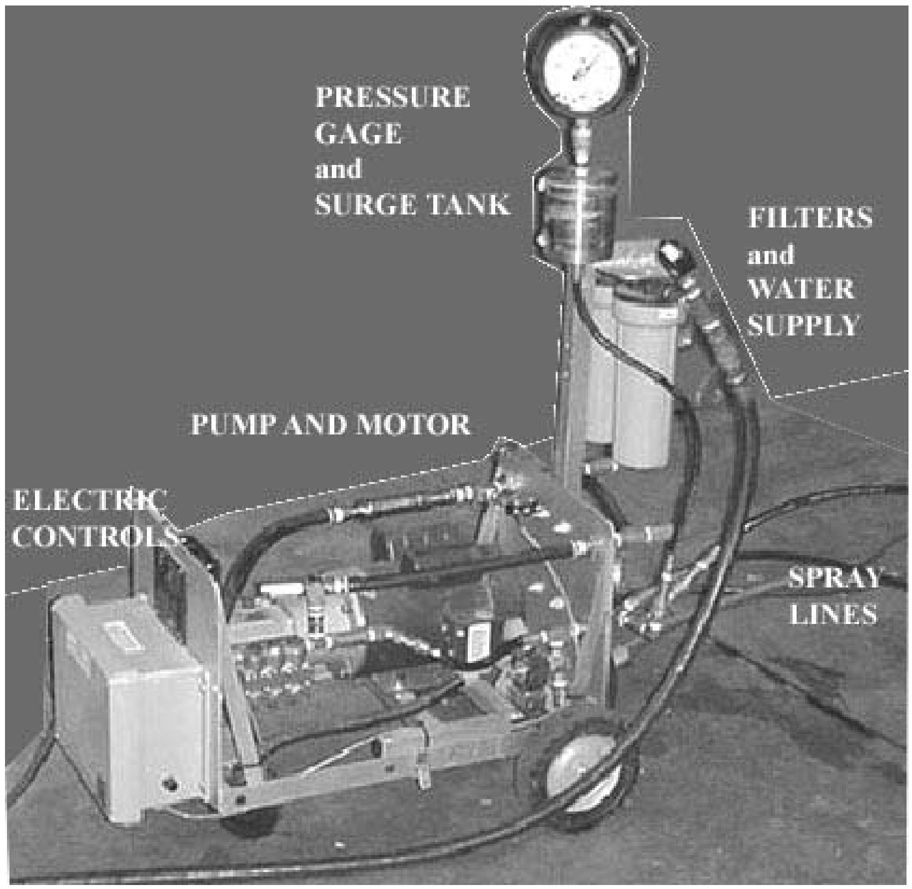

Figure A.3: Photo of spray system.

Figure A.4: Photo of grain chute from overhead bin into test chamber.

Figure A.5: Photo of test chamber and PC for data acquisition.

Figure A.6: Photo of dust and spray emissions during test.

Figure A.7: Photo of unloading grain from test chamber.

Appendix B: Propeller anemometer calibration

Two propeller anemometers were used with the test chamber. The propeller was 22 cm in diameter and the anemometer was mounted in 25.4 cm (10 in) stove pipe (figure B.1). The anemometers were acquired from R.M. Young Co. of Traverse City, MI, 231-946-3980. They were model 27106, Gill Propeller Anemometer. The anemometer produced a dc voltage which was proportional to the wind velocity. It was made with a light weight propeller and ball bearings and was able to sense low airflows.

Each anemometer and tube assembly was mounted to the KSU BAE Dept airflow chamber for calibration. The KSU airflow chamber contained an adjustable fan, precision airflow nozzles, and a micro-manometer for measuring the pressure across the nozzles at varied airflows. Twelve airflow measurements were obtained per instrument and per mounting direction. Two airflow calibration chart are shown in (figures B.2 and B.3).

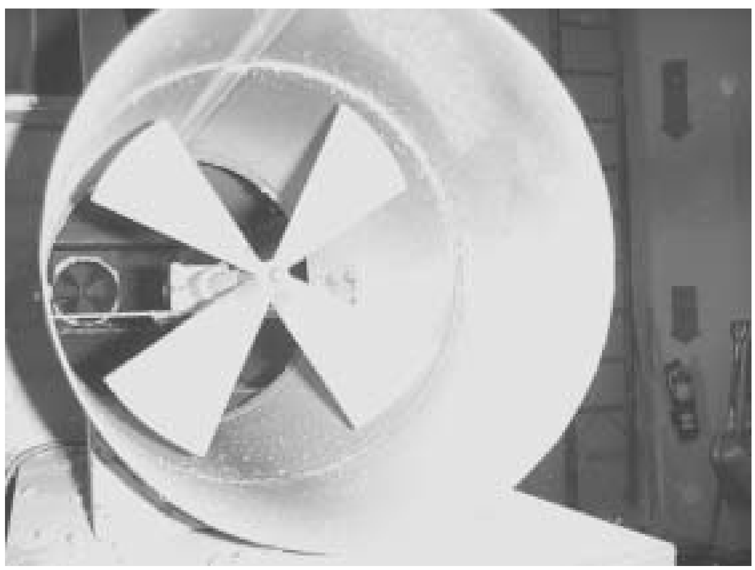

Figure B.1: Photo of propeller anemometer mounted inside tubing.

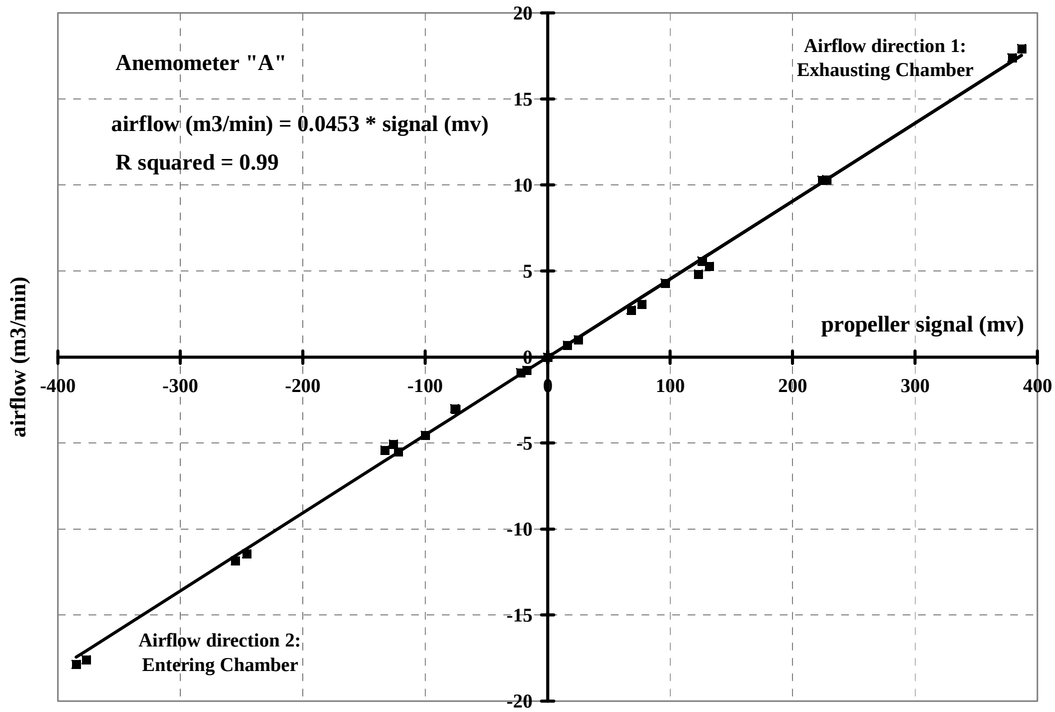

Figure B.2: Chart of calibration data and regression line for anemometer A.

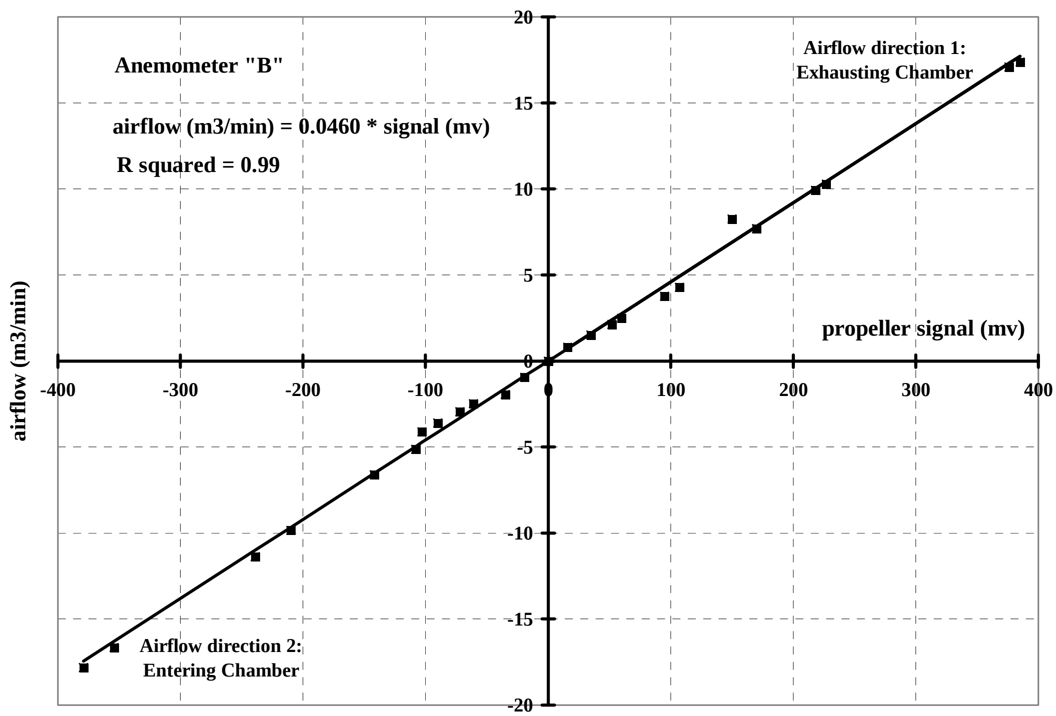

Figure B.3: Chart of calibration data and regression line for anemometer B.

Appendix C: High volume air sampler calibration

Two high-volume air samplers were used to collect dust and fog emission samples from the outlet of the propeller anemometers. The air sampler had a variable speed blower which was adjusted using a vari-ac control. A propeller anemometer assembly was used as the reference airflow measurement instrument. During calibration, a 50.8 cm (20 in.) extension tube and mounting flanged connected the sampler to the propeller anemometer assembly. The sampler's airflow rate was adjusted to one of nine levels and for three replicates. The static pressure at the air sampler's outlet was recorded and correlated to the airflow measured with the propeller anemometer.

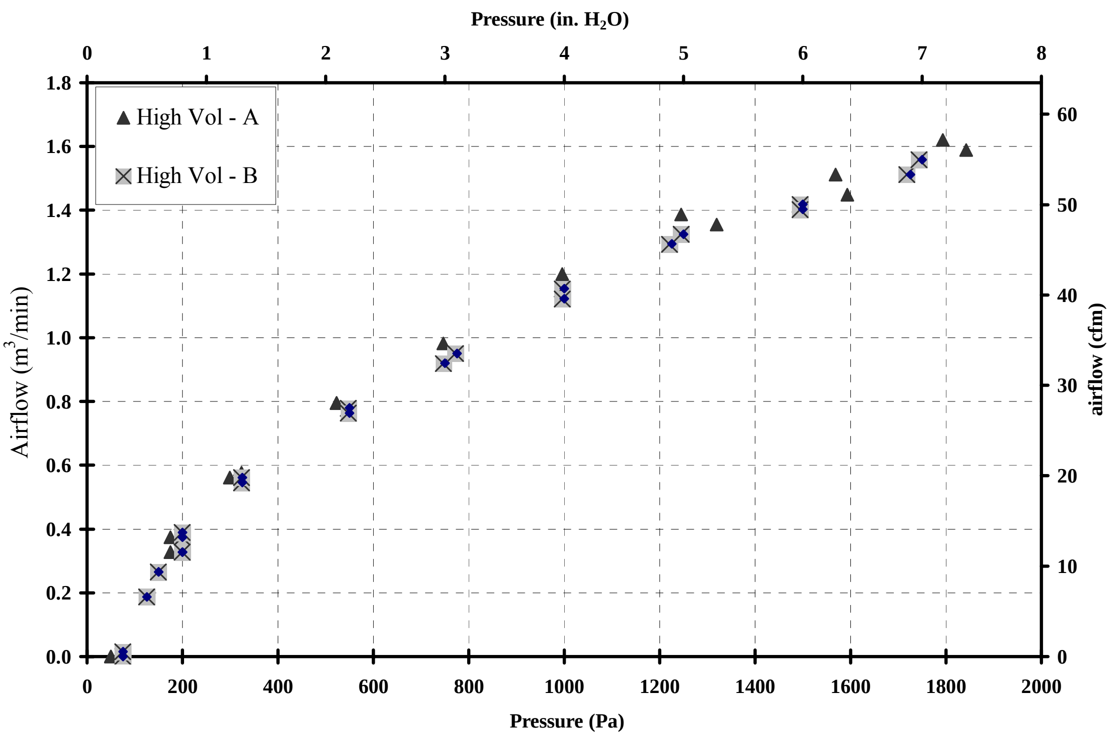

Figure C.1: Calibration chart for two high-volume air samplers.

Appendix D: Baseline grain dust emissions data

Corn and wheat grain shipments of 35 m^3 (1000 bu) were received. The grain drop trials used 2.1 m^3 (60 bu) sublots. To measure the dust emission variability between sublots, dust emissions were measured for 12 consecutive grain drops for each grain (720 bu). The first 4.2 m^3 (120 bu) were passed through the test chamber before grain drop #1 and collection of emission data. The entire 35 m^3 (1000 bu) was cycled through the elevator dump hopper and bucket elevator as one batch and stored into an overhead bin before each group of trials during subsequent testing.

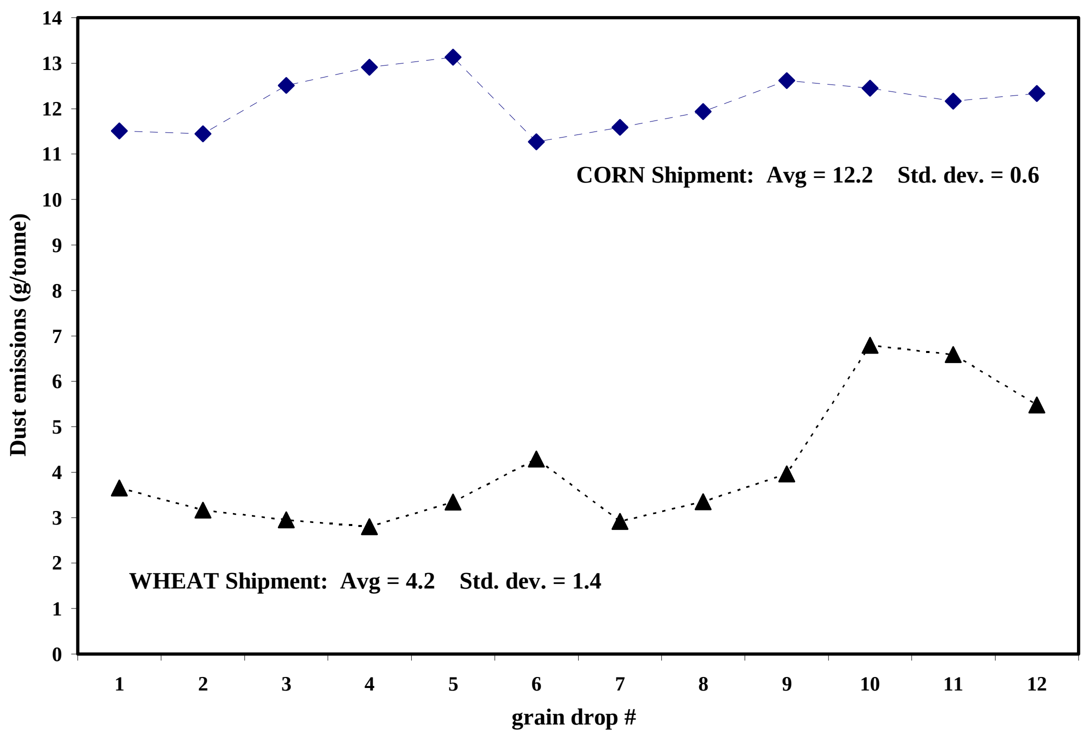

Figure D.1: Pretest grain dust emissions for 12 consecutive grain drops.

Appendix E: Test series I airflow, emissions, deposition data

Test series I studied four spray-fog treatments with two grains and and two grain flows. The experiment was organized as a randomized split-plot design. The wheat was tested in September of 2001 when the outside temperature was around 32.2°C (90°F) and the r.h. was 50%. The corn was tested in October of 2001 with outside temperatures near 29.5°C (85 °F).

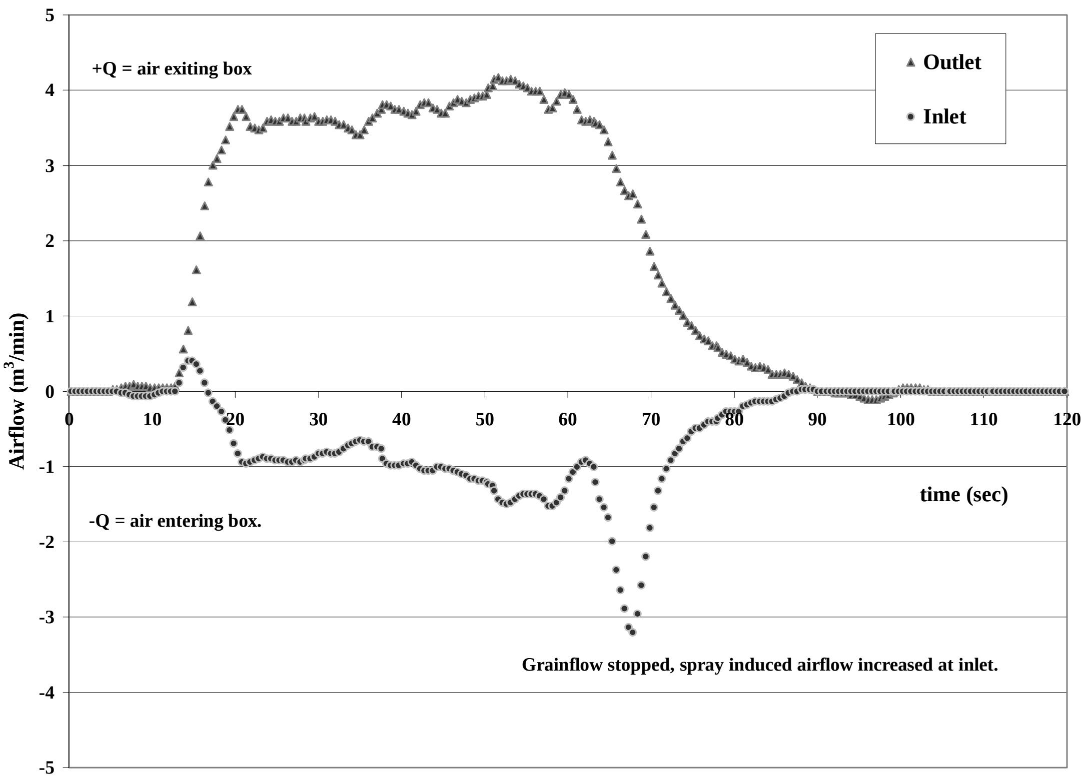

Figure E.1: PC data from the propeller anemometers.
For test W3-39 (9 nozzles @ 6.9 MPa with wheat and grain-flow at 2.5 m^3/min).

Table E.1: Index of grain drop trials for wheat

Trial #	Trt.	Grain-flow
w1-1	control	full
w1-2	control	part
w1-3	blower	full
w1-4	blower	part
w1-5b	S1	full
w1-6b	S1	part
w1-7b	S2	full
w1-8b	S2	part
w1-9b	S3	full
w1-10b	S3	part
w1-11	S4	full
w1-12	S4	part
w2-19	control	full
w2-20	control	part
w2-21	blower	full
w2-22	blower	part
w2-23	S2	full
w2-24	S2	part
w2-25	S1	full
w2-26	S1	part
w2-27	S4	full
w2-28	S4	part
w2-29	S3	full
w2-30	S3	part
w3-31	blower	full
w3-32	blower	part
w3-33	control	full
w3-34	control	part
w3-35	S3	full
w3-36	S3	part
w3-37	S4	full
w3-38	S4	part
w3-39	S1	full
w3-40	S1	part
w3-41	S2	full
w3-42	S2	Part

Table E.2: Average airflow rates at the inlet and exit during wheat drop test. A positive number represented outflow while a negative number represented inflow.

Wheat trials		Avg. airflow	
Trt.	Grain-flow	Outlet	Inlet
		m^3/min	m^3/min
control	f	1.4	1.4
blower	f	4.5	-2.4
S1	f	3.9	-1.1
S2	f	3.3	-0.4
S3	f	3.0	0.0
S4	f	2.3	0.6
control	p	1.1	1.1
blower	p	4.1	-2.4
S1	p	3.7	-1.4
S2	p	3.1	-0.8
S3	p	2.8	-0.4
S4	p	2.3	0.1

Table E.3: Airflows at the outlet and high-volume sampler airflow.

Exhaust air Filename	Trt.	Grain-flow	Avg1 full(20-60) m^3/min	High-vol. rate 25% * avg m^3/min
w1-1	control	full	1.33	0.34
w2-19	control	full	1.37	
w3-33	control	full	1.40	
w1-3	blower	full	4.41	1.10
w2-21	blower	full	4.51	
w3-31	blower	full	4.53	
w1-5b	S1	full	3.87	0.93
w2-25	S1	full	3.71	
w3-39	S1	full	3.75	
w1-7b	S2	full	3.26	0.82
w2-23	S2	full	3.23	
w3-41	S2	full	3.45	
w1-9b	S3	full	2.97	0.74
w2-29	S3	full	2.96	
w3-35	S3	full	2.97	
w1-11	S4	full	2.28	0.59
w2-27	S4	full	2.43	
w3-37	S4	full	2.42	

Table E.4: Dust and fog emission data for wheat-rep#1.

Trial no.	Trt.	Filter ID:	Before	After1	After2				
			tare wt.	wt(1): wet	wt(2): dry	dust wt	water wt	Dust	Water
			g	g	g	g	g	g	g
1	C, f	inlet	3.550	4.750	4.742	1.19	0.01	2.33	0.02
		outlet	3.552	4.700	4.690	1.14	0.01		
2	C, p	inlet	3.557	4.738	4.728	1.17	0.01	2.43	0.02
		outlet	3.550	4.813	4.807	1.26	0.01		
3	blw, f	inlet	3.538	3.548	3.547	0.01	0.00	1.72	-0.02
		outlet	3.550	5.240	5.262	1.71	-0.02		
4	blw, p	inlet	3.540	3.570	3.568	0.03	0.00	3.33	-0.03
		outlet	3.537	6.809	6.837	3.30	-0.03		
5	S1, f	out-1	3.550	9.308	3.838	0.29	5.47	0.56	8.70
		out-2	3.571	7.070	3.843	0.27	3.23		
6	S1, p	out-1	3.546	9.790	3.889	0.34	5.90	0.64	10.57
		out-2	3.559	8.524	3.857	0.30	4.67		
7	S2, f	out-1	3.549	7.380	3.884	0.34	3.50	0.59	5.76
		out-2	3.556	6.072	3.807	0.25	2.27		
8	S2, p	out-1	3.566	7.860	3.958	0.39	3.90	0.71	7.04
		out-2	3.571	7.030	3.889	0.32	3.14		
9	S3, f	inlet	3.566	3.585	3.614	0.05	-0.03	0.79	4.02
		outlet	3.629	8.423	4.372	0.74	4.05		
10	S3, p	inlet	3.536	3.543	3.548	0.01	0.00	0.75	4.76
		outlet	3.540	9.040	4.275	0.74	4.77		
11	S4, f	inlet	3.516	4.020	3.990	0.47	0.03	1.60	2.38
		outlet	3.533	7.015	4.662	1.13	2.35		
12	S4, p	inlet	3.540	3.968	3.944	0.40	0.02	2.35	2.87
		outlet	3.537	8.326	5.481	1.94	2.85		

Table E.5: Dust and fog emission data for wheat-rep#2.

Trial no.	Trt.	Filter ID:	Before	After1	After2				
			tare wt.	wt(1): wet	wt(2): dry	dust wt	water wt	Dust	Water
			g	g	g	g	g	g	g
19	C, f	inlet	3.542	4.850	4.829	1.29	0.02	2.53	0.04
		outlet	3.537	4.797	4.775	1.24	0.02		
20	C, p	inlet	3.559	4.912	4.892	1.33	0.02	2.71	0.04
		outlet	3.553	4.953	4.928	1.38	0.03		
21	blw, f	out-1	3.568	4.712	4.707	1.14	0.00	1.78	0.00
		out-2	3.564	4.205	4.208	0.64	0.00		
22	blw, p	out-1	3.571	5.002	4.800	1.23	0.20	2.30	0.21
		out-2	3.576	4.647	4.642	1.07	0.00		
23	S2, f	out-1	3.575	7.328	3.906	0.33	3.42	0.55	6.33
		out-2	3.571	6.696	3.792	0.22	2.90		
24	S2, p	out-1	3.604	7.782	4.105	0.50	3.68	0.81	7.45
		out-2	3.669	7.742	3.974	0.31	3.77		
25	S1, f	out-1	3.562	9.120	3.905	0.34	5.22	0.60	7.72
		out-2	3.565	6.327	3.824	0.26	2.50		
26	S1, p	out-1	3.573	10.025	4.001	0.43	6.02	0.69	10.31
		out-2	3.557	8.104	3.814	0.26	4.29		
27	S4, f	inlet	3.567	3.856	3.863	0.30	-0.01	1.02	2.23
		outlet	3.568	6.529	4.296	0.73	2.23		
28	S4, p	inlet	3.577	3.770	3.774	0.20	0.00	1.14	2.04
		outlet	3.582	6.568	4.524	0.94	2.04		
29	S3, f	inlet	3.578	3.593	3.594	0.02	0.00	0.75	4.08
		outlet	3.590	8.407	4.324	0.73	4.08		
30	S3, p	out-1	3.663	6.537	4.212	0.55	2.33	0.91	4.14
		out-2	3.648	5.820	4.009	0.36	1.81		

Table E.6: Dust and fog emission data for wheat-rep#3.

Trial no.	Trt.	Filter ID:	Before	After1	After2				
			tare wt.	wt(1): wet	wt(2): dry	dust wt	water wt	Dust	Water
			g	g	g	g	g	g	g
31	blw, f	out-1	3.604	4.700	4.704	1.10	0.00	1.66	0.00
		out-2	3.601	4.159	4.160	0.56	0.00		
32	blw, p	out-1	3.554	5.044	5.048	1.49	0.00	2.27	-0.01
		out-2	3.584	4.353	4.359	0.78	-0.01		
33	C, f	inlet	3.659	4.370	4.375	0.72	0.00	1.41	-0.01
		outlet	3.665	4.351	4.360	0.70	-0.01		
34	C, p	inlet	3.646	4.673	4.676	1.03	0.00	2.06	-0.01
		outlet	3.658	4.685	4.691	1.03	-0.01		
35	S3, f	inlet	3.670	3.687	3.687	0.02	0.00	0.72	3.64
		outlet	3.652	7.996	4.353	0.70	3.64		
36	S3, p	out-1	3.635	6.490	4.265	0.63	2.23	0.99	3.89
		out-2	3.648	5.675	4.007	0.36	1.67		
37	S4, f	inlet	3.622	3.805	3.805	0.18	0.00	0.66	1.98
		outlet	3.629	6.090	4.110	0.48	1.98		
38	S4, p	inlet	3.607	3.792	3.791	0.18	0.00	1.18	2.54
		outlet	3.616	7.148	4.608	0.99	2.54		
39	S1, f	out-1	3.587	9.122	3.918	0.33	5.20	0.56	7.71
		out-2	3.612	6.348	3.845	0.23	2.50		
40	S1, p	out-1	3.591	9.175	4.268	0.68	4.91	0.98	9.16
		out-2	3.602	8.155	3.907	0.31	4.25		
41	S2, f	out-1	3.591	8.060	3.991	0.40	4.07	0.58	6.03
		out-2	3.590	5.730	3.768	0.18	1.96		
42	S2, p	out-1	3.607	8.092	4.134	0.53	3.96	0.90	7.37
		out-2	3.610	7.388	3.979	0.37	3.41		

Table E.7: Dust and fog deposits for wheat at the outlet.

Wheat Trials		Deposits					
Trt.	Rep.	A1: ledge, exit		A2: front wall, exit		A3: Side wall, exit	
		Dust wt	Water wt	Dust wt	Water wt	Dust wt	Water wt
		g	g	g	g	g	g
control, f	1	0.034	-0.002	0.053	-0.001	0.049	0.007
control, p	1	0.025	-0.002	0.018	-0.001	0.016	-0.001
blower, f	1	0.020	-0.006	0.010	-0.006	0.010	-0.006
blower, p	1	0.040	-0.011	0.018	-0.012	0.017	-0.011
S1,f	1	0.006	0.608	-0.006	0.238	-0.008	0.113
S1,p	1	0.009	0.633	-0.003	0.126	-0.004	0.113
S2,f	1	0.016	0.468	0.000	0.076	0.000	0.095
S2,p	1	0.019	0.594	0.000	0.148	0.003	0.140
S3,f	1	0.016	0.212	-0.002	0.050	-0.003	0.046
S3,p	1	0.008	0.268	-0.007	0.051	-0.008	0.043
S4,f	1	0.049	0.133	0.029	0.023	0.031	0.052
S4,p	1	0.077	0.171	0.028	0.024	0.027	0.037
control, f	2	0.025	0.009	0.009	0.006	0.008	0.007
control, p	2	0.028	0.004	0.011	0.004	0.005	0.005
blower, f	2	0.021	0.000	0.010	-0.001	0.012	-0.002
blower, p	2	0.028	0.002	0.012	0.002	0.013	0.001
S2,f	2	0.024	0.490	0.014	0.125	0.017	0.118
S2,p	2	0.035	0.708	0.017	0.123	0.017	0.145
S1,f	2	0.025	0.426	0.013	0.118	0.014	0.139
S1,p	2	0.034	0.690	0.018	0.126	0.018	0.206
S4,f	2	0.030	0.144	0.012	0.019	0.012	0.011
S4,p	2	0.028	0.095	0.013	0.007	0.013	0.009
S3,f	2	0.028	0.198	0.013	0.045	0.011	0.026
S3,p	2	0.031	0.205	0.014	0.028	0.015	0.027
blower, f	3	0.030	-0.004	0.023	-0.009	0.025	-0.013
blower, p	3	0.029	-0.003	0.019	-0.008	0.021	-0.008
control, f	3	0.022	-0.006	0.014	-0.005	0.013	-0.004
control, p	3	0.024	-0.002	0.016	-0.003	0.013	-0.003
S3,f	3	0.037	0.173	0.022	0.029	0.022	0.022
S3,p	3	0.041	0.244	0.022	0.038	0.020	0.044
S4,f	3	0.035	0.153	0.021	0.031	0.019	0.024
S4,p	3	0.040	0.157	0.020	0.025	0.020	0.025
S1,f	3	0.043	0.610	0.051	0.178	0.026	0.133
S1,p	3	0.044	0.703	0.029	0.135	0.030	0.210
S2,f	3	0.042	0.444	0.028	0.123	0.027	0.127
S2,p	3	0.048	0.566	0.027	0.116	0.027	0.113

Table E.8: Dust and fog deposits for wheat at the inlet.

Wheat trials		Deposits					
Trt.	Rep.	B1: ledge, inlet		B2: front wall, inlet		B3: side wall, inlet	
		Dust wt	Water wt	Dust wt	Water wt	Dust wt	Water wt
		g	g	g	g	g	g
control, f	1	0.029	0.004	0.042	0.006	0.038	0.008
control, p	1	0.025	0.000	0.015	-0.001	0.014	-0.001
blower, f	1	0.011	-0.004	0.011	-0.006	0.011	-0.006
blower, p	1	0.015	-0.013	0.016	-0.012	0.015	-0.011
S1,f	1	-0.005	0.172	-0.004	0.124	-0.007	0.164
S1,p	1	-0.001	0.249	-0.003	0.126	0.000	0.267
S2,f	1	0.007	0.124	0.002	0.090	0.003	0.057
S2,p	1	0.007	0.098	0.001	0.038	0.001	0.033
S3,f	1	0.010	0.240	0.003	0.076	0.007	0.373
S3,p	1	-0.001	0.268	-0.002	0.093	-0.002	0.103
S4,f	1	0.032	0.118	0.033	0.041	0.053	0.022
S4,p	1	0.077	0.092	0.042	0.061	0.043	0.074
control, f	2	0.031	0.008	0.009	0.006	0.006	0.013
control, p	2	0.031	0.005	0.012	0.005	0.007	0.005
blower, f	2	0.009	0.000	0.010	0.000	0.011	-0.001
blower, p	2	0.008	0.004	0.011	0.002	0.011	0.001
S2,f	2	0.020	0.109	0.015	0.062	0.016	0.072
S2,p	2	0.020	0.118	0.017	0.092	0.018	0.092
S1,f	2	0.018	0.224	0.015	0.173	0.015	0.228
S1,p	2	0.021	0.208	0.020	0.165	0.026	1.334
S4,f	2	0.032	0.091	0.017	0.011	0.017	0.016
S4,p	2	0.029	0.069	0.016	0.035	0.015	0.009
S3,f	2	0.022	0.216	0.019	0.118	0.024	0.707
S3,p	2	0.023	0.251	0.017	0.118	0.026	1.054
blower, f	3	0.016	-0.002	0.020	-0.005	0.025	-0.011
blower, p	3	0.012	-0.003	0.014	-0.003	0.017	-0.006
control, f	3	0.025	-0.009	0.014	-0.006	0.013	-0.004
control, p	3	0.025	-0.004	0.016	-0.003	0.017	-0.004
S3,f	3	0.031	0.223	0.030	0.099	0.029	0.082
S3,p	3	0.030	0.248	0.028	0.087	0.035	0.546
S4,f	3	0.034	0.096	0.024	0.027	0.024	0.023
S4,p	3	0.039	0.149	0.023	0.029	0.025	0.028
S1,f	3	0.031	0.120	0.030	0.144	0.031	0.311
S1,p	3	0.029	0.170	0.029	0.105	0.034	0.278
S2,f	3	0.041	0.228	0.030	0.096	0.031	0.081
S2,p	3	0.036	0.172	0.029	0.108	0.029	0.082

Table E.9: Index of grain drop trials for corn.

Trial #	Trt.	Grain-flow
c1-43	control	full
c1-44	control	partial
c1-45	blower	full
c1-46	blower	partial
c1-47	S1	full
c1-48	S1	partial
c1-49	S2	full
c1-50	S2	partial
c1-51	S3	full
c1-52	S3	partial
c1-52r	S3	partial
c1-53	S4	full
c1-54	S4	partial
c1-55	control	full
c2-57	blower	full
c2-58	blower	partial
c2-59	control	full
c2-60	control	partial
c2-61	S3	full
c2-62	S3	partial
c2-63	S4	full
c2-64	S4	partial
c2-65	S2	full
c2-66	S2	partial
c2-67	S1	full
c2-68	S1	partial
c2-69	control	full
c3-71	S2	full
c3-72	S2	partial
c3-73	S1	full
c3-74	S1	partial
c3-75	S4	full
c3-76	S4	partial
c3-77	S3	full
c3-78	S3	partial
c3-79	control	full
c3-80	control	partial
c3-81	blower	full
c3-82	blower	partial
c3-83	control	full

Table E.10: Airflow data for corn at 2.5 m^3/min (72 bu/min).

Trt.	Outlet	Inlet
	m^3/min	m^3/min
blower	4.49	-2.41
S1	3.92	-1.12
S2	3.45	-0.48
S3	3.04	-0.03
S4	2.42	0.44
control	1.41	1.50

Note: positive number mean air exiting test-box and vice versa.

Test no.	Trt.	Grain-flow	Outlet m^3/min	Inlet m^3/min	Outlet avg.	Inlet avg.
c1-45	blower	full	4.42	-2.45	4.49	-2.41
c2-57	blower	full	4.54	-2.40		
c3-81	blower	full	4.51	-2.37		
c1-47	S1	full	3.79	-1.00	3.92	-1.12
c2-67	S1	full	4.00	-1.17		
c3-73	S1	full	3.96	-1.19		
c1-49	S2	full	3.46	-0.37	3.45	-0.48
c2-65	S2	full	3.41	-0.39		
c3-71	S2	full	3.49	-0.67		
c1-51	S3	full	3.21	-0.08	3.04	-0.03
c2-61	S3	full	3.03	0.00		
c3-77	S3	full	2.87	0.01		
c1-53	S4	full	2.47	0.38	2.42	0.44
c2-63	S4	full	2.43	0.41		
c3-75	S4	full	2.38	0.53		
c1-43	control	full	1.38	1.48	1.41	1.50
c1-55	control	full	1.35	1.48		
c2-59	control	full	1.44	1.51		
c2-69	control	full	1.43	1.58		
c3-79	control	full	1.42	1.46		
c3-83	control	full	1.45	1.52		

Table E.11: Airflow data for corn at 1.7 m^3/min (48 bu/min).

Trt.	Outlet	Inlet
	m^3/min	m^3/min
blower	4.21	-2.43
S1	3.96	-1.19
S2	3.51	-0.34
S3	3.01	-0.01
S4	2.32	0.48
control	1.40	1.39

Note: positive number mean air exiting test-box and vice versa.

Test no.	Trt.	Grain-flow	Outlet	Inlet	Outlet	Inlet
			m^3/min	m^3/min	avg.	avg.
c1-46	blower	partial	4.20	-2.48	4.21	-2.43
c2-58	blower	partial	4.25	-2.40		
c3-82	blower	partial	4.20	-2.41		
c1-48	S1	partial	3.88	-1.18	3.96	-1.19
c2-68	S1	partial	3.98	-1.21		
c3-74	S1	partial	4.01	-1.18		
c1-50	S2	partial	3.76	-0.40	3.51	-0.34
c2-66	S2	partial	3.38	-0.21		
c3-72	S2	partial	3.38	-0.40		
c1-52r	S3	partial	3.00	-0.01	3.01	-0.01
c2-62	S3	partial	3.02	-0.03		
c3-78	S3	partial	3.01	0.00		
c1-54	S4	partial	2.39	0.42	2.32	0.48
c2-64	S4	partial	2.40	0.44		
c3-76	S4	partial	2.16	0.58		
c2-60	control	partial	1.41	1.37	1.40	1.39
c3-80	control	partial	1.40	1.40		

Table E.12: Dust and fog emission data for corn-rep#1.

Trial no.	Trt.	Filter ID:	Before	After1	After2				
			tare wt.	wt(1): wet	wt(2): dry	dust wt	water wt	Dust	Water
			g	g	g	g	g	g	g
43	C, f	out	3.627	6.501	6.468	2.84	0.03	5.75	0.07
		inlet	3.649	6.594	6.556	2.91	0.04		
44	C, p	out	3.639	10.696	10.623	6.98	0.07	12.79	0.14
		inlet	3.641	9.510	9.447	5.81	0.06		
45	blw, f	out-1	3.636	6.438	6.410	2.77	0.03	6.50	0.07
		out-2	3.629	7.395	7.356	3.73	0.04		
46	blw, p	out-1	3.639	7.399	7.357	3.72	0.04	11.28	0.12
		out-2	3.653	11.296	11.214	7.56	0.08		
47	S1, f	out-1	3.653	9.901	4.621	0.97	5.28	1.52	6.82
		out-2	3.650	5.736	4.200	0.55	1.54		
48	S1, p	out-1	3.648	11.601	5.010	1.36	6.59	2.15	9.07
		out-2	3.645	6.920	4.437	0.79	2.48		
49	S2, f	out-1	3.632	10.690	5.000	1.37	5.69	1.37	5.69
		out-2				0.00	0.00		
50	S2, p	out-1	3.634	12.123	5.818	2.18	6.31	2.64	7.87
		out-2	3.634	5.653	4.086	0.45	1.57		
51	S3, f	out	3.636	8.930	5.289	1.65	3.64	1.69	3.64
		inlet	3.651	3.688	3.687	0.04	0.00		
52	S3, p	out-1	3.661	12.151	6.852	3.19	5.30	3.19	5.30
		out-2				0.00	0.00		
53	S4, f	out	3.657	7.953	5.209	1.55	2.74	2.48	2.78
		inlet	3.669	4.635	4.600	0.93	0.04		
54	S4, p	out	3.672	9.301	6.287	2.62	3.01	3.82	3.08
		inlet	3.664	4.940	4.873	1.21	0.07		
55	C, f	out	3.634	6.483	6.465	2.83	0.02	5.30	0.03
		inlet	3.646	6.134	6.119	2.47	0.02		
56	ref	ref	3.643	3.677	3.677	0.03	0.00	0.08	0.00
		ref	3.634	3.678	3.678	0.04	0.00		

Table E.13: Dust and fog emission data for corn-rep#2.

Trial no.	Trt.	Filter ID:	Before	After1	After2				
			tare wt.	wt(1): wet	wt(2): dry	dust wt	water wt	Dust	Water
			g	g	g	g	g	g	g
57	blw, f	out-1	3.631	6.489	6.438	2.81	0.05	5.29	0.10
		out-2	3.625	6.162	6.111	2.49	0.05		
58	blw, p	out-1	3.638	7.293	7.231	3.59	0.06	7.69	0.14
		out-2	3.638	7.818	7.737	4.10	0.08		
59	C, f	out	3.608	6.134	6.099	2.49	0.04	5.03	0.09
		inlet	3.614	6.198	6.148	2.53	0.05		
60	C, p	out	3.601	8.311	8.239	4.64	0.07	8.36	0.11
		inlet	3.603	7.364	7.326	3.72	0.04		
61	S3, f	out	3.586	8.515	4.565	0.98	3.95	1.00	3.95
		inlet	3.594	3.615	3.615	0.02	0.00		
62	S3, p	out-1	3.586	6.853	4.366	0.78	2.49	1.86	4.37
		out-2	3.584	6.547	4.665	1.08	1.88		
63	S4, f	out	3.607	7.010	4.764	1.16	2.25	1.84	2.33
		inlet	3.594	4.360	4.274	0.68	0.09		
64	S4, p	out	3.600	8.296	5.793	2.19	2.50	3.10	2.68
		inlet	3.602	4.681	4.509	0.91	0.17		
65	S2, f	out-1	3.678	7.014	4.339	0.66	2.68	1.15	5.82
		out-2	3.680	7.310	4.169	0.49	3.14		
66	S2, p	out-1	3.689	7.550	4.335	0.65	3.22	1.34	8.16
		out-2	3.674	9.313	4.372	0.70	4.94		
67	S1, f	out-1	3.628	8.357	4.040	0.41	4.32	0.67	7.90
		out-2	3.627	7.467	3.880	0.25	3.59		
68	S1, p	out-1	3.627	8.900	4.219	0.59	4.68	1.19	10.79
		out-2	3.616	10.320	4.211	0.60	6.11		
69	C, f	out	3.608	5.699	5.67	2.06	0.03	4.27	0.02
		inlet	3.741	5.943	5.948	2.21	-0.01		
70	ref.	ref	3.046	3.046	3.047	0.00	0.00	0.00	0.00
		ref	3.080	3.080	3.083	0.00	0.00		

Table E.14: Dust and fog emission data for corn-rep#3.

Trial no.	Trt.	Filter ID:	Before	After1	After2				
			tare wt.	wt(1): wet	wt(2): dry	dust wt	water wt	Dust	Water
			g	g	g	g	g	g	g
71	S2, f	out-1	3.047	5.920	3.607	0.56	2.31	0.86	5.65
		out-2	3.086	6.726	3.386	0.30	3.34		
72	S2, p	out-1	3.629	8.055	4.242	0.61	3.81	1.35	8.43
		out-2	3.625	8.978	4.360	0.74	4.62		
73	S1, f	out-1	3.624	7.852	4.119	0.50	3.73	0.80	8.28
		out-2	3.631	8.485	3.936	0.31	4.55		
74	S1, p	out-1	3.640	9.830	4.176	0.54	5.65	1.01	11.82
		out-2	3.636	10.273	4.106	0.47	6.17		
75	S4, f	out	3.632	6.854	4.550	0.92	2.30	1.41	2.57
		inlet	3.643	4.394	4.130	0.49	0.26		
76	S4, p	out	3.652	8.043	5.716	2.06	2.33	2.86	3.01
		inlet	3.651	5.130	4.451	0.80	0.68		
77	S3, f	out	3.650	8.400	4.499	0.85	3.90	0.92	3.91
		inlet	3.648	3.726	3.716	0.07	0.01		
78	S3, p	out-1	3.629	7.010	4.200	0.57	2.81	1.47	5.39
		out-2	3.641	7.116	4.537	0.90	2.58		
79	C, f	out	3.642	5.530	5.530	1.89	0.00	3.60	0.00
		inlet	3.637	5.345	5.345	1.71	0.00		
80	C, p	out	3.661	7.000	7.000	3.34	0.00	6.28	0.00
		inlet	3.652	6.596	6.596	2.94	0.00		
81	blw, f	out-1	3.667	6.294	6.294	2.63	0.00	4.90	0.00
		out-2	3.666	5.942	5.942	2.28	0.00		
82	blw, p	out-1	3.652	7.406	7.406	3.75	0.00	8.14	0.00
		out-2	3.649	8.032	8.032	4.38	0.00		
83	C	out	3.618	5.973	5.973	2.36	0.00	4.61	0.00
		inlet	3.878	6.130	6.130	2.25	0.00		

Table E.15: Dust and fog deposits for corn at the outlet.

Corn trials			Deposits					
			A1: ledge, exit		A2: front wall, exit		A3: side wall, exit	
Trt.	Grain flow	Rep.	Dust wt	Water wt	Dust wt	Water wt	Dust wt	Water wt
			g	g	g	g	g	g
control	F	1	0.108	0.005	0.042	0.005	0.036	0.006
control	P	1	0.283	0.008	0.085	0.005	0.028	0.008
blower	F	1	0.143	0.007	0.037	0.004	0.029	0.002
blower	P	1	0.230	0.007	0.057	0.003	0.074	0.004
S1	F	1	0.089	0.641	0.039	0.250	0.022	0.126
S1	P	1	0.136	0.729	0.045	0.264	0.032	0.153
S2	F	1	0.084	0.469	0.032	0.108	0.025	0.097
S2	P	1	0.140	0.697	0.035	0.134	0.039	0.161
S3	F	1	0.072	0.204	0.016	0.043	0.013	0.032
S3	P	1	0.157	0.483	0.034	0.109	0.026	0.068
S4	F	1	0.071	0.208	0.013	0.043	0.015	0.046
S4	P	1	0.102	0.187	0.014	0.031	0.029	0.064
blower	F	2	0.112	0.014	0.022	0.008	0.019	0.009
blower	P	2	0.184	0.009	0.043	0.007	0.042	0.006
control	F	2	0.094	0.007	0.031	0.007	0.025	0.006
control	P	2	0.189	0.010	0.073	0.007	0.057	0.013
S3	F	2	0.049	0.246	0.008	0.061	0.007	0.065
S3	P	2	0.080	0.347	0.012	0.054	0.014	0.047
S4	F	2	0.061	0.191	0.008	0.041	0.008	0.041
S4	P	2	0.117	0.221	0.017	0.049	0.015	0.036
S2	F	2	0.091	0.527	0.038	0.168	0.032	0.131
S2	P	2	0.103	1.075	0.030	0.177	0.053	0.406
S1	F	2	0.060	0.792	0.035	0.518	0.021	0.114
S1	P	2	0.089	1.002	0.042	0.456	0.039	0.249
S2	F	3	0.065	0.587	0.026	0.173	0.017	0.128
S2	P	3	0.097	0.878	0.032	0.329	0.033	0.296
S1	F	3	0.063	0.708	0.030	0.348	0.019	0.191
S1	P	3	0.086	0.953	0.036	0.578	0.024	0.229
S4	F	3	0.057	0.209	0.011	0.070	0.008	0.057
S4	P	3	0.115	0.246	0.017	0.071	0.016	0.059
S3	F	3	0.044	0.251	0.007	0.073	0.009	0.065
S3	P	3	0.077	0.345	0.011	0.090	0.014	0.083
control	F	3	0.084	0.000	0.022	0.000	0.020	0.000
control	P	3	0.176	0.000	0.062	0.000	0.046	0.000
blower	F	3	0.119	0.000	0.024	0.000	0.019	0.000
blower	P	3	0.218	0.000	0.051	0.000	0.041	0.000

Table E.16: Dust and fog deposits for corn at the inlet.

Corn trials			Deposits					
			B1: ledge, inlet		B2: front wall, inlet		B3: side wall, inlet	
Trt.	Grain flow	Rep.	Dust wt	Water wt	Dust wt	Water wt	Dust wt	Water wt
			g	g	g	g	g	g
control	F	1	0.094	0.004	0.037	0.004	0.029	0.005
control	P	1	0.216	0.004	0.082	0.004	0.062	0.003
blower	F	1	0.017	0.002	0.035	0.004	0.033	0.004
blower	P	1	0.030	0.001	0.058	0.002	0.050	0.003
S1	F	1	0.051	0.365	0.049	0.181	0.045	0.426
S1	P	1	0.051	0.457	0.037	0.192	0.065	0.839
S2	F	1	0.121	0.205	0.030	0.065	0.040	0.078
S2	P	1	0.139	0.201	0.045	0.110	0.057	0.100
S3	F	1	0.035	0.203	0.047	0.110	0.033	0.093
S3	P	1	0.063	0.381	0.047	0.110	0.101	1.242
S4	F	1	0.103	0.128	0.027	0.045	0.036	0.044
S4	P	1	0.119	0.159	0.033	0.051	0.040	0.049
blower	F	2	0.011	0.008	0.024	0.008	0.019	0.007
blower	P	2	0.017	0.005	0.029	0.005	0.022	0.006
control	F	2	0.093	0.008	0.028	0.006	0.025	0.005
control	P	2	0.137	0.009	0.039	0.006	0.035	0.006
S3	F	2	0.024	0.239	0.017	0.061	0.032	0.309
S3	P	2	0.036	0.300	0.022	0.072	0.069	1.257
S4	F	2	0.068	0.059	0.019	0.045	0.019	0.056
S4	P	2	0.091	0.161	0.025	0.048	0.030	0.045
S2	F	2	0.123	0.322	0.044	0.150	0.047	0.188
S2	P	2	0.088	0.195	0.037	0.164	0.042	0.099
S1	F	2	0.030	0.286	0.034	0.164	0.031	0.077
S1	P	2	0.042	0.479	0.039	0.157	0.063	0.915
S2	F	3	0.075	0.263	0.028	0.126	0.034	0.138
S2	P	3	0.090	0.342	0.037	0.248	0.043	0.173
S1	F	3	0.034	0.631	0.034	0.287	0.029	0.431
S1	P	3	0.024	0.479	0.033	0.291	0.034	0.459
S4	F	3	0.074	0.187	0.019	0.071	0.018	0.066
S4	P	3	0.088	0.255	0.024	0.103	0.028	0.097
S3	F	3	0.031	0.407	0.021	0.101	0.034	0.514
S3	P	3	0.037	0.465	0.025	0.142	0.032	0.443
control	F	3	0.073	0.000	0.019	0.000	0.013	0.000
control	P	3	0.124	0.000	0.024	0.000	0.020	0.000
blower	F	3	0.016	0.000	0.016	0.000	0.015	0.000
Blower	P	3	0.020	0.000	0.023	0.000	0.025	0.000

```
dm 'log; clear; output; clear;';

options date number ls=120 ps=36;

Data;
Input  Number grain $ rep gflow $ trt $ dust mist;

datalines;
43     corn   1      f      control      14.4   0.2
44     corn   1      p      control      32.0   0.4
45     corn   1      f      blower       16.3   0.2
46     corn   1      p      blower       28.2   0.3
47     corn   1      f      S1           3.8    17.1
48     corn   1      p      S1           5.4    22.7
49     corn   1      f      S2           3.4    14.2
50     corn   1      p      S2           6.6    19.7
51     corn   1      f      S3           4.2    9.1
52     corn   1      p      S3           8.0    13.3
53     corn   1      f      S4           6.2    7.0
54     corn   1      p      S4           9.6    7.7
57     corn   2      f      blower       13.2   0.3
58     corn   2      p      blower       19.2   0.4
59     corn   2      f      control      12.6   0.2
60     corn   2      p      control      20.9   0.3
61     corn   2      f      S3           2.5    9.9
62     corn   2      p      S3           4.7    10.9
63     corn   2      f      S4           4.6    5.8
64     corn   2      p      S4           7.8    6.7
65     corn   2      f      S2           2.9    14.6
66     corn   2      p      S2           3.4    20.4
67     corn   2      f      S1           1.7    19.8
68     corn   2      p      S1           3.0    27.0
71     corn   3      f      S2           2.2    14.1
72     corn   3      p      S2           3.4    21.1
73     corn   3      f      S1           2.0    20.7
74     corn   3      p      S1           2.5    29.6
75     corn   3      f      S4           3.5    6.4
76     corn   3      p      S4           7.2    7.5
77     corn   3      f      S3           2.3    9.8
78     corn   3      p      S3           3.7    13.5
79     corn   3      f      control      9.0    0.0
80     corn   3      p      control      15.7   0.0
81     corn   3      f      blower       12.3   0.0
82     corn   3      p      blower       20.4   0.0
```

```
proc print;

run;

proc mixed;
classes grain rep gflow trt;
model dust = gflow trt gflow*trt/ddfm = satterth;
random rep rep*trt;
lsmeans gflow trt gflow*trt/pdiff;
run;

proc mixed;
classes grain rep gflow trt;
model mist= gflow trt gflow*trt/ddfm = satterth;
random rep rep*trt;
lsmeans gflow trt gflow*trt/pdiff;
run;
```

Table F.1: Probability of differences between test treatment emission

Differences of Least Squares Means for corn dust emissions									
Effect	gflow	trt	_gflow	_trt	Diff.	Error	DF	t Value	Pr > |t|
gflow	f		p		-1.87	0.27	12	-7.07	0.00
trt		S1		S2	-0.23	0.58	10	-0.39	0.70
trt		S1		S3	-0.47	0.58	10	-0.8	0.44
trt		S1		S4	-1.36	0.58	10	-2.34	0.04
trt		S1		blower	-6.08	0.58	10	-10.46	0.00
trt		S1		control	-5.75	0.58	10	-9.89	0.00
trt		S2		S3	-0.24	0.58	10	-0.41	0.69
trt		S2		S4	-1.13	0.58	10	-1.95	0.08
trt		S2		blower	-5.85	0.58	10	-10.07	0.00
trt		S2		control	-5.52	0.58	10	-9.5	0.00
trt		S3		S4	-0.90	0.58	10	-1.54	0.15
trt		S3		blower	-5.61	0.58	10	-9.66	0.00
trt		S3		control	-5.28	0.58	10	-9.09	0.00
trt		S4		blower	-4.72	0.58	10	-8.12	0.00
trt		S4		control	-4.38	0.58	10	-7.55	0.00
trt		blower		control	0.33	0.58	10	0.57	0.58
gflow*trt	f	S1	f	S2	-0.13	0.74	19.9	-0.18	0.86
gflow*trt	f	S1	f	S3	-0.21	0.74	19.9	-0.28	0.78
gflow*trt	f	S1	f	S4	-0.91	0.74	19.9	-1.23	0.23
gflow*trt	f	S1	f	blower	-4.57	0.74	19.9	-6.17	0.00
gflow*trt	f	S1	f	control	-3.80	0.74	19.9	-5.13	0.00
gflow*trt	f	S2	f	S3	-0.08	0.74	19.9	-0.10	0.92
gflow*trt	f	S2	f	S4	-0.78	0.74	19.9	-1.06	0.30
gflow*trt	f	S2	f	blower	-4.44	0.74	19.9	-5.99	0.00
gflow*trt	f	S2	f	control	-3.67	0.74	19.9	-4.95	0.00
gflow*trt	f	S3	f	S4	-0.71	0.74	19.9	-0.95	0.35
gflow*trt	f	S3	f	blower	-4.36	0.74	19.9	-5.89	0.00
gflow*trt	f	S3	f	control	-3.59	0.74	19.9	-4.85	0.00
gflow*trt	f	S4	f	blower	-3.65	0.74	19.9	-4.93	0.00
gflow*trt	f	S4	f	control	-2.88	0.74	19.9	-3.89	0.00
gflow*trt	f	blower	f	control	0.77	0.74	19.9	1.04	0.31

Differences of Least Squares Means of corn dust emission (continued)

Effect	gflow	trt	_gflow	_trt	Diff.	Error	DF	t Value	Pr > |t|
gflow*trt	p	S1	p	S2	-0.33	0.74	19.9	-0.44	0.66
gflow*trt	p	S1	p	S3	-0.72	0.74	19.9	-0.98	0.34
gflow*trt	p	S1	p	S4	-1.81	0.74	19.9	-2.44	0.02
gflow*trt	p	S1	p	blower	-7.59	0.74	19.9	-10.25	0.00
gflow*trt	p	S1	p	control	-7.69	0.74	19.9	-10.39	0.00
gflow*trt	p	S2	p	S3	-0.40	0.74	19.9	-0.54	0.60
gflow*trt	p	S2	p	S4	-1.48	0.74	19.9	-2.00	0.06
gflow*trt	p	S2	p	blower	-7.26	0.74	19.9	-9.80	0.00
gflow*trt	p	S2	p	control	-7.37	0.74	19.9	-9.95	0.00
gflow*trt	p	S3	p	S4	-1.09	0.74	19.9	-1.47	0.16
gflow*trt	p	S3	p	blower	-6.86	0.74	19.9	-9.27	0.00
gflow*trt	p	S3	p	control	-6.97	0.74	19.9	-9.41	0.00
gflow*trt	p	S4	p	blower	-5.78	0.74	19.9	-7.80	0.00
gflow*trt	p	S4	p	control	-5.88	0.74	19.9	-7.95	0.00
gflow*trt	p	blower	p	control	-0.11	0.74	19.9	-0.14	0.89
gflow*trt	f	S1	p	S1	-0.45	0.65	12	-0.70	0.50
gflow*trt	f	S2	p	S2	-0.65	0.65	12	-1.00	0.34
gflow*trt	f	S3	p	S3	-0.97	0.65	12	-1.49	0.16
gflow*trt	f	S4	p	S4	-1.35	0.65	12	-2.08	0.06
gflow*trt	f	blower	p	blower	-3.47	0.65	12	-5.35	0.00
gflow*trt	f	control	p	control	-4.35	0.65	12	-6.70	<.0001

Appendix G: Test series II emissions and deposition data

The main objective of test series II, was to test the direct application of the spray-fog to the incoming grain as it entered the test chamber and to see if wetting the grain reduced dust emissions. A second objective to series II was to see if the S2 spray significantly wet the incoming grain and reduced emission. For this test, a removable, 45.7 cm (18 in.) tall chute extension (xchute) was added to cover the incoming grain from the spray plume and minimized S2 fog deposits on grain column. Results showed that the use of the xchute had no effect on reducing amount of dust emissions. But it did affect the amount of side wall deposits because the cross section of the chamber was reduced.

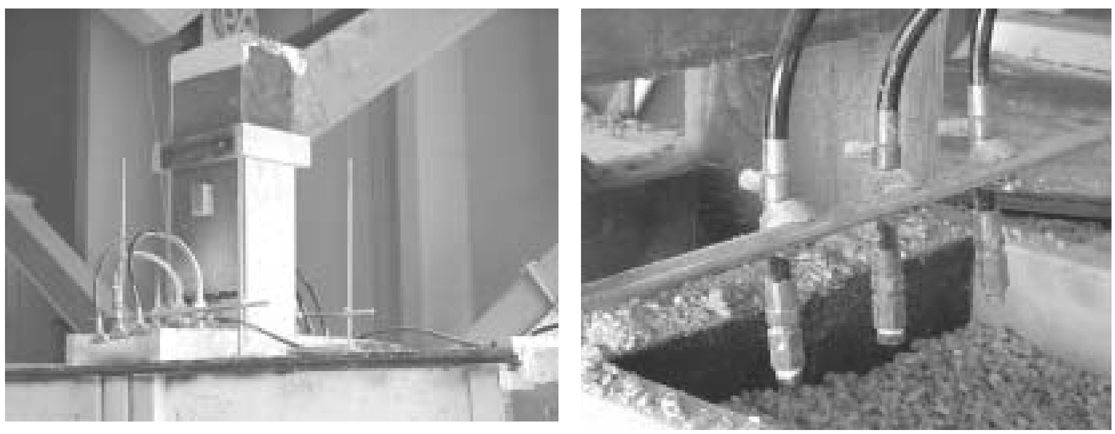

Figure G.1: Spray fog system positioned above test chamber.

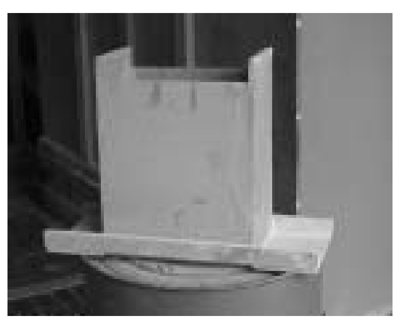

Figure G.2: Wooden, chute extension to cover incoming grain.

Table G.1: Test series II trials and high-volume pressure settings.

Rep	Test #	Treatment	High-vol pressure		Time change for hi-vol2[1]
			Inlet (hv B)	Exit (hv A)	
1	1	Control	0.8"	0.8"	
1	2	Spray S2		2.5"	X-25sec
1	3	Control - xchute	0.8"	0.8"	
1	4	Spray - xchute		2.5"	X-25sec
1	5	Wet Grain 1, 6 nozzles	1	1	
1	6	Wet Grain 1, 6 nozzles	2	2	
2	7	Spray S2		2.6 / 2.5	X-25sec
2	8	Wet Grain 2, 4 nozzles	2	2.1	
2	9	Wet Grain 1, 6 nozzles	2.1	2.2	
2	10	Control	0.8	0.9	
2	11	Control - xchute	0.8	0.9	
2	12	Spray - xchute		2.6 / 2.5	X-25sec
3	13	Wet Grain 1, 6 nozzles	2.1	2.2	
3	14	Wet Grain 2, 4 nozzles	2	2.1	
3	15	Control - xchute	0.8	0.9	
3	16	Spray - xchute		2.6 / 2.5	X-25sec
3	17	Spray S2		2.6 / 2.5	X-25sec
3	18	Control	0.8	0.9	
4	19	Wet Grain 2, 4 nozzles	2	2.1	
4	20	Wet Grain 1, 6 nozzles	2.1	2.2	
4	21	Spray S2		2.6 / 2.5	X-25sec
4	22	Spray - xchute		2.6 / 2.5	X-25sec
4	23	Control - xchute	0.8"	0.9	
4	24	Control	0.8"	0.9	

[1] When the exhaust and emissions were directed out one end, both high volume samplers were used to collect the emission at that end. This column represents the approximate time when the samplers were changed during the grain drop trial.

Table G.2: Test series II dust and fog emissions data.

	Avg.	Std. dev.	Avg.	Std. dev.
	Dust	Dust	Water	Water
Description	g/tonne	g/tonne	g/tonne	g/tonne
Control	17.0	3.1	0.1	0.2
Control + xchute	16.7	4.1	0.2	0.1
Spray S2	4.0	1.1	12.4	1.2
Spray + xchute	4.4	1.6	13.8	1.7
Wet Grain 4 nozzles	22.6	2.6	0.4	0.2
Wet Grain 6 nozzles	23.1	4.2	0.8	0.4

	Rep #1		Rep #2		Rep #3		Rep #4	
	Dust	Water	Dust	Water	Dust	Water	Dust	Water
Description	g	g	g	g	g	g	g	g
Control	8.1	0.0	6.6	0.0	6.0	0.1	5.3	0.1
Control + xchute	7.8	0.0	7.6	0.1	4.7	0.1	5.4	0.1
Spray S2	1.9		1.8	5.0	1.2	4.2	1.2	5.0
Spray + xchute	2.3	5.5	2.1	6.0	1.1	4.6	1.2	4.8
Wet Grain 4nozzles	8.8	0.2	9.9	0.1	8.3	0.2	7.5	0.2
Wet Grain 6 nozzles	10.2	0.5	9.9	0.3	8.5	0.3	6.7	0.2

Table G.3: Test series II dust and fog side wall deposits ($mg/cm^2/min$).

Test ID	Sample location	Avg. dust wt	Std. dev. dust wt	Avg. water wt	Std. dev. water wt
		g	g	g	g
Control	mid(0)	0.2	0.1		
	mid(30)	0.3	0.1		
	mid(90)	0.4	0.1		
Control	mid(0)	0.3	0.1		
+ xchute	mid(30)	0.2	0.1		
	mid(90)	0.3	0.1		
Spray-1	mid(0)	1.2	0.2	11.0	2.8
S2	mid(30)	0.9	0.1	5.3	1.2
	mid(90)	0.5	0.2	1.5	0.3
Spray-2	mid(0)	1.5	0.2	17.4	0.5
S2	mid(30)	0.9	0.1	7.1	1.6
+ xchute	mid(90)	0.5	0.1	2.3	0.4
Xchute	front	1.0	0.1	3.1	0.6
Wet Grain-1	mid(0)	0.3	0.1		
4 nozzles	mid(30)	0.2	0.1		
	mid(90)	0.2	0.0		
Wet Grain-2	mid(0)	0.4	0.0		
6 nozzles	mid(30)	0.3	0.1		
	mid(90)	0.3	0.0		

Table G.4: Test series II dust and fog side wall deposit data.

Test ID	Sample location	Rep#1		Rep#2		Rep#3		Rep#4	
		dust wt	water wt	dust wt	water wt	dust wt	water wt	dust wt	water wt
		g	g	g	g	g	g	g	g
Control	mid(0)	0.029		0.029		0.011		0.015	
	mid(30)	0.043		0.025		0.030		0.031	
	mid(90)	0.055		0.034		0.022		0.031	
Control	mid(0)	0.022		0.032		0.015		0.031	
+ xchute	mid(30)	0.030		0.024		0.012		0.027	
	mid(90)	0.037		0.040		0.023		0.030	
Spray-1	mid(0)			0.095	0.79	0.129	1.33	0.129	1.19
S2	mid(30)			0.082	0.61	0.095	0.60	0.086	0.40
	mid(90)			0.027	0.18	0.053	0.14	0.057	0.12
Spray-2	mid(0)	0.136	1.74	0.158	1.69	0.177	1.80	0.146	1.72
S2	mid(30)	0.085	0.88	0.101	0.79	0.090	0.66	0.091	0.52
+ xchute	mid(90)	0.044	0.28	0.036	0.23	0.064	0.23	0.058	0.18
Xchute	front			0.905	3.13	1.082	3.09	0.832	2.17
Wet Grain-1	mid(0)			0.042		0.027		0.030	
4 nozzles	mid(30)			0.028		0.021		0.010	
	mid(90)			0.020		0.027		0.025	
Wet Grain-2	mid(0)	0.047		0.041		0.037		0.045	
6 nozzles	mid(30)	0.030		0.032		0.027		0.021	
	mid(90)	0.032		0.026		0.022		0.024	

Appendix H: Spray nozzles and liquid flow

Nozzles were tested using the same individual line and at 5.5 MPa (800 psi) and in duplicate. Each nozzle was directed into a graduated cylinder while the pump operated for 30 seconds. The manufacturer stated the flow at those conditions should be 84 cc/min. The flow ranged from 58 to128 cc/min for the group. A subset of 16 nozzles was selected from the batch of 32 nozzles.

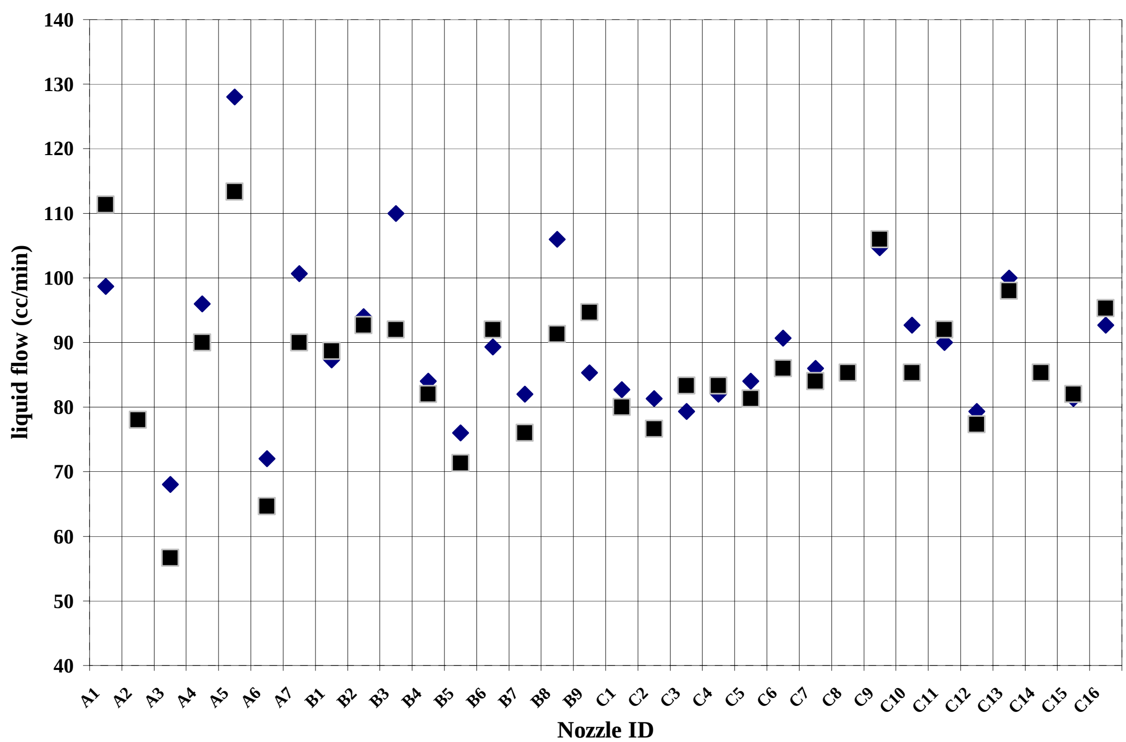

Figure H.1: Chart of liquid flow data from 32 nozzles.

Appendix I: Spray drop size and velocity data.

Two nozzles were sent to a private laboratory for analysis. One nozzle was tested at three pressures: 5.5 MPa (800 psi), 6.9 MPa (1000 psi), 8.3 MPa (1200 psi). The second nozzle was tested at one pressure: 6.9 MPa (1000 psi). An Aerometrics Phase Doppler Particle Analyzer, PDPA, instrument was used. It had a 100 mWatt Argon-Ion laser as a light source. The receiver was mounted at 30 degrees forward collection angle. The transmitter and receiver were mounted on rails with rotary plates. Optical lens were set for capturing 2 – 212 um drops. At each test point, either 30,000 samples or 30 seconds of data were collected.

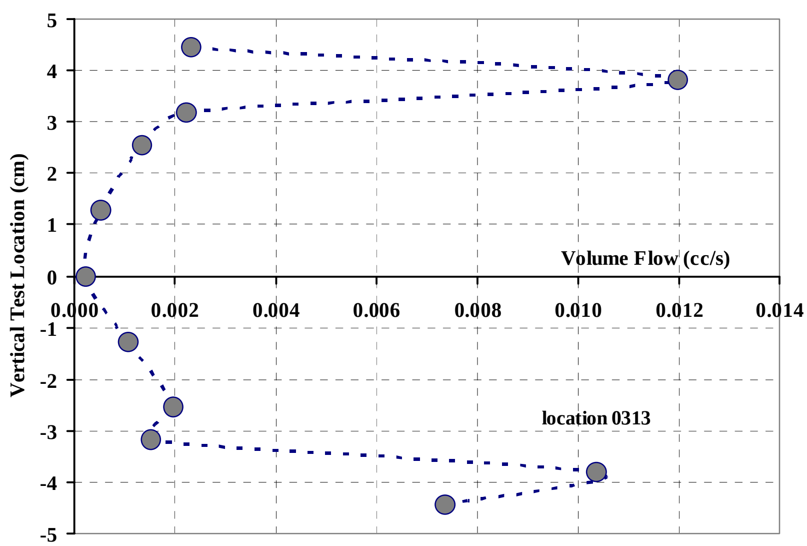

Figure I.1: Liquid flow distribution for spray nozzle.

Measurements were taken at 7.6 cm (3 in.) from the tip and at 11 vertical test locations. The nozzle was pressurized to 6.9 MPa (1000 psi). The distribution indicated the spray was a hollow cone.

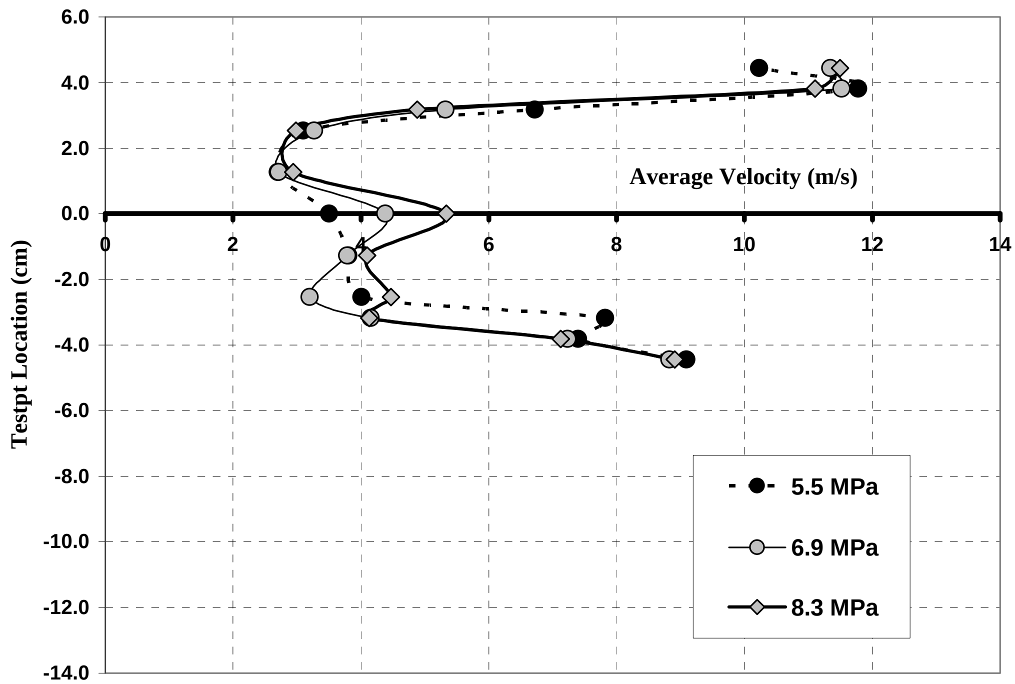

Figure I.2: Average drop velocity at 7.6 cm from nozzle and 3 pressures.

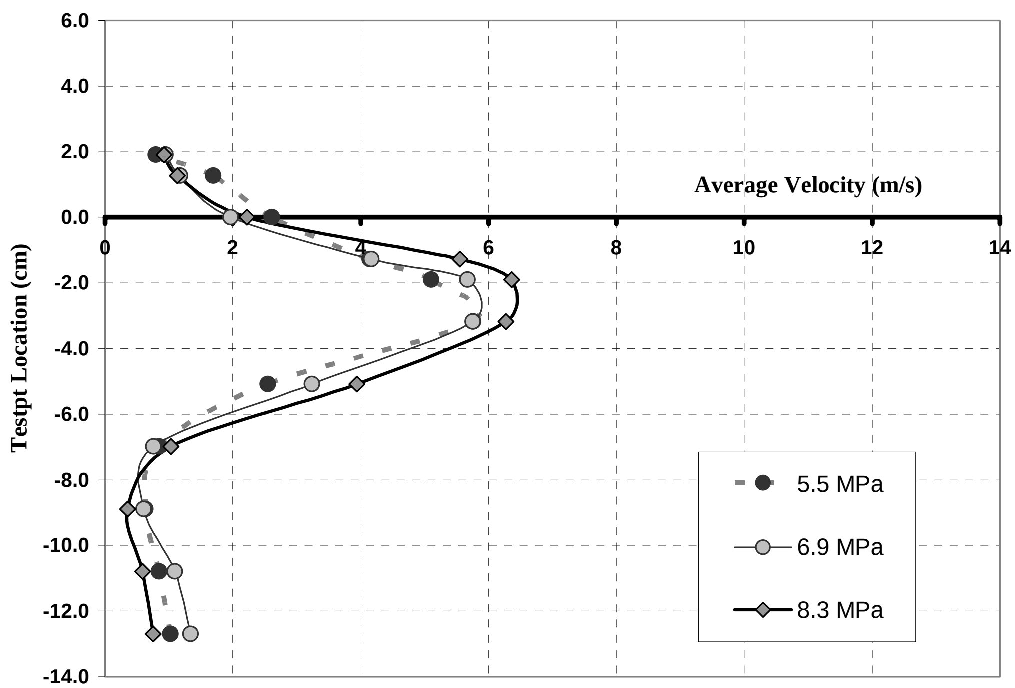

Figure I.3: Average drop velocity at 30.5 cm from nozzle and 3 pressures.

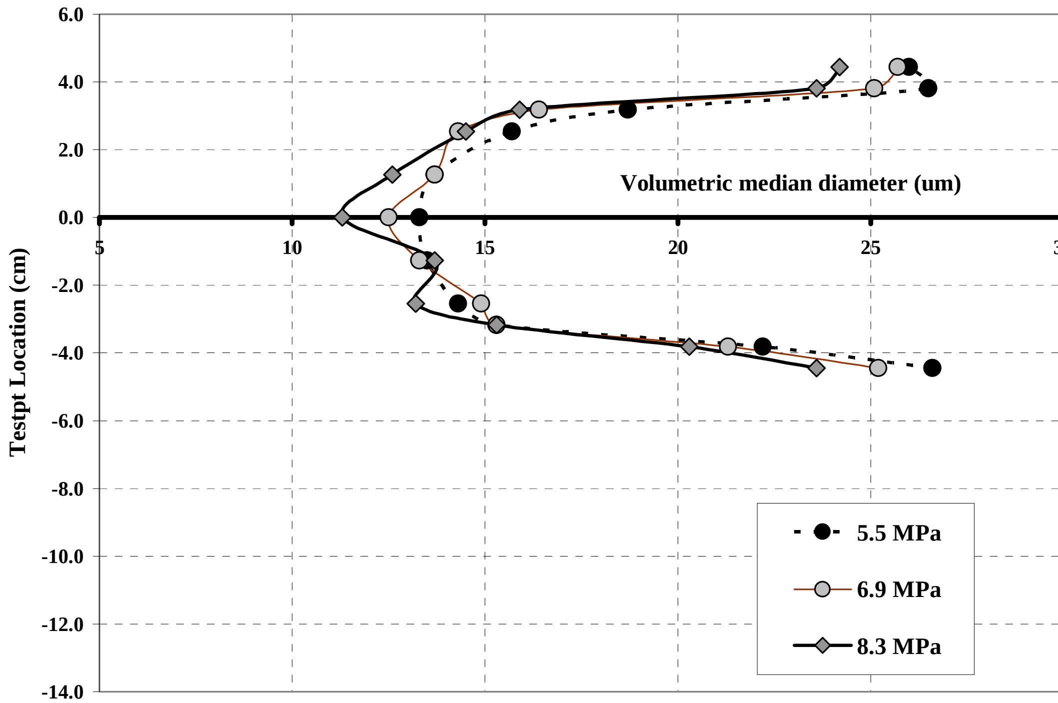

Figure I.4: VMD of drops at 7.6 cm from a nozzle and at 3 pressures.

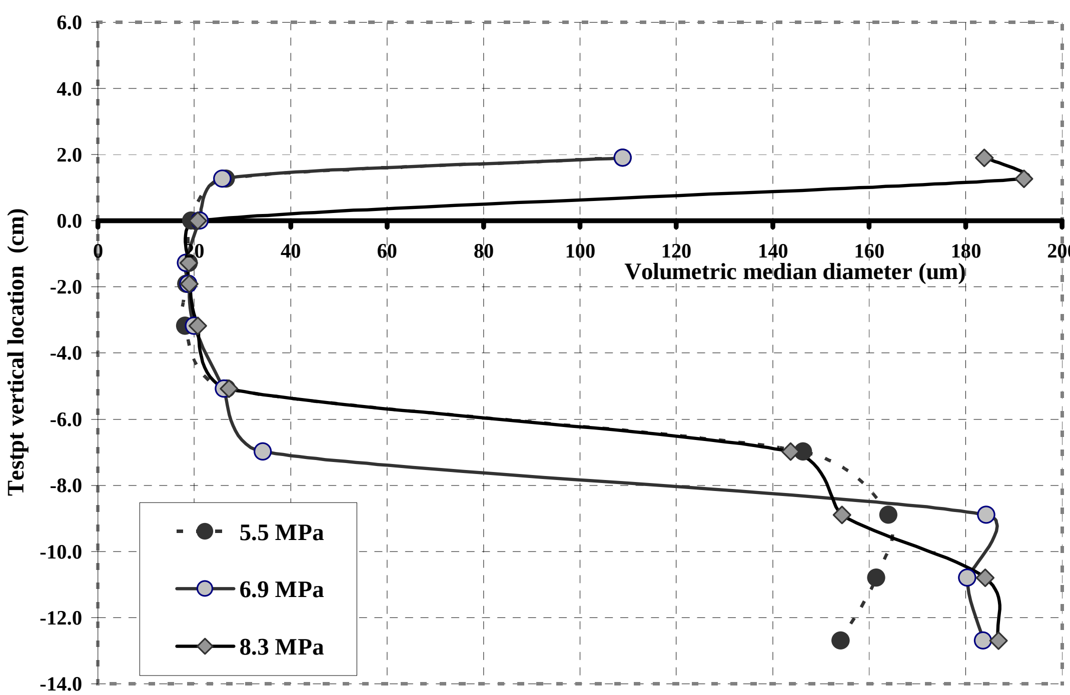

Figure I.5: VMD of drops at 30.5 cm from a nozzle and at 3 pressures.

Table I.1: Spray drop size and velocity data for a single test location 0313.

The following table is one of 44 individual data sheets. This data was collected at 7.6 cm (3 in.) from the nozzle and at 3.8 cm (1.5 in.) from the centerline. At this location, the larger drops are the faster drops. Drops with diameters of 16 to 31 um account for over 85% of the liquid volume at this location.

Diameter	Velocity		Count	Vol.	%Vol	Cumulative
	Avg.	Std. dev				
um	m/s	m/s		$(cm)^3$		%vol.
4.3	2.5	1.2	14	5.8E-07	0.0%	0.0
7.3	2.5	1.4	79	1.6E-05	0.0%	0.0
10.2	2.7	2.2	429	2.4E-04	0.2%	0.2
13.2	2.8	1.7	2563	3.1E-03	2.0%	2.1
16.2	3.3	2.1	8664	1.9E-02	12.3%	14.4
19.2	4.5	2.9	8317	3.1E-02	19.6%	34.0
22.1	7.4	4.2	3803	2.2E-02	13.8%	47.8
25.1	12.6	5.0	2027	1.7E-02	10.7%	58.6
28.1	18.8	5.2	1928	2.2E-02	14.3%	72.9
31.1	22.0	4.4	1793	2.8E-02	18.0%	90.8
34.0	24.0	5.6	440	9.1E-03	5.8%	96.6
37.0	23.8	7.4	123	3.3E-03	2.1%	98.7
40.0	25.7	6.2	24	8.0E-04	0.5%	99.2
42.9	18.0	12.3	13	5.4E-04	0.3%	99.6

Appendix J: Airflow measurement for test chamber with large inlet

To obtain initial airflow measurements during spray operation, a cover was placed on the test chamber leaving large 30.5 cm x 76.2 cm (1 ft x 2.5 ft) openings for the inlet and outlet. To measure spray induced airflow, a 10 cm (4 in.) diameter vane anemometer was placed at nine locations of the inlet while seven nozzles were operated at 6.9 MPa (1000 psi). The vane anemometer was a mechanical device which recorded rotary distance of the vane while a stop watch measured the time.

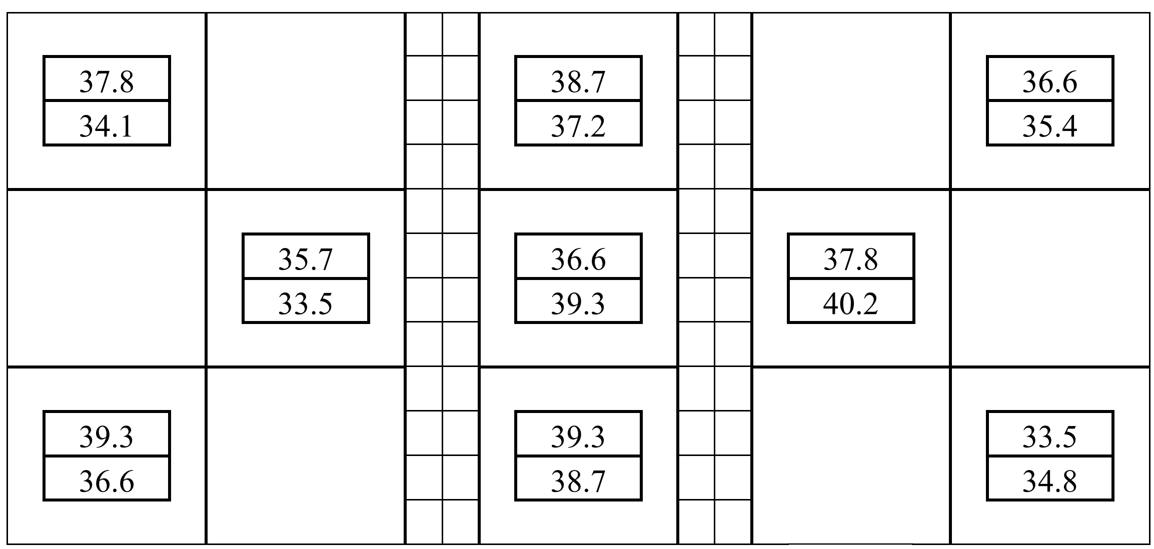

Figure J.1: Schematic of test chamber inlet and vane anemometer test locations. Values are velocities in m/min.

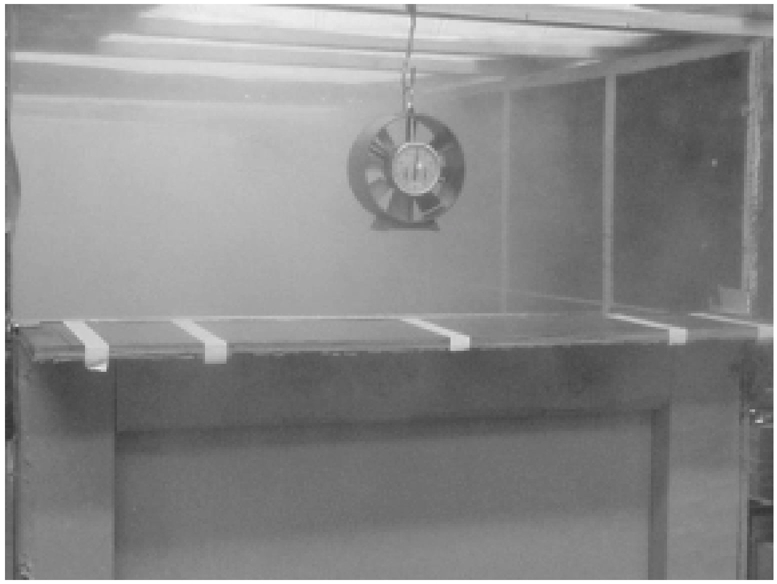

Figure J.2: Photo of the vane anemometer at the spray chamber outlet.

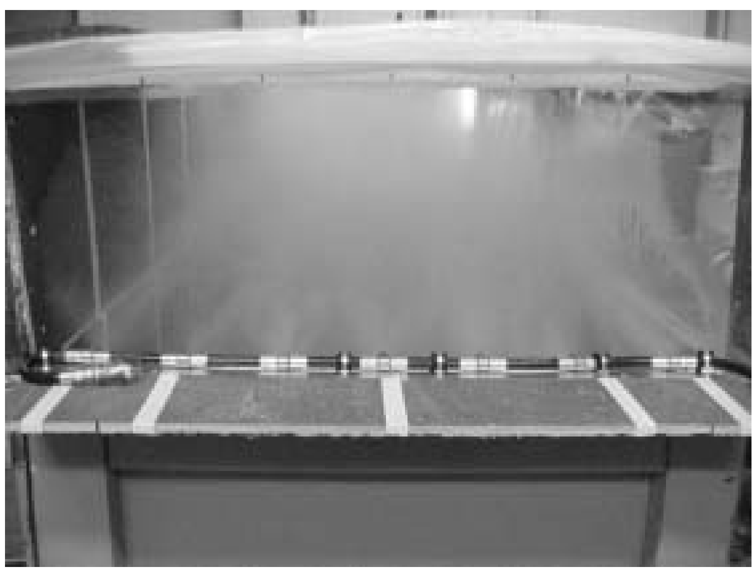

Figure J.3: Photo of test chamber inlet during spray-fog generation.

Appendix K: CFD software models and settings.

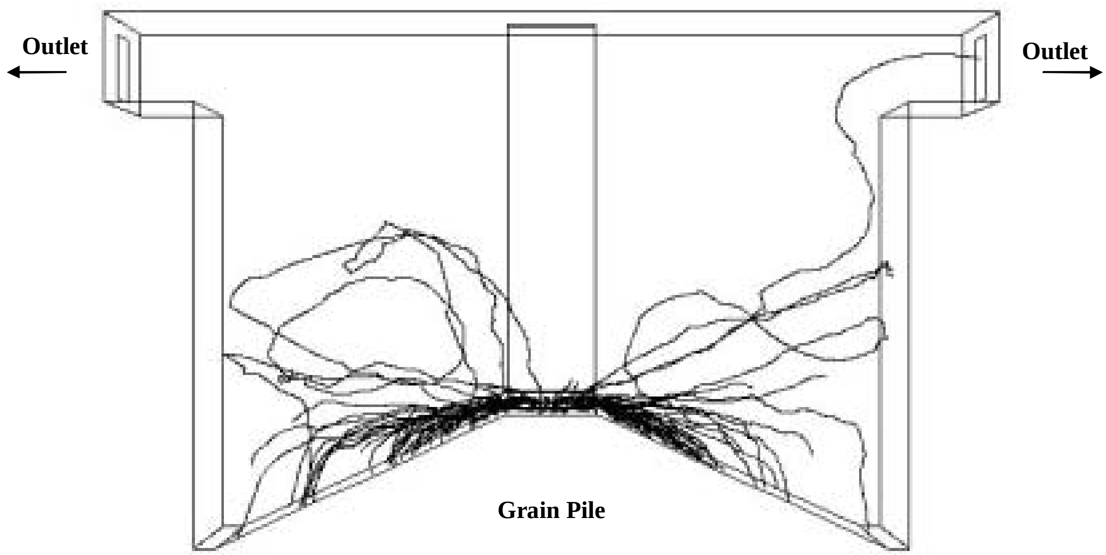

Figure K.1: CFD dust particle tracks of 30 μm particles in test chamber. Particles were initially positioned near the top of the grain pile and approximately 16% escaped through the outlet.

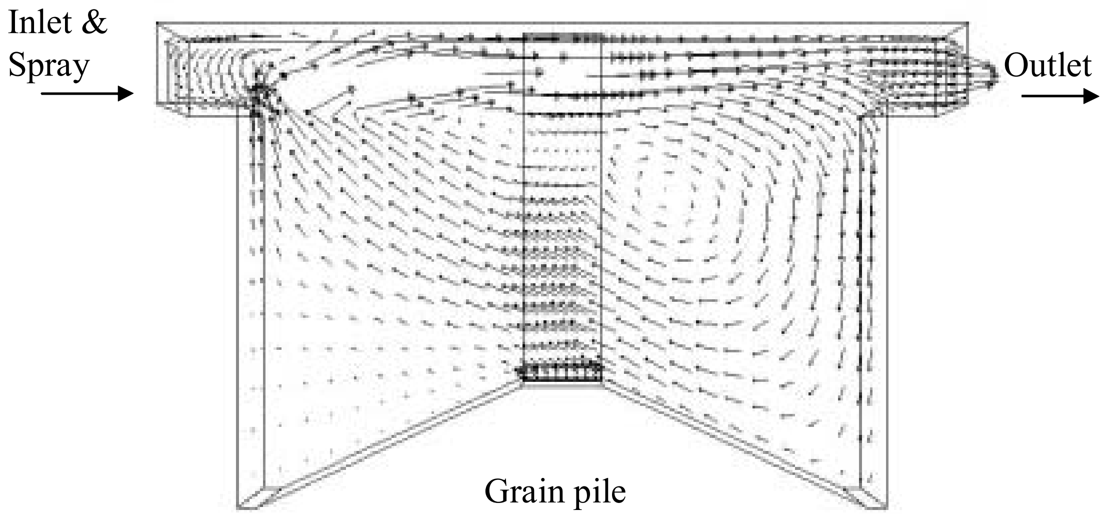

Figure K.2: CFD airflow profile during spray operations.

Airflow was affected by both the incoming grain and the induced airflow of the nozzle. The dominant airflow is across the top of the chamber, but a recirculating airflow is in the lower section of the chamber.

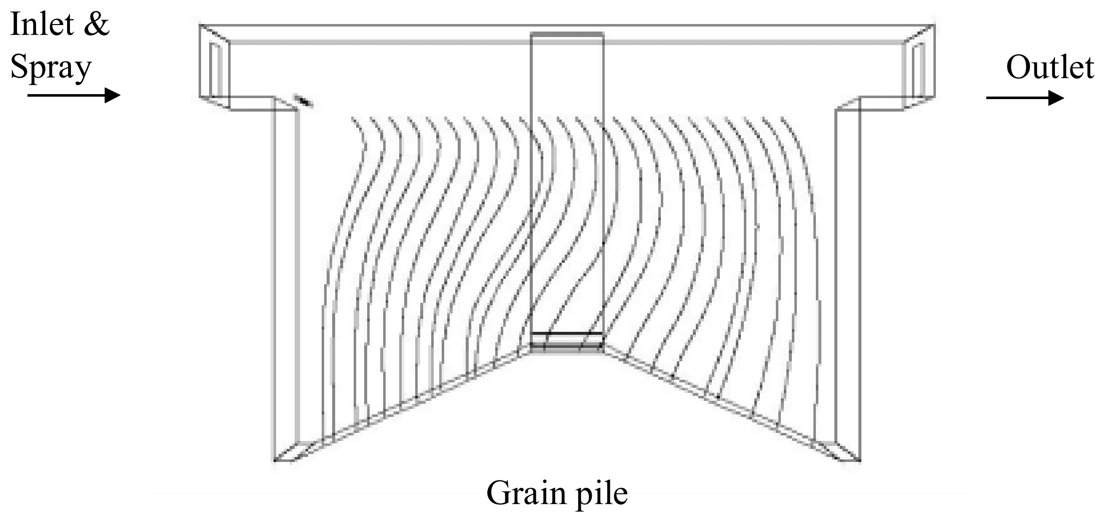

Figure K.3: CFD particle tracking for agglomerated drops as simulated by 180 µm drops released along the x-axis and below the spray plume during incoming grain and the induced airflow from seven nozzles.

```
FLUENT Modeling equations selection, test chamber boundaries
conditions, computational parameter selections, and fluid properties.

Version: 3d, segregated, ske (3d, segregated, standard k-epsilon)
Release: 6.0.20
Models
------
   Model                        Settings
   -----------------------------------------------------------------
   Space                        3D
   Time                         Steady
   Viscous                      Standard k-epsilon turbulence model
   Wall Treatment               Standard Wall Functions
   Heat Transfer                Disabled
   Solidification and Melting   Disabled
   Species Transport            Disabled
   Coupled Dispersed Phase      Disabled
   Pollutants                   Disabled
   Soot                         Disabled

Boundary Conditions
-------------------

   Zones

      name                 id   type
      ---------------------------------------
      fluid                2    fluid
      default-interior     25   interior

      outlet               22   pressure-outlet
      out2                 17   wall

      inlet                23   pressure-inlet
      in2                  16   wall

      7fans                21   fan

      g-impact             18   velocity-inlet
      g-wall               19   wall
      g-pile-a             20   velocity-inlet
      g-pile-b             9    velocity-inlet
      g-pile-m             8    velocity-inlet

      wall                 3    wall
      side0                14   wall
      side30               7    wall
      side90               6    wall
      side-low2            4    wall
      side-low-back        5    wall
      side-low-frt         15   wall

      ledge-near           10   wall
      ledge-far            11   wall
      end-near             12   wall
      end-far              13   wall
```

Boundary Conditions

g-impact

Condition	Value
Velocity Specification Method	2
Velocity Magnitude	0.12 m/s
Turbulence Intensity	0.05
Turbulence Length Scale	0.0305

g-wall

Condition	Value
Wall Motion	1
Velocity Magnitude	1.4 m/s
X-Component of Wall Translation	0
Y-Component of Wall Translation	-1
Z-Component of Wall Translation	0
Wall Roughness Constant	0.5

g-pile-a

Condition	Value
Velocity Specification Method	2
Velocity Magnitude	0.02 m/s
Turbulence Intensity	0.005
Turbulence Length Scale	0.762

7fans

Condition	Value
Flow Direction (-1,0,1)	-1
Pressure-Jump	175 Pa

outlet

Condition	Value
Gauge Pressure	0
Backflow Turbulence Intensity	0.03
Backflow Turbulence Length Scale	0.244

inlet

Condition	Value
Gauge Total Pressure	0
Turbulence Intensity	0.02
Turbulence Length Scale	0.244

Solver Controls

Equations

Equation	Solved
Flow	yes
Turbulence	yes

Relaxation

Variable	Relaxation Factor
Pressure	0.3
Momentum	0.7
Turbulence Kinetic Energy	0.8
Turbulence Dissipation Rate	0.8
Turbulent Viscosity	1

Linear Solver

Variable	Solver Type	Termination Criterion	Residual Reduction Tolerance
Pressure	V-Cycle	0.1	
X-Momentum	Flexible	0.1	0.7
Y-Momentum	Flexible	0.1	0.7
Z-Momentum	Flexible	0.1	0.7
Turbulence Kinetic Energy	Flexible	0.1	0.7
Turbulence Dissipation Rate	Flexible	0.1	0.7

Discretization Scheme

Variable	Scheme
Pressure	Standard
Pressure-Velocity Coupling	SIMPLE
Momentum	First Order Upwind
Turbulence Kinetic Energy	First Order Upwind
Turbulence Dissipation Rate	First Order Upwind

Material Properties

Material: air (fluid)

Property	Units	Method	Value(s)
Density	kg/m3	constant	1.225
Viscosity	kg/m-s	constant	1.7894e-05
Molecular Weight	kg/kgmol	constant	28.966

Table K.1: Drop injection location for a single nozzle location.

NO	(X) m	(Y) m	(Z) m	(U) m/s	(V) m/s	(W) m/s	(T) ^{o}K	(DIAM) M	(MFLOW) kg/s
0	0.38	1.53	0.24	6.74	-4.74	5.66	300	1.8E-05	4.7E-05
1	0.38	1.54	0.23	6.74	-3.55	6.48	300	1.8E-05	4.7E-05
2	0.38	1.55	0.23	6.74	-2.21	7.04	300	1.8E-05	4.7E-05
3	0.38	1.55	0.23	6.74	-0.80	7.34	300	1.8E-05	4.7E-05
4	0.38	1.56	0.22	6.74	0.65	7.35	300	1.8E-05	4.7E-05
5	0.38	1.56	0.22	6.74	2.07	7.09	300	1.8E-05	4.7E-05
6	0.38	1.57	0.21	6.74	3.41	6.55	300	1.8E-05	4.7E-05
7	0.38	1.57	0.21	6.74	4.63	5.75	300	1.8E-05	4.7E-05
8	0.38	1.57	0.20	6.74	5.66	4.74	300	1.8E-05	4.7E-05
9	0.38	1.57	0.19	6.74	6.48	3.55	300	1.8E-05	4.7E-05
10	0.38	1.57	0.18	6.74	7.04	2.21	300	1.8E-05	4.7E-05
11	0.38	1.56	0.18	6.74	7.34	0.80	300	1.8E-05	4.7E-05
12	0.38	1.56	0.17	6.74	7.35	-0.65	300	1.8E-05	4.7E-05
13	0.38	1.55	0.17	6.74	7.09	-2.07	300	1.8E-05	4.7E-05
14	0.38	1.55	0.16	6.74	6.55	-3.41	300	1.8E-05	4.7E-05
15	0.38	1.54	0.16	6.74	5.75	-4.63	300	1.8E-05	4.7E-05
16	0.38	1.53	0.16	6.74	4.74	-5.66	300	1.8E-05	4.7E-05
17	0.38	1.53	0.16	6.74	3.55	-6.48	300	1.8E-05	4.7E-05
18	0.38	1.52	0.16	6.74	2.21	-7.04	300	1.8E-05	4.7E-05
19	0.38	1.51	0.17	6.74	0.80	-7.34	300	1.8E-05	4.7E-05
20	0.38	1.51	0.17	6.74	-0.65	-7.35	300	1.8E-05	4.7E-05
21	0.38	1.50	0.18	6.74	-2.07	-7.09	300	1.8E-05	4.7E-05
22	0.38	1.50	0.18	6.74	-3.41	-6.55	300	1.8E-05	4.7E-05
23	0.38	1.50	0.19	6.74	-4.63	-5.75	300	1.8E-05	4.7E-05
24	0.38	1.50	0.20	6.74	-5.66	-4.74	300	1.8E-05	4.7E-05
25	0.38	1.50	0.21	6.74	-6.48	-3.55	300	1.8E-05	4.7E-05
26	0.38	1.50	0.21	6.74	-7.04	-2.21	300	1.8E-05	4.7E-05
27	0.38	1.50	0.22	6.74	-7.34	-0.80	300	1.8E-05	4.7E-05
28	0.38	1.51	0.22	6.74	-7.35	0.65	300	1.8E-05	4.7E-05
29	0.38	1.51	0.23	6.74	-7.09	2.07	300	1.8E-05	4.7E-05
30	0.38	1.52	0.23	6.74	-6.55	3.41	300	1.8E-05	4.7E-05
31	0.38	1.53	0.23	6.74	-5.75	4.63	300	1.8E-05	4.7E-05

Table K.2: Dust injection locations around the grain impact zone.

NO	(X) m	(Y) m	(Z) m	(U) m/s	(V) m/s	(W) m/s	(T) °K	(DIAM) M	(MFLOW) kg/s
dust14 injections-left side of impact zone: x=1.34m									
0	1.34	0.49	0.27	-2.00	2.00	0.00	300	1.4E-05	4.0E-03
1	1.34	0.49	0.29	-2.00	2.00	0.00	300	1.4E-05	4.0E-03
2	1.34	0.49	0.31	-2.00	2.00	0.00	300	1.4E-05	4.0E-03
3	1.34	0.49	0.33	-2.00	2.00	0.00	300	1.4E-05	4.0E-03
4	1.34	0.49	0.34	-2.00	2.00	0.00	300	1.4E-05	4.0E-03
5	1.34	0.49	0.36	-2.00	2.00	0.00	300	1.4E-05	4.0E-03
6	1.34	0.49	0.38	-2.00	2.00	0.00	300	1.4E-05	4.0E-03
7	1.34	0.49	0.40	-2.00	2.00	0.00	300	1.4E-05	4.0E-03
dust14 injections-right side of impact zone: x=1.71m									
NO	(X)	(Y)	(Z)	(U)	(V)	(W)	(T)	(DIAM)	(MFLOW)
0	1.71	0.49	0.27	2.00	2.00	0.00	300	1.4E-05	4.0E-03
1	1.71	0.49	0.29	2.00	2.00	0.00	300	1.4E-05	4.0E-03
2	1.71	0.49	0.31	2.00	2.00	0.00	300	1.4E-05	4.0E-03
3	1.71	0.49	0.33	2.00	2.00	0.00	300	1.4E-05	4.0E-03
4	1.71	0.49	0.34	2.00	2.00	0.00	300	1.4E-05	4.0E-03
5	1.71	0.49	0.36	2.00	2.00	0.00	300	1.4E-05	4.0E-03
6	1.71	0.49	0.38	2.00	2.00	0.00	300	1.4E-05	4.0E-03
7	1.71	0.49	0.40	2.00	2.00	0.00	300	1.4E-05	4.0E-03
dust14 injections-back side of impact zone: z=0.26m									
NO	(X)	(Y)	(Z)	(U)	(V)	(W)	(T)	(DIAM)	(MFLOW)
0	1.37	0.49	0.26	0.00	2.00	-2.00	300	1.4E-05	4.0E-03
1	1.39	0.49	0.26	0.00	2.00	-2.00	300	1.4E-05	4.0E-03
2	1.40	0.49	0.26	0.00	2.00	-2.00	300	1.4E-05	4.0E-03
3	1.42	0.49	0.26	0.00	2.00	-2.00	300	1.4E-05	4.0E-03
4	1.44	0.49	0.26	0.00	2.00	-2.00	300	1.4E-05	4.0E-03
5	1.45	0.49	0.26	0.00	2.00	-2.00	300	1.4E-05	4.0E-03
6	1.47	0.49	0.26	0.00	2.00	-2.00	300	1.4E-05	4.0E-03
7	1.48	0.49	0.26	0.00	2.00	-2.00	300	1.4E-05	4.0E-03
8	1.50	0.49	0.26	0.00	2.00	-2.00	300	1.4E-05	4.0E-03
9	1.52	0.49	0.26	0.00	2.00	-2.00	300	1.4E-05	4.0E-03
10	1.53	0.49	0.26	0.00	2.00	-2.00	300	1.4E-05	4.0E-03
11	1.55	0.49	0.26	0.00	2.00	-2.00	300	1.4E-05	4.0E-03
12	1.56	0.49	0.26	0.00	2.00	-2.00	300	1.4E-05	4.0E-03
13	1.58	0.49	0.26	0.00	2.00	-2.00	300	1.4E-05	4.0E-03
14	1.60	0.49	0.26	0.00	2.00	-2.00	300	1.4E-05	4.0E-03
15	1.61	0.49	0.26	0.00	2.00	-2.00	300	1.4E-05	4.0E-03
16	1.63	0.49	0.26	0.00	2.00	-2.00	300	1.4E-05	4.0E-03
17	1.64	0.49	0.26	0.00	2.00	-2.00	300	1.4E-05	4.0E-03
18	1.66	0.49	0.26	0.00	2.00	-2.00	300	1.4E-05	4.0E-03
19	1.68	0.49	0.26	0.00	2.00	-2.00	300	1.4E-05	4.0E-03
dust14 injections-front side of impact zone: z=0.40m									
NO	(X)	(Y)	(Z)	(U)	(V)	(W)	(T)	(DIAM)	(MFLOW)
0	1.37	0.49	0.40	0.00	2.00	2.00	300	1.4E-05	4.0E-03
1	1.39	0.49	0.40	0.00	2.00	2.00	300	1.4E-05	4.0E-03
2	1.40	0.49	0.40	0.00	2.00	2.00	300	1.4E-05	4.0E-03
3	1.42	0.49	0.40	0.00	2.00	2.00	300	1.4E-05	4.0E-03
4	1.44	0.49	0.40	0.00	2.00	2.00	300	1.4E-05	4.0E-03
5	1.45	0.49	0.40	0.00	2.00	2.00	300	1.4E-05	4.0E-03
6	1.47	0.49	0.40	0.00	2.00	2.00	300	1.4E-05	4.0E-03
7	1.48	0.49	0.40	0.00	2.00	2.00	300	1.4E-05	4.0E-03
8	1.50	0.49	0.40	0.00	2.00	2.00	300	1.4E-05	4.0E-03
9	1.52	0.49	0.40	0.00	2.00	2.00	300	1.4E-05	4.0E-03
10	1.53	0.49	0.40	0.00	2.00	2.00	300	1.4E-05	4.0E-03
11	1.55	0.49	0.40	0.00	2.00	2.00	300	1.4E-05	4.0E-03
12	1.56	0.49	0.40	0.00	2.00	2.00	300	1.4E-05	4.0E-03
13	1.58	0.49	0.40	0.00	2.00	2.00	300	1.4E-05	4.0E-03
14	1.60	0.49	0.40	0.00	2.00	2.00	300	1.4E-05	4.0E-03
15	1.61	0.49	0.40	0.00	2.00	2.00	300	1.4E-05	4.0E-03
16	1.63	0.49	0.40	0.00	2.00	2.00	300	1.4E-05	4.0E-03
17	1.64	0.49	0.40	0.00	2.00	2.00	300	1.4E-05	4.0E-03
18	1.66	0.49	0.40	0.00	2.00	2.00	300	1.4E-05	4.0E-03
19	1.68	0.49	0.40	0.00	2.00	2.00	300	1.4E-05	4.0E-03

Appendix L: Deposits of grain dust and spray

Figure L.1: Dust deposits on test chamber wall after 72 drop trials.

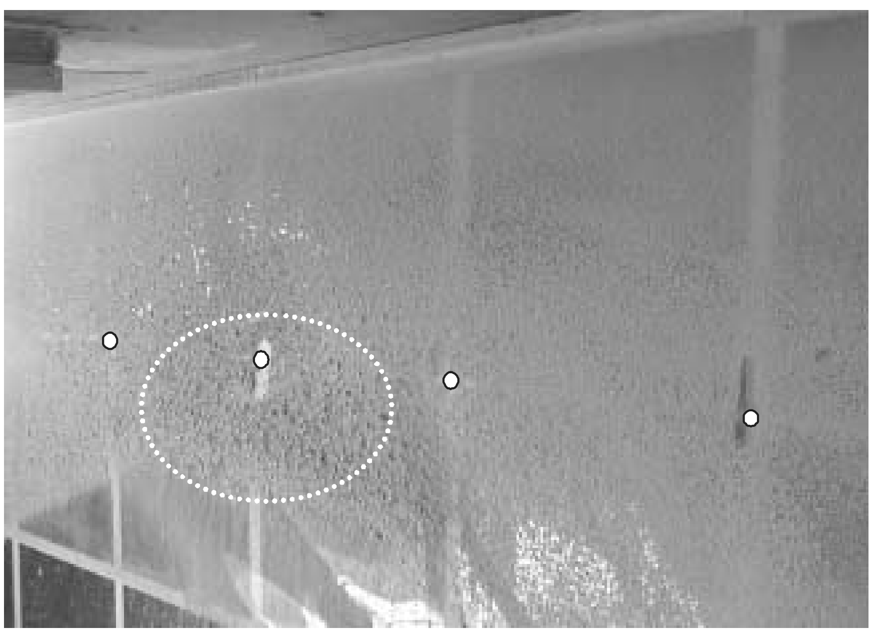

Figure L.2: Dust deposit gradient on side wall of test chamber.

The largest dust deposits were in the middle, where the cross section narrowed from the incoming grain. Below the grain surface, dust was rubbed off the walls.

Figure L.3: Filters and pans on grain surface for fog deposition test.
Three pans were on the front slope and three were on the back slope of the grain pile.

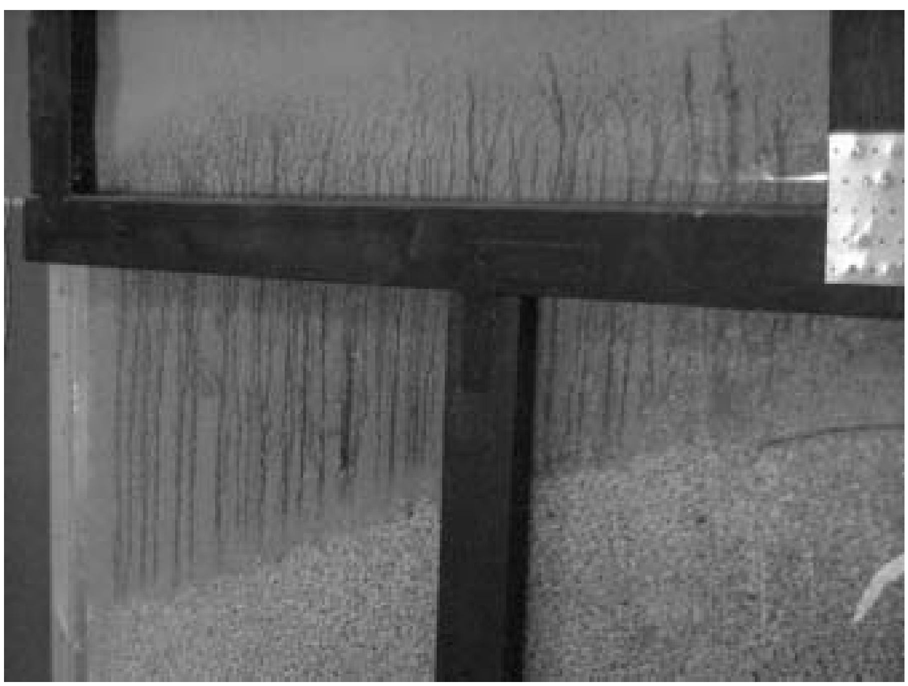

Figure L.4: Spray fog deposits on side of test chamber.
Water streaks were made in the dust on the side wall and close to the nozzles.

Figure L.5: Barrier used to model incoming grain during spray deposit test. The barrier was placed inside the grain chute and sat on the grain surface.

Appendix M: Grain dust particle size data

Dust samples were sent to a private laboratory (Micromeritics of Norcross, GA) for size distribution measurements. The laboratory used an Elzone particle sizing instrument. The Elzone analyzer measures particles which are dispersed in an electrolyte solution and passed through the electrical sensing orifice. The electrical conductivity measurement varies with particle size vs. test orifice diameter. The instrument could sense particles from 0.4 to 1200 µm at rates of up to 2000 particles per second. The laboratory ran duplicates to confirm similar results but sent data from only one run.

The first dust sample was grain dust from the USDA elevator's pneumatic dust collection system. A second sample was taken from the high-volume air sampler filters after the grain drop test (control trial). The dust size distributions resulted from different processes and depend on the grain process, airflows, and the proximity of the dust collections. The elevator dust sample contained fractions of larger particles which were captured by the high inlet airflows of the pneumatic system. The airflow for the grain drop test was generated by the displaced grain and entrained air which was rather low and thus able to lift only smaller sizes of dust.

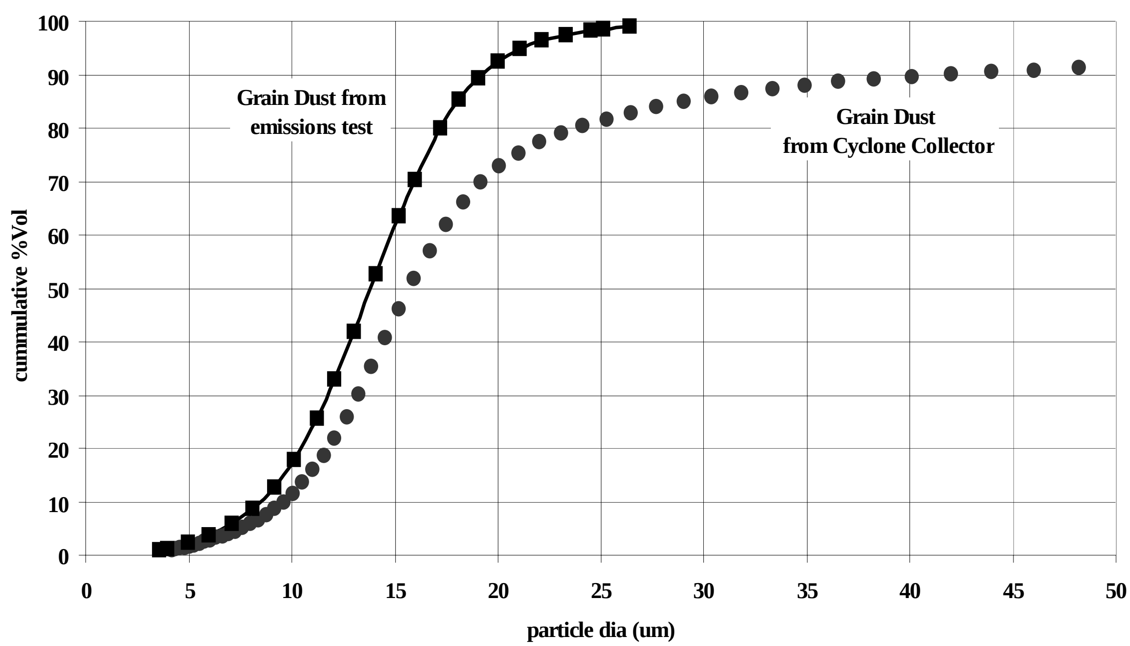

Figure M.1: Particle size distributions of dust samples.
Sample 1: Elevator's pneumatic dust collection system (circles).
Sample 2: High-volume air sample (squares) during grain drop.

Appendix N: Full scale grain receiving modeling

Prelimary efforts were made at modeling the USDA Grain Marketing Research Center's grain receiving hopper. The geometry was defined, meshed, and initial CFD computations were performed. The basic airflow modeling strategy has the grain pile displacing the majority of air volume at a low velocity while the impact zone, displaces a low volume of air at a relatively higher velocity.

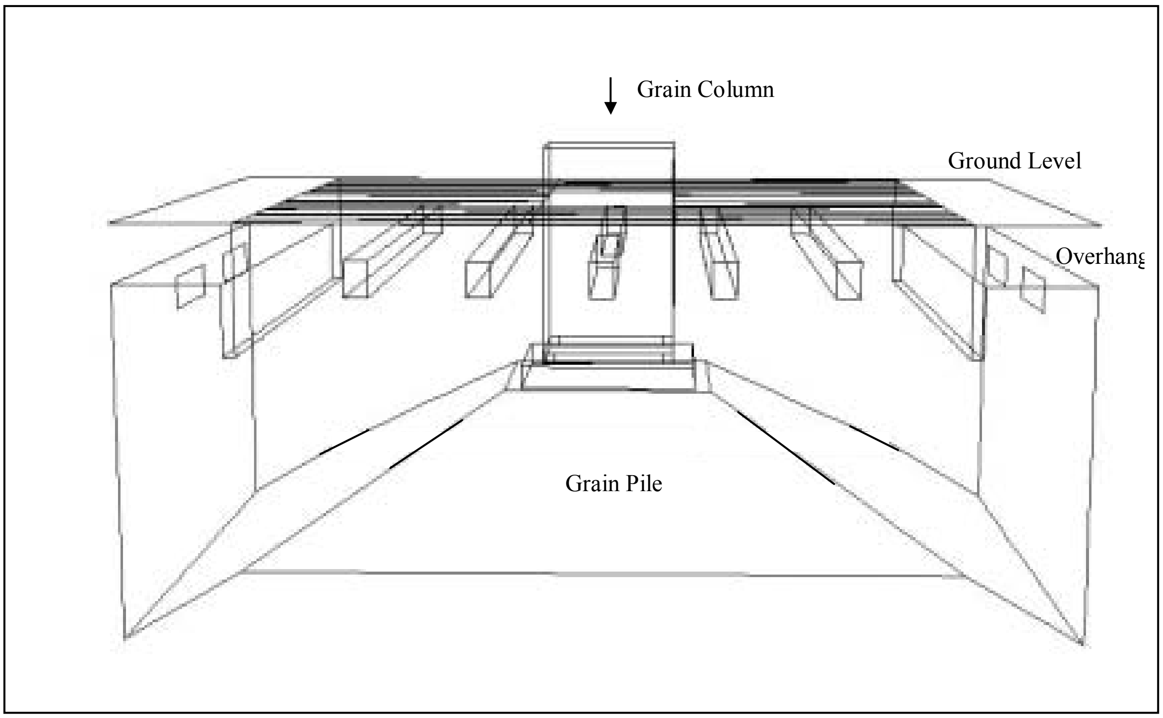

Figure N.1: Full scale grain receiving hopper geometry
with grain pile in lower section.

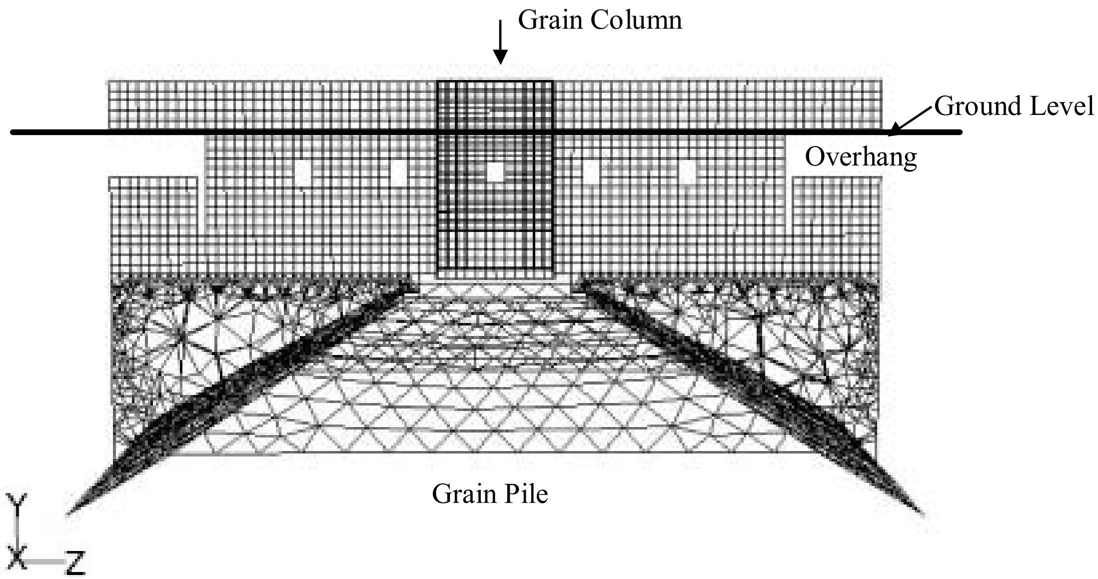

Figure N.2: Side view of CFD mesh for full scale receiving hopper.
The upper portion was meshed with hexahedrals
and lower portion was meshed with tetrahedrals.

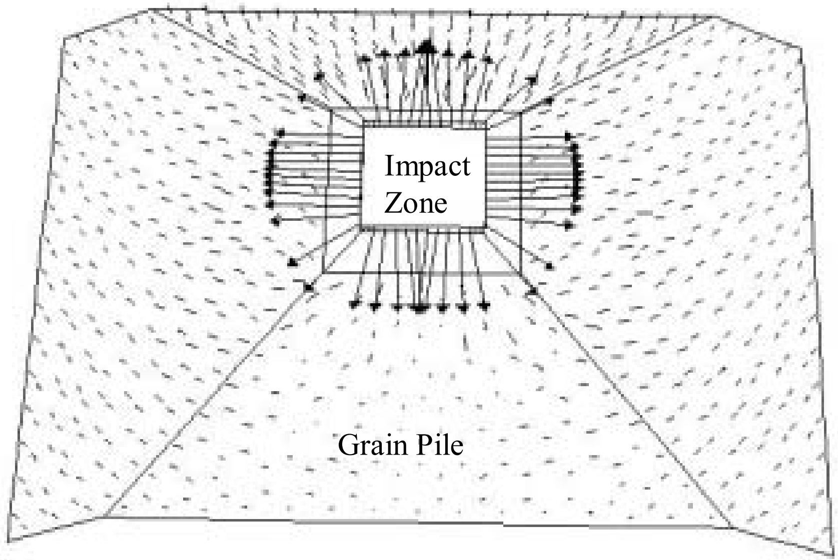

Figure N.3: Top view of impact zone and grain pile velocity vectors.
The velocity and airflow at the impact zone were 0.3 m/s and 3.1 m^3/min, respectively.
The velocity and airflow at the grain pile were 0.025 m/s and 30 m^3/min, respectively.

Appendix O: Electro-static measurements with spray-fog

A small test was performed to evaluate electro-static charge from the spray-fog. A glass rod was rubbed vigorously with two types of material to build a charge on the glass. One material was a paper towel and the second material was a clothe, which was made from polyester and cotton. The charge on the glass rod was measured with a hand held electro-static field meter as over 16 kVolts. The meter was model Hand*E*Stat from Simco, Hatfield, PA (215-822-6401). An individual nozzle was operated at 6.9 MPa (1000 psi). The glass rod was passed through the spray plume and the charge on the glass was measured. With a single pass through the plume, the charge was reduced to less than 4 kV. After the glass rod was held in the spray plume for several seconds, the charge on the glass rod measured 0. From this limited trial, the spray-fog appeared to neutralize a highly charged glass rod.

Appendix P: Laboratory scale dust emission measurement

The dust emission potential of a grain lot was determined using a laboratory aspiration method. Two, 2000 g samples of each grain were passed through a laboratory aspirator (Model: 6DT4, Kice Mft, Wichita, KS). The air baffle was set so the pressure at the inlet of the cyclone was 1 inch water. The grain flow gate was set for the grain to pass in 18-20 seconds. The fines and broken material collected with the cyclone and separated with 2 sieves and a pan. The sieve stack contained a #30 sieve (595 μm), #70 sieve (210 μm), and a pan and the material was shaken manually for 30 strokes. The filter bag on the exhaust of the cyclone was weighed before and after each sample. The material collected in the pan was summed with the weight of fines in the exhaust filter and correlated with the dust emissions data collected from the grain receiving test.

The corn and wheat laboratory emissions averaged 0.46 g/kg and 0.17 g/kg, respectively. The ratio of the corn/wheat emissions was 2.7. From the grain receiving test data, the ratio of corn/wheat emissions was 12.5/5.5 or 2.3. The relative dustiness of the material was evident for both size of test. Many methods could be developed to estimate grain-dust emission potential which would use an air and filter collection system. A grain-dust test could be correlated with many grain quality parameters such as insect damage or grain breakage or the amount of potential weight lost into the pneumatic dust collection system.